

See discussions, stats, and author profiles for this publication at: <https://www.researchgate.net/publication/313164879>

Geothermal Energy

Chapter · January 2006

DOI: 10.1007/b83039

CITATIONS

9

READS

3,732

1 author:



[Christoph Clauser](#)

RWTH Aachen University

240 PUBLICATIONS 6,826 CITATIONS

[SEE PROFILE](#)

8	GEOTHERMAL ENERGY.....	1
8.1	THE EARTH'S THERMAL REGIME	1
8.1.1	<i>The Structure of the Earth</i>	1
8.1.2	<i>Energy Budget of the Earth</i>	4
8.1.2.1	Heat Income	5
8.1.2.1.1	External Heat Sources	5
8.1.2.1.2	Internal Heat Sources	6
8.1.2.2	Heat Expenditure.....	8
8.1.2.3	Heat Budget.....	9
8.1.3	<i>The Thermal Regime of the Earth's Crust</i>	9
8.1.4	<i>Heat Storage</i>	10
8.1.4.1	Measuring Techniques	12
8.1.4.2	Calculated Heat Capacity	12
8.1.5	<i>Heat Transport</i>	23
8.1.5.1	Heat Conduction.....	23
8.1.5.1.1	Measuring Techniques	23
8.1.5.1.2	Indirect Methods.....	24
8.1.5.1.3	Thermal Conductivity of Minerals	28
8.1.5.2	Thermal Conductivity of Rocks	35
8.1.5.2.1	Thermal Conductivity of Sedimentary, Volcanic, Plutonic, and Metamorphic Rocks	36
8.1.5.2.2	Influence of Various Factors on Thermal Conductivity	46
8.1.5.3	Heat Advection.....	52
8.1.5.4	Heat Radiation and Thermal Conductivity in the Earth's Mantle.....	56
8.2	GEOTHERMAL ENERGY RESOURCES.....	59
8.3	TYPES OF GEOTHERMAL ENERGY USE	61
8.3.1	<i>Direct Use</i>	61
8.3.1.1	Space Heating.....	64
8.3.1.1.1	Earth Coupled Heat Extraction Systems.....	65
8.3.1.1.2	Hydrothermal Heating Systems.....	68
8.3.1.2	Commercial and Industrial Applications.....	69
8.3.2	<i>Power Generation</i>	71
8.4	TECHNOLOGICAL AND ECONOMICAL ASPECTS OF GEOTHERMAL ENERGY	75
8.4.1	<i>Direct Use</i>	76
8.4.1.1	Earth Coupled Heat Extraction Systems.....	76
8.4.1.2	Hydrothermal Heating Systems.....	82
8.4.2	<i>Power Generation</i>	84
8.4.2.1	Natural Steam Power Plants	85
8.4.2.2	Binary Power Plants	89
8.4.2.3	Power Plants for Hot Dry Rock or Enhanced Geothermal Systems	91
8.4.2.4	Technical, Economic, and Ecological Aspects of Geothermal Power Production.....	94
8.4.2.4.1	Efficiency	94
8.4.2.4.2	Cost and Life Time.....	95
8.4.2.4.3	Pollution	99
8.5	SUMMARY	104
	REFERENCES	106

8 Geothermal Energy

Geothermal energy is the heat contained in the solid Earth and its internal fluids. This sets it apart from other terrestrial energy sources such as

- fossil or fissional fuels in the subsurface;
- biomass, solar energy, and hydropower on the surface of the solid Earth and in its rivers and seas;
- wind energy in the atmosphere.

Geothermal energy is stored as sensible or latent heat. Supplied by both internal and external sources, it represents a vast supply which is only started to be tapped by mankind for space heating, process heat, and generation of electric power. The options and challenges involved in turning this promising potential into operational, efficient, and economic technologies are the topic of this assessment.

The major topics associated with an enhanced future use of geothermal energy are reviewed in four main chapters: (1) *The Earth's thermal regime*: where on Earth is heat, how much is there, where does it come from, and how is it transferred? (2) *Geothermal energy resources*: what kinds of resources are available in which reservoirs and how big are they? (3) *Types of geothermal energy use*: how can geothermal heat be used directly or converted into electricity and what is the present use of geothermal energy?; (4) *Technological and economical aspects of geothermal energy use*: which technologies are available to produce geothermal energy, and how much does it cost? A summary and outlook concludes this review.

8.1 The Earth's Thermal Regime

Since the conditions under which geothermal energy can be exploited strongly depend on both the origin of geothermal heat and the environment in which it is stored, we first need to examine briefly the internal structure of the Earth. Next we analyze the energy budget of the Earth and quantify the contributions of the various external and internal sources and sinks of heat. Then we examine the thermal regime of the Earth' crust and the magnitudes of heat storage and transport and the associated physical properties specific heat capacity, thermal conductivity, and diffusivity.

8.1.1 The Structure of the Earth

Our information on the internal structure of the Earth and the variation of its physical properties (pressure, temperature, density, seismic velocities) and chemical composition are derived from seismology, i.e. the interpretation of travel time curves of earthquakes which passed through the Earth. The variation with depth of the observed seismic velocities and elastic constants combined with Maxwell's four thermodynamic relations between pressure P, volume V, entropy S ($\Delta S = \Delta Q/T$; Q: heat), and temperature T yield the predominantly radial structure of the Earth.

From Maxwell's relation $(\partial T/\partial P)_S = (\partial V/\partial S)_P$ one obtains an expression for the adiabatic temperature gradient in terms of temperature, the volume coefficient of thermal expansion $\alpha = (\partial V/\partial T)_P/V$, and the isobaric specific heat capacity c_P (at constant pressure):

$$\left(\frac{\partial T}{\partial z}\right)_S = T \frac{\alpha g}{c_P}, \quad (8.1)$$

where g is gravity and subscripts P and S refer to isobaric and adiabatic conditions, respectively, i.e. constant pressure and constant entropy.

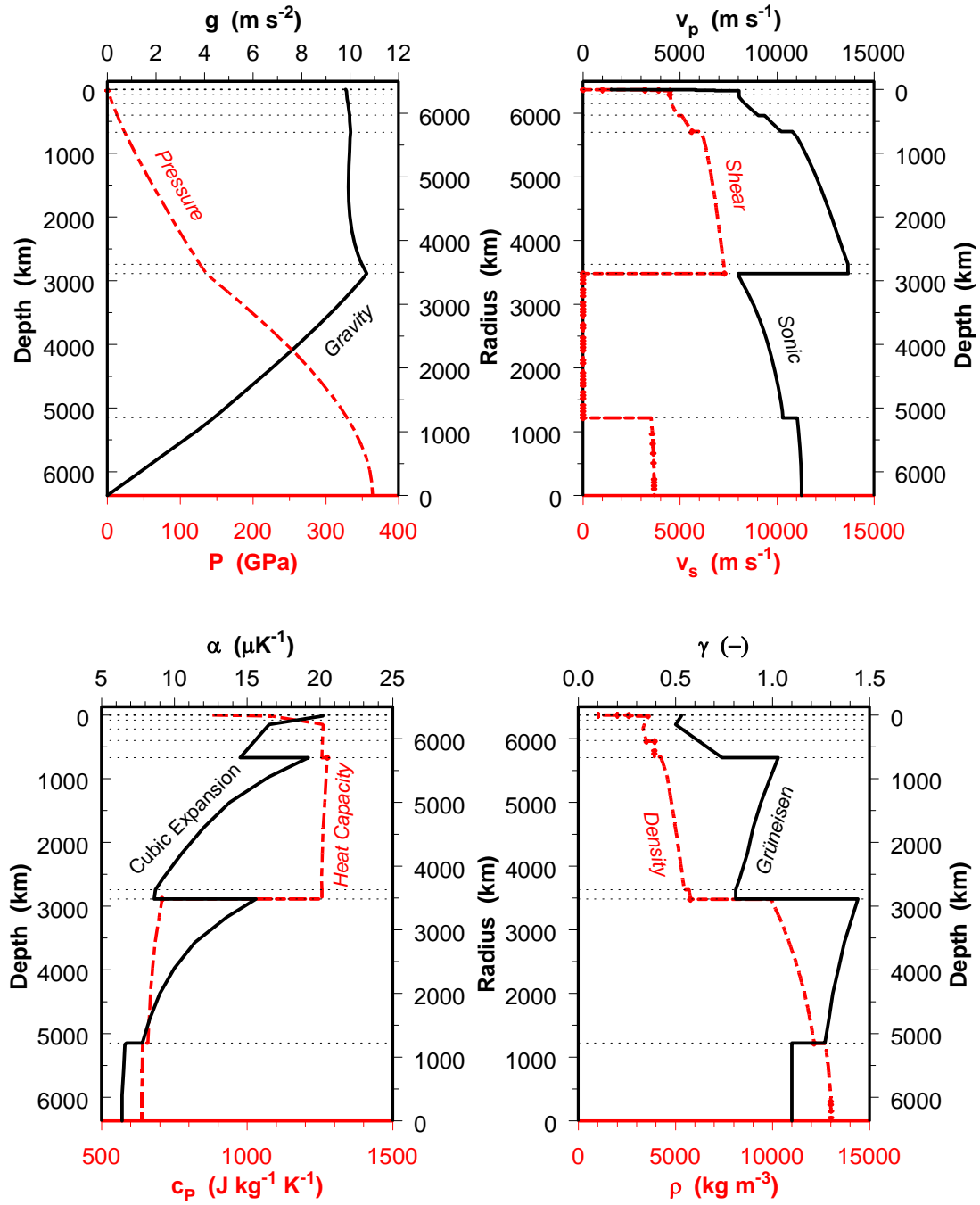


Fig. 8.1 Variation of selected properties versus depth in the Earth according to the Earth models PREM (gravity g , pressure P , coefficient of thermal volume expansion α and isobaric specific heat capacity c_p ; Grüneisen parameter γ) [1981Dzi; data: 1992Sta] and AK135-f (sonic and shear wave velocities v_p and v_s ; density ρ) [1995Ken; 1995Mon].

Assuming lower mantle values (at about 1500 km depth) of $T=2400$ K, $g=9.9$ m s⁻², $c_p=1200$ J kg⁻¹ K⁻¹, and $\alpha=14$ μ K⁻¹, yields an adiabatic temperature gradient of about 0.3 K km⁻¹; the corresponding values for the outer core (at about 3500 km depth) of $T=4000$ K, $g=10.1$ m s⁻², $c_p=700$ J kg⁻¹ K⁻¹, and $\alpha=14$ μ K⁻¹ (Fig. 8.1), yield an adiabatic temperature gradient of about 0.8 K km⁻¹ [1992Sta; 1997Low].

Approximate estimates for the adiabatic temperature inside the Earth can be obtained with the aid of the dimensionless thermodynamic Grüneisen parameter $\gamma = \alpha K_S / (\rho c_p)$, where K_S is the adiabatic incompressibility or bulk modulus and ρ is density (Fig. 8.1):

$$\frac{\partial T}{T} = \gamma \frac{d\rho}{\rho}, \quad \text{or: } T = T_0 \left(\frac{\rho}{\rho_0} \right)^\gamma. \quad (8.2)$$

From a known temperature T_0 and density ρ_0 at a given depth, eq. (8.2) allows computing the adiabatic temperature from the density profile in a region where the Grüneisen parameter is known. Fortunately, the Grüneisen parameter does not vary too much within large regions of the Earth's interior (Fig. 8.1). However, eq. (8.2) cannot be applied across the boundaries between these domains, where γ is discontinuous. But if T_0 and ρ_0 are known at calibration points, the adiabatic temperature profile can be computed in an iterative fashion within these depth intervals. The currently accepted estimate of the temperature profile is characterized by steep gradients in the lithosphere, asthenosphere and in the lower mantle D'' layer (immediately above the core-mantle boundary). Neglecting large lateral variations in the crust and lithosphere it indicates, on average, temperatures of less than 1000 K in the lithosphere, close to 3750 K at the core-mantle boundary, and around 5100 K at the center of the Earth (Fig. 8.2) [1992Sta; 1997Low;].

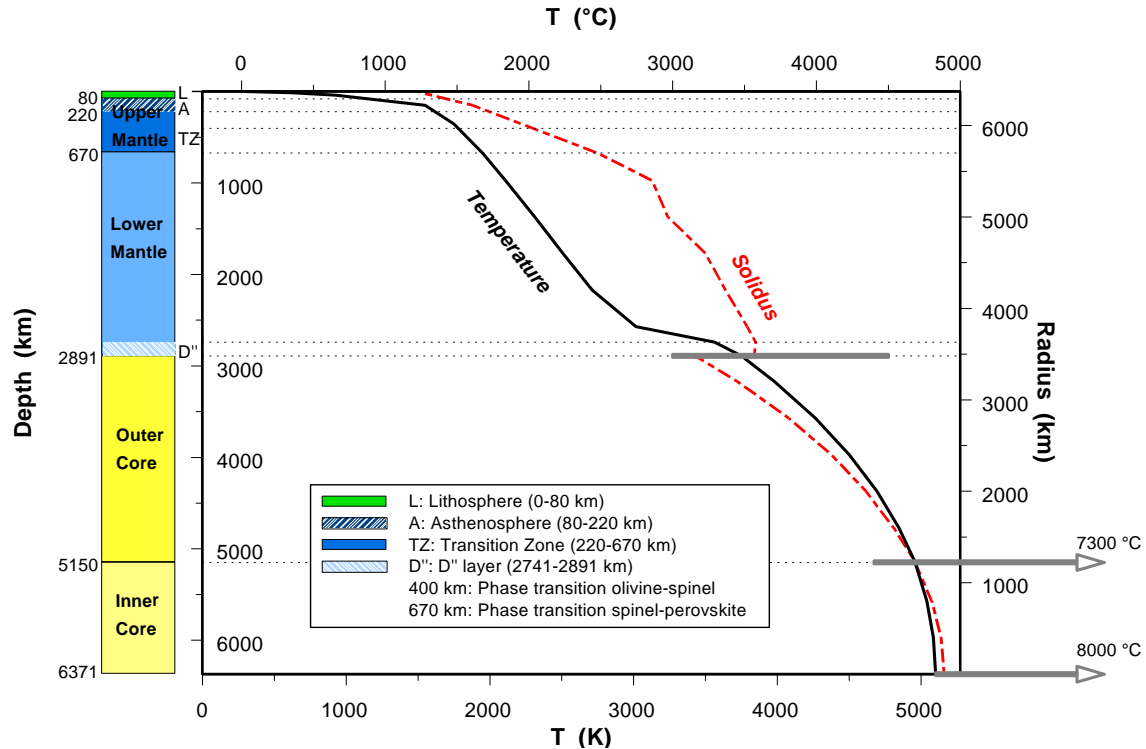


Fig. 8.2. Variation of estimated temperature and melting point in the Earth with depth; Data according to Stacey [1992Sta] selected to be representative and consistent with the Preliminary Reference Earth Model (PREM) [1981Dzi]. Temperature is poorly constrained in the deeper sections, indicated by large error bars; data: [1993Bro].

However, there are large uncertainties, particularly in the mantle and core [1993Bro; 2001Bea], indicating ranges for conceivable minimum and maximum temperatures of 3000 °C – 4500 °C at the core-mantle boundary, 4400 °C – 7300 °C at the transition between outer and inner core, and a maximum temperature at the center of the Earth of less than 8000 °C (Fig. 8.2).

From another one of Maxwell's thermodynamic relations, $(\partial S/\partial P)_T = -(\partial V/\partial T)_P$, one can derive the fractional variation of the melting point temperature T_{mp} with depth within the Earth:

$$\frac{1}{T_{mp}} \frac{dT_{mp}}{dz} = \frac{g}{L} \frac{(\rho_{solid} - \rho_{liquid})}{\rho_{liquid}}, \quad (8.3)$$

where L is the latent heat of fusion, and ρ_{solid} and ρ_{liquid} are the densities of the solid and liquid phases, respectively. With the information on the variation of gravity and density with depth derived from seismic travel times (Fig. 8.1) one may obtain a profile of the melting point temperature with depth. Assuming outer core values (at about 3300 km depth) of $T=4000$ K, $g=10.1$ m s⁻², $\rho_{solid}=13000$ kg m⁻³, $\rho_{liquid}=11000$ kg m⁻³, and $L=7$ MJ kg⁻¹ for iron yields a melting point temperature gradient of about 1 K km⁻¹ (Fig. 8.2) [1997Low]. Thus, the melting point temperature increases more rapidly with depth than the adiabatic temperature. However, the variation of the properties (e.g. L , g , c_p) in the Earth is known only with large uncertainty, and an accordingly large uncertainty is associated with the temperature profiles based on eqs. (8.2) and (8.3).

8.1.2 Energy Budget of the Earth

In order to avoid numbers with too many digits energy budgets are usually quantified in multiples of 1000 of the base units Joule and Kilowatt-hour (Table 8.1; Table 8.2).

Table 8.1 Abbreviations, prefixes, and names for various powers of ten in different systems.

American	system British/French/German	prefix	abbreviation	factor
thousand	thousand	Kilo	k	10 ³
million	million	Mega	M	10 ⁶
billion	milliard	Giga	G	10 ⁹
trillion	billion	Tera	T	10 ¹²
quadrillion	–	Peta	P	10 ¹⁵
quintillion	trillion	Exa	E	10 ¹⁸
sextillion	–	Zetta	Z	10 ²¹
septillion	quadrillion	Yotta	Y	10 ²⁴

The Earth's energy budget is determined by its thermal income and expenditure. The Earth receives remarkable amounts of energy from both external and internal sources. Their enormous size can be best illustrated by comparison with the global production of primary energy in the year 2001, about 420 EJ [2003IEA¹] or the annual primary energy requirements predicted for the current century, estimated to 600 EJ – 1800 EJ depending on various assumptions [1997Edw; 1997Nak; 2000Nak; 2002IEA] (Fig. 8.3).

Table 8.2 Units and conversion factors for energy and power.

quantity	unit	abbreviation	conversion
Energy (e.g. heat)	Joule	J	1 GJ = (1000/3.6) MJ ≈ 278 kW h
	Kilowatt-hours	kW h	1 kW h = 3.6 MJ
Power	Watt	W	1 W = 1 J s ⁻¹

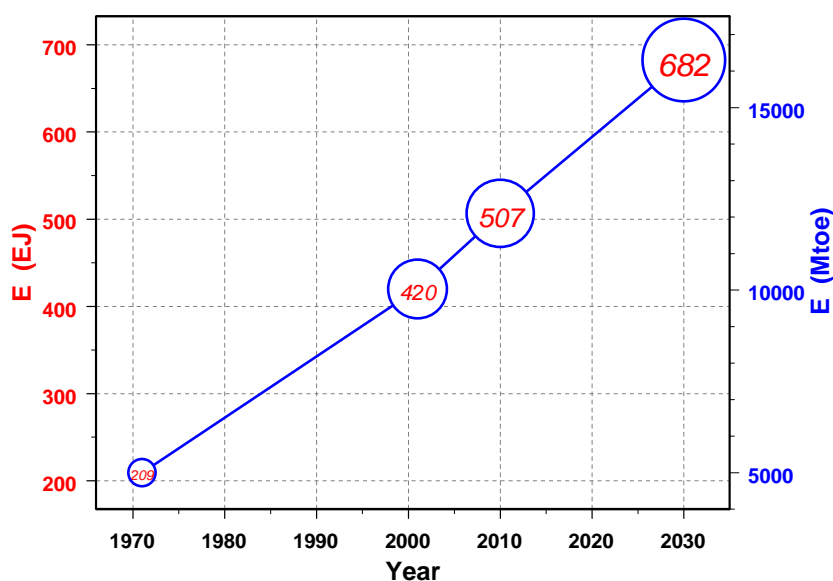


Fig. 8.3. Global primary energy consumption in 1971 and 2001 and expected primary energy demand in 2010 and 2030 in EJ (left axis) or Megatonnes of oil equivalent (Mtoe, right axis) [2002IEA; 2003IEA]; 1 Mtoe = 41.868 PJ.

8.1.2.1 Heat Income

The largest *external* energy source of the Earth is the solar irradiation. The incident energy of the Sun's rays falling on the Earth for just one day, 1.5×10^{22} J (computed from the solar irradiance given below), correspond to about 35 years worth of the global production of primary energy in the year 2001 (Fig. 8.3). In other terms, 4–12 days of solar irradiation corresponds to the expected cumulative primary energy requirements for the entire current century. However, only regrettably small amounts of the irradiated solar energy are converted into forms of energy which can be stored relatively permanently by the Earth, mainly as fossil fuels, as will be seen below. The conversion of solar energy reaching the Earth's surface into heat and electricity is the topic of Chap. 4 of this book.

The largest *internal* energy source of the Earth is provided by the decay of radiogenic isotopes in the rocks of the Earth's crust. The heat thus produced within one year, 8.6×10^{20} J (computed from the average terrestrial heat generation rate given below), corresponds to more than twice the global production of primary energy in the year 2000 (Fig. 8.3). This huge energy source by itself clearly exceeds the world's energy demands expected for the period 2000–2030 [2002IEA]. If it could be harnessed, it would suffice alone to satisfy the primary energy demand of the entire 21st century.

8.1.2.1.1 External Heat Sources

The Earth receives energy from two major external sources: electromagnetic energy from the *solar radiation* and *gravitational energy* due to forces of the Sun and Moon exerted on the rotating Earth.

Solar Radiation: The solar constant $S = 1373 \text{ W m}^{-2}$ [2000Lid] is the solar irradiance (or incident solar radiation flux) on a plane normal to the Sun's rays, just outside the Earth's atmosphere, when the Earth is at a distance of one astronomical unit ($1 \text{ AU} = 1.496 \times 10^8 \text{ km}$) from the Sun. Long-term observations of the solar irradiation from satellites [1999Kyl; 2002NGD] indicate a variability of the solar "constant" on the order of fractions of a percent due to changes in the solar activity. With its cross section of $\pi (R_E)^2$ the Earth intercepts from the total solar radiation a radiation power $P = S \pi (R_E)^2 \approx 1.75 \times 10^{17} \text{ W}$, where

$R_E=6371$ km is the radius of the best-fitting sphere for the Earth. Of this solar energy flux, about 35 % (6.1×10^{16} W) are directly reflected as short wavelength radiation, and 65 % (1.14×10^{17} W) are scattered and absorbed in atmosphere, hydrosphere, and lithosphere, and finally re-emitted as long-wavelength radiation. Of this absorbed fraction of the total incident solar energy, 31 % (3.53×10^{16} W) are absorbed in the atmosphere, while 69 % (**7.87×10^{16} W**) reach the surface of the Earth. Thus less than half of the total solar irradiation of the Earth, just about 45 % can be considered an external source to the terrestrial heat budget. But most of this energy is directly re-emitted as long-wavelength radiation (see Sect.). Only a tiny fraction of less than 1 ppm (3.2×10^9 W – 3.2×10^{10} W) of this absorbed energy flux is converted into biomass by photosynthesis and finally stored in the Earth's crust as fossil fuels, such as coal and hydrocarbons [1981Bro]. A small fraction of the solar energy incident on the Earth's surface is used to heat up the surface, but it penetrates only to very shallow depth, some decimeters for the daily cycle and some tens of meters for the annual seasonal changes. As a result, large as it may be, solar energy has negligible influence on the Earth's thermal regime. However, the solar heating of the very surface of the Earth contributes to some extent to the heat that can be extracted from the shallow subsurface with Earth coupled heat exchangers (see section 8.3.1.1.1).

Gravitational Energy: Exchange of gravitational energy between the Earth and the Moon and Sun is the source of tidal energy both in the oceans and the body of the solid Earth. Among the Earth's celestial neighbors only the Sun and the Moon are sufficiently massive or close to cause significant tides on the Earth. This is owing to the fact that tidal accelerations and the associated torques are linearly and inversely proportional to the mass and the cube of the distance between the two bodies, respectively. Tidal deceleration of the Earth results in a decrease of rotational kinetic energy at a rate of about 3×10^{12} W – 6×10^{12} W [1980Ver]. This energy is dissipated by tidal friction and finally converted into heat. Most of this heat, at least 80 %, is dissipated in the oceans, and only a fraction of less than 20 % in the Earth's mantle. Thus, heat derived from gravitational energy is accumulated in the solid Earth at a rate of about **6×10^{11} W – 12×10^{11} W** [1980Ver; 1981Bro]. Clearly, there is considerable uncertainty attached to these numbers, and it should be realized that they are probably correct only with respect to the order of magnitude. They indicate, however, that the heat delivered to the Earth by conversion of gravitational energy into heat is 1–2 orders of magnitude less than that which is produced by the decay of radioactive isotopes in the rocks of the Earth (see below). However, the relative importance of gravitational and radioactive heating might have changed during the Earth's life time.

8.1.2.1.2 Internal Heat Sources

The interior of the Earth is gaining heat from four main sources: *radiogenic heat* from the decay of unstable, radioactive isotopes; *original heat*, i.e. the heat content of the infant Earth immediately after formation; *potential energy* released as heat during the creation of new crust, the enrichment of heavy metals in the Earth's mantle or the formation iron core of the Earth; *frictional heat* from elastic energy released in earthquakes.

Radiogenic Heat: When radioactive isotopes decay, they emit energetic particles (α - and β -particles; neutrinos and antineutrinos without mass or charge) and γ -rays. Matter is almost transparent to neutrinos and antineutrinos and most of the energy carried by them is transmitted into space. In contrast, α - and β -particles (helium nuclei and electrons) do interact with the surrounding rock which absorbs their kinetic energy thus generating heat. In order to be a significant source of heat to the Earth, a radioactive isotope must be sufficiently abundant, have a half-life comparable to the age of the Earth, and most of its decay energy must be converted into heat. Mainly uranium, thorium, and potassium isotopes fulfill these conditions: ^{238}U and ^{235}U (natural uranium: 99.28 % ^{238}U + 0.71 % ^{235}U + 0.01 % ^{234}U), ^{232}Th , and ^{40}K (natural Potassium: 0.01167 % ^{40}K). The low concentration of the ^{40}K isotope is made up for by the abundance of potassium in rocks. Therefore the heat production of ^{40}K is not negligible. The ratios of the initial concentrations of uranium, thorium and potassium in the infant bulk Earth are believed to be: $c_K/c_U = 1.1 \times 10^4$ – 1.3×10^4 ; $c_{Th}/c_U = 3.7$ – 4.0 ; $c_K/c_U = 1.1 \times 10^4$. By comparison, the potassium-uranium ratio in chondrites, believed to be remnants of the early universe, is $c_K/c_U = 7 \times 10^4$ [1995Van]. The heat production

of a bulk rock can be determined from its concentrations in uranium, thorium and potassium. The current heat generation rate of average Earth A_{av} determined from estimated concentrations of the radiogenic isotopes ^{238}U , ^{235}U , ^{232}Th and ^{40}K equals about $A_{av} = 2.75 \times 10^{13} \text{ W}$ [1995Van]. In the geological past, when less radioactive isotopes had yet decayed, heat generation was considerably larger. The total heat production E accumulated over a period of 4.6×10^9 years can be computed from the current value and the different half-lives of uranium, thorium, and potassium to $E \sim 8.9 \times 10^{30} \text{ J}$ [1995Van]. This is equivalent to several millions of years of solar irradiation received by the Earth. The Earth loses heat by conduction (see Heat Expenditure below) at a rate of $Q_{\text{global}} = 4.42 \times 10^{13} \text{ W}$ [1993Pol]. Combined with the total accumulated heat production this global heat loss yields a typical cooling time τ for the Earth of

$$\tau = E / Q_{\text{global}} = 8.9 \times 10^{30} \text{ J} / 4.42 \times 10^{13} \text{ W} = 2.0 \times 10^{17} \text{ s} \approx 6.4 \times 10^9 \text{ a} .$$

In view of the age of the Earth (4.6×10^9 a) this means that the current terrestrial heat flow could be sustained by radioactive heat alone at least for another 1.8×10^9 years. This period is more than doubled if the original heat and the latent heat which would be liberated during a further solidification of the Earth's core are also considered. The ratio of radiogenic heat generation to global heat loss is $2.75 \times 10^{13} \text{ W} / 4.42 \times 10^{13} \text{ W} = 0.62$. This means that slightly less than $\frac{2}{3}$ of the Earth's heat output can be accounted for by radioactivity.

Original Heat: It is generally accepted that the cooling of the Earth since its early history, when internal temperatures were much higher than they are now, contributes a significant amount to the present terrestrial heat flow comparable to that from radiogenic heat. Assuming an average specific heat capacity of $1088 \text{ J kg}^{-1} \text{ K}^{-1}$ and a temperature drop of 650 K over a cooling time of 4.6×10^9 years yields $2.9 \times 10^{13} \text{ W}$ as the average rate for the loss of original heat [1991Vac; 1992Vac]. As the heat loss was much larger for the hotter and not yet solidified young Earth than today, this contribution is certainly lower at present (see below). Original heat is believed to derive (1) from gravitational contraction of the interstellar material, and (2) in part from the Moon-forming collision of a proto-planet the size of Mars and the proto-Earth providing an enormous energy on the order of 10^{31} J [1990Mel; 2000Can].

Potential Energy: Potential energy is liberated by the formation of

- the iron core of the Earth at an average rate of: $\sim 3.2 \times 10^{11} \text{ W}$ [1981Bro] – $4.5 \times 10^{13} \text{ W}$ [1992Vac] over the past 4.6×10^9 years;
- new crust or the enrichment of heavy metals in the Earth's mantle at rates of $\sim 3.2 \times 10^{10} - 3.2 \times 10^{12} \text{ W}$ [1981Bro].

In summary, $3.5 \times 10^{10} \text{ W} - 4.8 \times 10^{13} \text{ W}$ is released by the conversion of potential energy into heat.

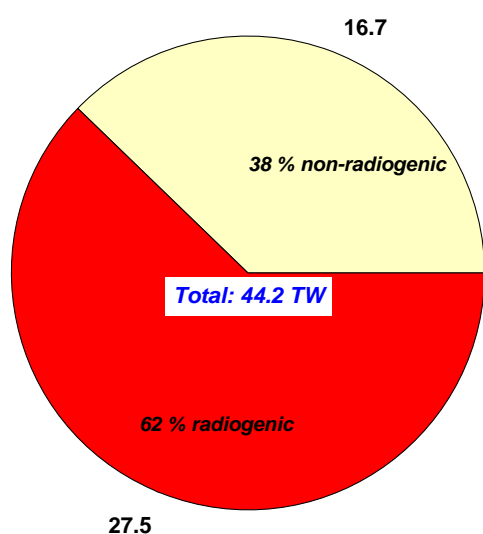


Fig. 8.4. Thermal power (TW) received by the Earth from different sources.

Frictional Heat: Heat due to release of elastic energy in earthquakes (for 10–40 earthquakes per year of surface wave magnitudes $M_s > 7$) is dissipated at a rate of $1.6 \times 10^{10} \text{ W} - 1.3 \times 10^{12} \text{ W}$ [1997Low].

Thus the maximum estimate for the non-radiogenic heat generation rate from original heat, potential energy, and frictional heat amounts to $7.8 \times 10^{13} \text{ W}$. The true value, however, is certainly much lower. The rate at which non-radiogenic heat is actually generated in the Earth today can be estimated by subtracting the current average radiogenic heat production rate of $2.75 \times 10^{13} \text{ W}$ [1995Ste] from the Earth's total heat loss of $4.42 \times 10^{13} \text{ W}$ [1993Pol] (see Heat Expenditure below). This calculation yields $1.67 \times 10^{13} \text{ W}$ for the current rate of non-radiogenic heat generation in the Earth. Thus radiogenic exceeds non-radiogenic heat generation by a factor of 5/3 (Fig. 8.4).

8.1.2.2 Heat Expenditure

The Earth is losing heat owing mainly to three processes: *Long-wavelength heat radiation, volcanism, and global heat flow*. By far the largest heat loss is due to global heat flow. As a process contributing to global heat flow, thermal and compositional convection in the Earth's fluid outer core provide the energy which drives the geomagnetic dynamo. However, this comprises no heat sink since this electromagnetic energy is finally dissipated again as heat (Fig. 8.5).

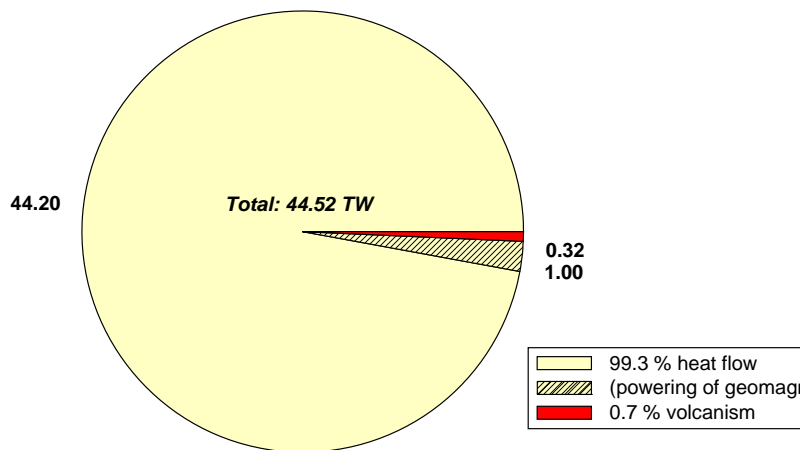


Fig. 8.5. Thermal power (TW) spent by the Earth via different processes (disregarding long-wavelength heat radiation).

Long-Wavelength Heat Radiation: Of the Sun's irradiation power of $3.53 \times 10^{16} \text{ W}$ which are absorbed in the atmosphere, 73 % are directly heating the atmosphere, while about 27 % are converted into kinetic wind energy. These transmit about 10 % of their energy to waves on the Earth's water surface [1981Bro]. Ultimately, all wind and wave energy is again converted into heat and re-emitted as long-wavelength radiation. Because rocks and soil are poor heat conductors, most of the energy flux of $7.87 \times 10^{16} \text{ W}$ incident at the Earth's surface does not penetrate to any depth greater than one meter and must be re-emitted as long-wavelength radiation, particularly at night. Since only small amounts of solar energy are converted into energy forms that can be permanently stored in the Earth, any disturbance of the delicate balance between solar income and terrestrial radiation will lead to a heating of the Earth's surface.

Global Heat Flow: The global rate of heat loss across the surface of the Earth is: $Q_{\text{global}} = Q_{\text{oceans}} + Q_{\text{continents}} = 3.1 \times 10^{13} \text{ W} + 1.32 \times 10^{13} \text{ W} = (4.42 \pm 1.0) \times 10^{13} \text{ W}$ [1993Pol]. Of the heat loss to the oceans, $34 \pm 12 \%$ or $(1.1 \pm 0.4) \times 10^{13} \text{ W}$ are associated with hydrothermal flow [1995Ste]. The average global specific heat flow $\bar{q} = 87 \text{ mW m}^{-2}$ was determined in a global compilation [1993Pol] of 24774 observations at 20201 locations (10337 continental; 9864 marine). The average on the continents $\bar{q}_{\text{continents}} = 67 \text{ mW m}^{-2}$ is

lower than in the oceans $\bar{q}_{\text{oceans}} = 101 \text{ mW m}^{-2}$. Fig. 8.5 summarizes the contributions of heat flow, energy supply to the geomagnetic dynamo, and volcanism to the energy expenditure of the Earth. The contribution by emission of long-wavelength heat radiation is disregarded since it is almost totally canceled by the corresponding contribution to the energy income.

Depending on various assumptions the powering of the geomagnetic dynamo consumes electromagnetic energy at a rate of $3.2 \times 10^9 \text{ W} - 1 \times 10^{12} \text{ W}$ [1980Ver; 1981Bro; 2003Buf]. A recent combined analysis of laboratory dynamo experiments and numerical simulations indicates a more constrained range of $2 \times 10^{11} \text{ W} - 5 \times 10^{11} \text{ W}$ [2004Chr]. This is two orders of magnitude less than the conductive heat loss. With Carnot-style efficiencies of 5% - 15% for the conversion of thermal and compositional convection into magnetic field energy [2002Buf; 2003Buf; 2003Rob], this yields a heat flow on the order of 10^{12} W required to drive the geomagnetic dynamo. Due to the very low frequencies in which the Earth's magnetic field varies virtually none of its electromagnetic energy is radiated.

8.1.2.3 Heat Budget

The budget of the heat income and heat expenditure of the Earth based on the numbers discussed above and shown in Fig. 8.4 and Fig. 8.5 is negative. It shows that the Earth is cooling at a rate of approximately **1.4 TW**. This number is based on the balance calculated between the Earth's global heat loss by heat flow and the estimated radiogenic heat generation rate. Its uncertainty is largely dominated by the uncertainty of this estimate and future estimates may modify this number to a certain extent. However, there is no doubt that the Earth has been losing heat since its formation and still continues to do so at a rate equivalent to roughly 2 ppm of the total solar irradiation intercepted by the Earth.

8.1.3 The Thermal Regime of the Earth's Crust

In the Earth's crust, the variation of temperature with depth is more irregular than in the mantle and core and shows large lateral variations. It depends strongly on the content of radioactive isotopes in the rocks (see below) and on the tectonic and hydrological regime. Typically, average values vary from $10 \text{ K km}^{-1} - 60 \text{ K km}^{-1}$ for the continental crust of 25 km – 45 km thickness. In the 5 km – 8 km thin oceanic crust these values may be much exceeded due to hydrothermal activity. The temperature regime has been compiled from observations in boreholes and mapped for several regions in the continental crust [e.g. 1980Hän; 1988Hän; 1991Gho; 1992Bla; 1992Hur; 1995Gup; 1996Ham; 1996Wan; 1998Ano; 2002Hur]. These maps and atlases provide reasonable general information on the regional variability of temperature at drilling depth in the crust. More specific local information on the temperature field requires, as a rule, additional analyses of the thermal regime. In particular, this involves some sort of analytical or numerical modeling based on measured thermal properties, such as thermal conductivity, thermal diffusivity, specific heat capacity, density, radiogenic heat generation rate, of the dominating local rocks.

Studies of the specific heat flow, the loss of heat across the surface of the Earth per unit time and area, based on observations at 20201 sites worldwide reveal remarkable variability and characteristic trends [1993Pol]. In general, there is a decrease of specific heat flow with age: Specific heat flow is lower in old stable platforms than in young, tectonically active crust, on average by a factor of $1 \frac{1}{2}$ (Fig. 8.6). As a consequence, the mean specific heat flow is larger in the generally young oceans (101 mW m^{-2}) than on the continents (67 mW m^{-2}).

Surprising as this may appear, the earth has been drilled to a maximum depth of only 12.262 km, less than 1 % of its diameter. In contrast, our universe has been explored by spacecraft beyond the limits of our solar system. Unfortunately, data from existing commercial boreholes of several kilometers depth, drilled for hydrocarbons, is rarely available for geothermal research. Therefore, the vast majority of marine and continental data is derived from measurements with heat flow probes penetrating only a few meters into

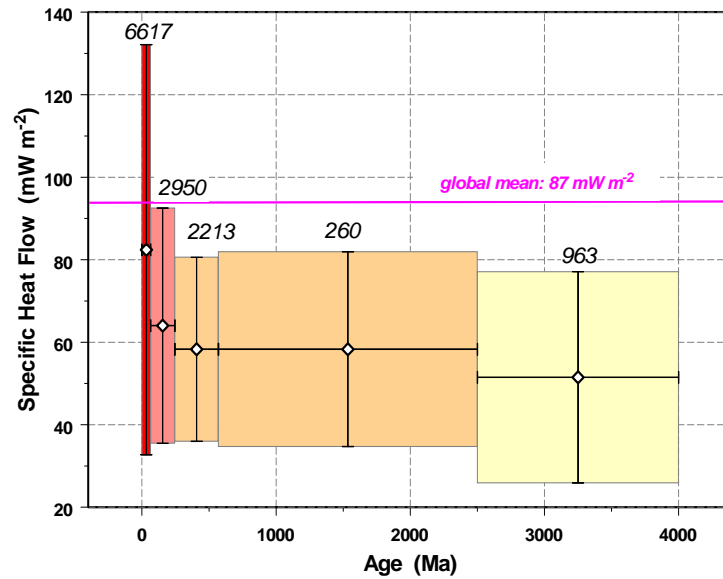


Fig. 8.6. Variation of specific heat flow with age based on 13003 observations in the continental crust. Diamonds show mean values for specific heat flow. The number of observations in each geologic era is shown above the corresponding box. Width and height of each box represents the duration of the different eras (from left to right: Cenozoic, Mesozoic, Paleozoic, Proterozoic, Archean) and one standard deviation above and below the mean specific heat flow, respectively; data: [1993Pol].

deep-sea sediments and in shallow boreholes of a few hundred meters depth, respectively. Therefore, specific heat flow derived from this data comprises signatures from a variety of factors and processes, both steady-state and transient, such as topography, contrasts in thermal properties in a heterogeneous subsurface, groundwater flow, paleoclimatic variations of the Earth's mean surface temperature, and others. This has to be considered when using heat flow data for thermal regime analyses, in particular for temperature predictions beyond the drilled depth.

Large anomalies occur both in the oceans and on the continents where heat is not only diffused to the surface but also advected by moving fluids. This occurs in particular near mid-ocean ridges, where upwelling magma maintains large lateral temperature gradients in the high-porosity sediments, but also in volcanic regions and many sedimentary basins on the continents where heat is redistributed by regional or focused groundwater flow [see e.g. 2002Cla for a summary of the literature].

Economic production of geothermal energy is facilitated, but not restricted to, regions of elevated heat flow. Various types of geothermal energy extraction schemes are available, suitable for both power production and direct thermal use (see section 8.3), which can be implemented in high and low temperature regimes, respectively.

8.1.4 Heat Storage

Heat is stored in the Earth by virtue of the heat capacity of its rocks and fluids. In comparison, the amount of heat stored in gas in the Earth is negligible. Heat capacity C is defined as the ratio of heat ΔQ required to raise the temperature of a body by ΔT . For each molecule this temperature increase requires an energy of $(f/2) k \Delta T$, where f is the number of degrees of freedom of the molecules and $k=1.3806503 \times 10^{-23} \text{ J K}^{-1}$ the Boltzmann constant. For a body of mass $M=m N_A$ (where m is the mass of the molecules and N_A is the

Avogadro's number $N_A = M/m = 6.022 \times 10^{23} \text{ mol}^{-1}$) a temperature increase by ΔT requires an energy of $\Delta Q = (M/m) (f/2) k \Delta T$. Thus the heat capacity of the body is:

$$C = \frac{\Delta Q}{\Delta T} = \frac{M}{m} k \frac{f}{2} = N_A k \frac{f}{2}. \quad (8.4)$$

Specific heat capacity c of a substance is defined as heat capacity C related to unit mass:

$$c = \frac{\Delta Q}{M \Delta T} = \frac{f}{2} \frac{k}{m} = \frac{f k}{2 \mu m_H}, \quad (8.5)$$

where μ is atomic mass relative to the mass of the hydrogen atom $m_H = 1.67 \times 10^{-27} \text{ kg}$.

For single gas molecules $f=3$, corresponding to the three degrees of freedom of translation along each direction in space. For solids, $f=6$, corresponding to the three degrees of freedom of potential and kinetic lattice vibration energy in each space direction. Isobaric specific heat capacity c_p (at constant pressure) is larger than isochoric specific heat capacity c_v (at constant volume) because additional work is required for volume expansion. Their ratio, the adiabatic exponent, is:

$$\frac{c_p}{c_v} = \frac{f+2}{f}, \quad (8.6)$$

Alternatively, isobaric specific heat capacity c_p can be expressed by means of enthalpy $H(T, P) = E + P V$, a state function of temperature and pressure, where E is internal energy, P pressure and V volume [e.g. 1989Hem]. In a closed system, the change in internal energy (dE) is the sum of the change in heat (dQ) and the work delivered (dW): $dE = dQ + dW$. If we only consider volume expansion work: $dW = -P dV$, the change in enthalpy dH becomes:

$$dH(T, P) = dE + P dV + V dP = dQ + V dP = \left(\frac{\partial H}{\partial T} \right)_P dT + \left(\frac{\partial H}{\partial P} \right)_T dP. \quad (8.7)$$

Comparing coefficients, we obtain:

$$\frac{dQ}{dT} = \left(\frac{\partial H}{\partial T} \right)_P \doteq c_p. \quad (8.8)$$

Thus, eq. (8.8) defines isobaric specific heat capacity c_p as the first derivative of enthalpy with respect to temperature. Comparing eqs. (8.5) and (8.8) we see that both expressions are equivalent for $dQ = \Delta Q/M$, and the isobaric enthalpy change is equal to the specific heat content $\Delta H = \Delta Q/M$.

Isobaric and isochoric specific heat capacity are related to compressibility $\beta = \Delta V / (V \Delta P)$ and its inverse, incompressibility or bulk modulus $K = V \Delta P / (\Delta V)$, by $c_p/c_v = \beta_T/\beta_S = K_S/K_T$ [e.g. 1992Sta]. Subscripts T and S refer to isothermal and adiabatic conditions, respectively, i.e. constant temperature and constant entropy. Inserting the thermodynamic relation $\beta_T = \beta_S + \alpha^2 T / (\rho c_p)$ [e.g. 1966Bir] between isothermal and adiabatic compressibility yields the relative difference between isobaric and isochoric specific heat capacity:

$$c_p/c_v = 1 + \alpha \gamma T, \quad (8.9)$$

where ρ is density, $\alpha = \Delta V / (V \Delta T)$ the volume expansion coefficient, and

$$\gamma = \frac{\alpha K_S}{\rho c_p} = \frac{\alpha K_T}{\rho c_v}, \quad (8.10)$$

the dimensionless Grüneisen parameter. Inserting the expressions for α and K in eq. (8.10) yields:

$$\gamma = \frac{1}{\rho c_p} \frac{\Delta V}{V \Delta T} \frac{V \Delta P}{\Delta V} = \frac{\Delta P}{\rho c_p \Delta T}, \quad (8.11)$$

Thus the Grüneisen parameter γ is the relative pressure change in a material heated at constant volume.

The absolute difference between isobaric and isochoric specific heat capacity follows from eqs. (8.9) and (8.6), assuming $f = 6$:

$$c_p - c_v = \frac{K_T \alpha^2 T}{\rho} = \frac{3 K_s \alpha^2 T}{4 \rho}. \quad (8.12)$$

For crustal rocks ($\gamma = 0.5$; $\alpha = 20 \mu\text{K}^{-1}$; $T < 10^3 \text{ K}$; $\rho = 2600 \text{ kg m}^{-3}$; $K_s < 75 \text{ GPa}$ [1981Dzi; 1992Sta]), the difference between isobaric and isochoric specific heat capacity is less than 1 % or $9 \text{ J kg}^{-1} \text{ K}^{-1}$ according to eqs. (8.9) and (8.12), respectively. Thus, the distinction between isobaric and isochoric specific heat capacity is negligible for crustal rocks at temperatures below 1000 K. Therefore, from here on, “specific heat capacity” will always refer to isobaric specific heat capacity, denoted simply by the letter c without the subscript “P”.

For temperatures above the Debye temperature this classical treatment of heat capacity is sufficient. In the Earth, the actual temperature exceeds the Debye temperature everywhere, except in the crust [1992Sta]. Therefore we observe deviations from the classical Dulong-Petit values (eqs. (8.5)–(8.12)) in experiments at room temperature and atmospheric pressure – the lower the temperature, lighter the element, and stronger the lattice bonding the larger the deviations are. An adequate treatment of specific heat capacity under these conditions requires quantum mechanics. This is, however, beyond the scope of this text and interested readers are referred to standard physics textbooks [e.g. 1991Tip; 2002Mes].

8.1.4.1 Measuring Techniques

Specific heat capacity c can be measured directly or derived as the isobaric derivative of enthalpy H with respect to temperature. Specific heat capacity of rocks varies with temperature, pressure, porosity, and saturants. Accordingly, in situ values deviate from laboratory data according to temperature, pressure, and type and content of pore fluid.

There are numerous steady-state and transient calorimetric methods available for direct measurement of specific heat capacity. The most popular are mixing or drop calorimeters and heat flux differential scanning (DSC) calorimeters. The first method yields an absolute value, the second one is a comparative method. All of these methods are discussed in detail in the literature [1984Hem; 1989Hem; 1997Höh; 1998Gal; 2001Bro; 2001Sch; 2002Hai]. They are therefore not addressed here and readers are referred to the literature for details on measurements.

The isobaric enthalpy change (or specific heat content) ΔH of solids may be determined by the method of mixtures using a Bunsen-type calorimeter in which the unknown isobaric enthalpy change of a sample relative to a base temperature, for instance 25°C , is compared to the corresponding known isobaric enthalpy change of platinum [1960Kel; 1992Som].

8.1.4.2 Calculated Heat Capacity

When no direct measurements can be performed, isobaric enthalpy change and specific heat capacity of rocks can be calculated as the arithmetic mean from the contributions of the individual mineralogical constituents and saturating fluids of the rock weighted by the volume fractions n_i of the N individual phases relative to total rock volume, where $1 = \sum n_i$:

$$\Delta H = \sum_{i=1}^N n_i \Delta H_i ; \quad c = \sum_{i=1}^N n_i c_i . \quad (8.13)$$

This is frequently referred to as Kopp’s law. As specific heat capacity is a scalar quantity, we need not be concerned with a loss of information on anisotropy in this case, unlike in the case of thermal conductivity (see section 8.1.5.1.2 below). From eq. (8.13) and based on the data in Table 8.3, the isobaric enthalpy change ΔH can be computed for rocks such as sandstones, shales, and limestones which consist of complex mineral assemblages of a combination of various oxides [1992 Som].

By suitable combinations of the data for different oxides in Table 8.3 enthalpy changes can be computed for various other mineral components; the enthalpy change for CaCO_3 , for instance, is computed as the sum of the enthalpy changes for CaO and CO_2 . For temperatures above 100°C , the loss of combined water needs to be accounted for in the calculations. It is considered to be linear between the drying temperature (105°C) and the ignition loss temperature (800°C); Somerton [1992Som] discusses further details of the calculations.

Table 8.3. Isobaric enthalpy change ΔH of common rock forming oxides relative to the corresponding enthalpies at 25°C for various temperatures; for water, subscripts “c” and “f” refer to combined and free water [1992Som; data: 1960Kel].

Oxide	Enthalpy change: $\Delta H = H(T) - H_{25^\circ\text{C}} \text{ (kJ kg}^{-1}\text{)}$									
	50°C	75°C	100°C	150°C	200°C	300°C	400°C	500°C	600°C	700°C
SiO_2	20.93	41.87	61.96	103.41	149.47	251.21	362.58	478.97	619.65	734.78
Al_2O_3	20.93	43.96	66.99	115.14	162.03	267.12	378.86	494.04	615.46	736.88
Fe_2O_3	16.71	33.41	50.33	85.91	125.60	210.43	301.53	392.72	492.79	592.43
CaO	20.93	39.90	58.87	100.73	140.01	228.98	314.01	405.70	497.39	595.36
K_2O	31.40	58.62	87.92	150.72	211.43	337.58	463.06	596.62	732.69	879.23
Na_2O	31.40	58.62	88.00	150.81	211.48	336.91	462.64	597.04	737.71	880.07
CO_2	24.87	50.37	75.24	132.81	190.37	320.54	458.04	608.34	765.35	929.05
$(\text{H}_2\text{O})_c$	50.66	102.16	154.91	264.23	379.07	628.86	907.70	1216.68	1558.75	1932.21
$(\text{H}_2\text{O})_f$	104.67	209.34	314.01	-	-	-	-	-	-	-

Based on the variation with temperature of isobaric enthalpy change ΔH measured for various oxides, Kelley [1960Kel] suggested a second order polynomial as fitting function for ΔH [1992Som]; according to eq. (8.8) this yields a corresponding polynomial for specific heat capacity c :

$$\Delta H = A_1 T + A_2 T^2 + \frac{A_3}{T} + A_4 ; \quad c = A_1 + 2 A_2 T - \frac{A_3}{T^2} \quad (T \text{ in K}). \quad (8.14)$$

The coefficients A_1 – A_4 shown in Table 8.4 are obtained from a least-squares fit of the polynomial (eq. (8.14)) for isobaric enthalpy change ΔH on the data in Table 8.3. Based on these coefficients ΔH and c can be computed from eq. (8.14) in kJ kg^{-1} and in $\text{kJ kg}^{-1} \text{K}^{-1}$, respectively. For ΔH , Fig. 8.7 compares the corresponding curves with the data in Table 8.3.

Table 8.4. Coefficients A_1 – A_4 for computing isobaric enthalpy change ΔH in kJ kg^{-1} relative to the corresponding enthalpies at 25°C and specific heat capacity c in $\text{kJ kg}^{-1} \text{K}^{-1}$ from eq. (8.14) (where temperature is in K) for common rock forming oxides and temperatures between 50°C – 700°C ; subscript “c” indicates that water and carbon dioxide are combined into the crystal lattice.

Oxide	A_1	$10^4 \times A_2$	A_3	A_4
SiO_2	1.0174	1.8785	50032	-479.87
Al_2O_3	0.95893	1.6540	22674	-375.39
Fe_2O_3	0.86410	0.97545	33080	-374.74
CaO	0.74142	1.2062	4493.2	-245.74
K_2O	0.87153	2.9471	-16396	-232.29
$(\text{CO}_2)_c$	1.0468	3.4676	33043	-451.55
$(\text{H}_2\text{O})_c$	0.59822	16.747	-39591	-195.23

Using the coefficients A_1 – A_4 in Table 8.4 the enthalpy changes ΔH_i and specific heat capacities c_i of individual mineral phases of a rock can be computed from eq. (8.14); Table 8.5 lists specific heat capaci-

ties of various minerals measured at different temperatures and coefficients A_1 – A_3 for calculating the specific heat capacities of a rock's mineral phases from eq. (8.14). According to eq. (8.13), these values combined with the specific heat capacity of the pore space and weighted by their volume fractions yield the specific heat capacity of the bulk rock. Rosen and Hashin [1970Ros] derived an exact expression for a two component medium which subtracts a temperature dependent, negative correction term from the empirical law in eq. (8.13) [1995Ber, p. 218].

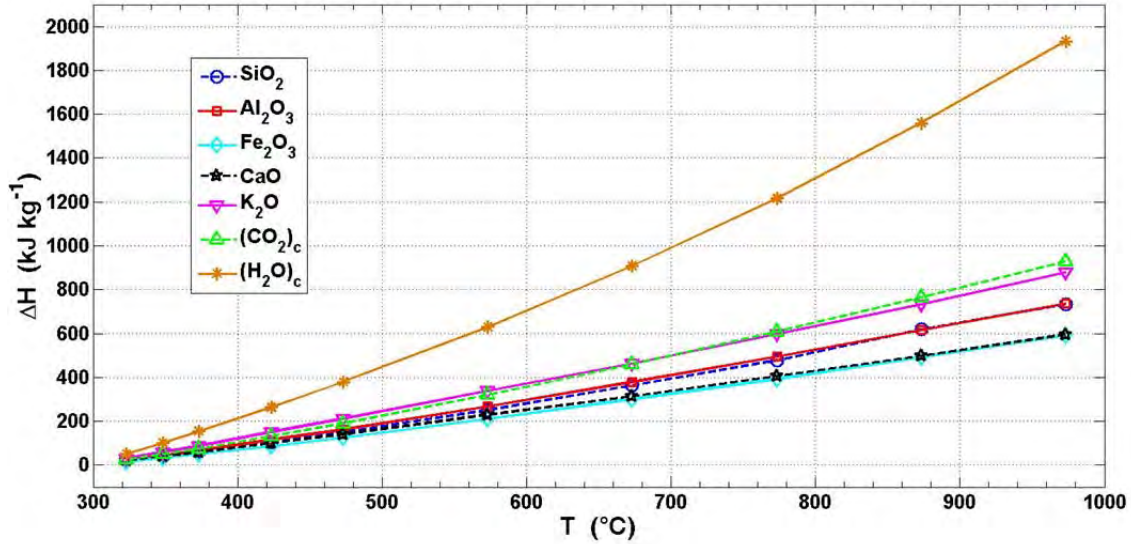


Fig. 8.7. Variation of isobaric enthalpy change ΔH with temperature T for common rock forming oxides: data (symbols; Table 8.3) and computed from eq. (8.14) (lines) with coefficients A_1 – A_4 in Table 8.4; data: [1960Kel; 1992Som]; subscript “c” indicates that water and carbon dioxide are combined into the crystal lattice.

For temperatures on the order of 300 K, however, this correction remains small: Assuming reasonable values for the quantities in eq. (58) of [1995Ber], it remains below -10 %. This is confirmed by a comparison of isobaric enthalpy changes measured over the temperature range of 127 °C – 527 °C on various clean to silty sandstones, siltstones, shale, and limestone with values calculated according to eq. (8.13) [1992Som]: Data and calculated values agree within a maximum deviation of less than 4.5 %, in most cases of better than 2 % (Fig. 8.8). Thus it appears acceptable to omit this correction for upper crustal conditions.

The heat capacity of the fraction of the rock volume occupied by pores and fractures is determined by the properties of its fluids: air, water, gas or oil. Table 8.6 and Table 8.7 list values for the specific heat capacity of air, water, and some gas and liquid hydrocarbons. However, because of the large density contrasts between different fluid and solid phases the heat capacity of saturated rocks is best calculated on a volumetric basis from thermal capacity.

Thermal capacity, also referred to as volumetric heat capacity, i.e. the product of specific heat capacity c and density ρ , is related to thermal conductivity λ and diffusivity κ :

$$\rho c = \lambda / \kappa. \quad (8.15)$$

In analogy to eq. (8.13) for specific heat capacity, Kopp's law yields rock bulk thermal capacity $(\rho c)_b$ as:

$$(\rho c)_b = (1 - \phi)(\rho c)_s + \phi \sum_i^N S_i (\rho c)_i, \quad (8.16)$$

where ϕ is porosity, $(\rho c)_s$ thermal capacity of the rock skeleton, S_i fractional saturation, and $(\rho c)_i$ thermal capacity of the i^{th} fluid phase in the pore space. Because of the low density of air and gas – about three

orders of magnitude lower than that of water and rock – the contribution of the gas phase to thermal capacity can often be ignored. In this case, $N=2$ for the fluid phases water and oil or $N=1$ for water only.

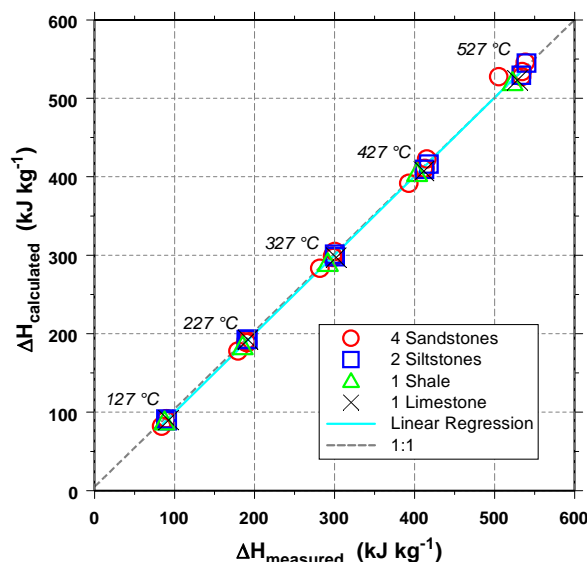


Fig. 8.8. Calculated versus measured isobaric enthalpy change ΔH relative to 25 °C at different temperatures for various sedimentary rocks. Linear regression (solid line): $y = (-0,4387 \pm 1.6236) + (1.0028 \pm 0.0048) x$, correlation coefficient: $R^2 = 0.9991$; broken line: $y = x$; data: [1992Som].

Table 8.5. Specific heat capacity c measured at different temperatures T and coefficients A_1 – A_3 for computing specific heat capacity c in $\text{kJ kg}^{-1} \text{K}^{-1}$ from eq. (8.14) (where temperature is in K) for different minerals (Ab: albite $\text{NaAlSi}_3\text{O}_8$; An: anorthite $\text{CaAl}_2\text{Si}_2\text{O}_8$). The last column shows the error Δc in % between specific heat capacity measured and calculated from eq. (8.14) and the temperature range for the coefficients (after [1942Gor]).

Compound	Mineral	c ($\text{kJ kg}^{-1} \text{K}^{-1}$) at T in °C						A_1	$2A_2 \times 10^4$	A_3	Δc (%); T-range (°C)
		-200	0	200	400	800	1200				
2Ab-3An	labradorite	0.82 at 60 °C									
3Ab-2An	andesine		0.7	0.97	1.07	1.18		0.991	2.0	25500	1; 0-900
	glass		0.7	0.99	1.09	1.21		1.016	2.06	27800	1; 0-900
4Ab-1An	oligoclase	0.85 at 60 °C									
Ag	native silver	0.146	0.233	0.24	0.26	0.28		0.217	0.58	0	1; 0-961
Ag	liquid						0.32	0.318	0	0	3; 961-1300
AgCl	cerargyrite	0.251	0.354	0.41	0.46			0.280	2.71	0	2; 0-453
Ag ₃ AsS ₃	proustite	0.34 at 50 °C									5; 453-533
Ag ₂ S	acanthite		0.32					0.317	0	0	5; 0-175
	argentite			0.37				0.368	0	0	5; 175-325
Ag ₃ SbS ₃	pyrargyrite	0.32 at 50 °C									
Al ₂ O ₃	corundum	0.069	0.72	1	1.1	1.19	1.26	1.067	1.40	28900	4; 0-1700
Al ₂ SiO ₅	andalusite	0.152	0.77	1.03	1.11	1.17	1.2	1.136	0.50	28100	3; 0-1300
	cyanite	0.077	0.7	1	1.1	1.2	1.27	1.080	1.36	31300	2; 0-1400

Pre-Print from:

Clauser, C., 2006. Geothermal Energy, In: K. Heinloth (ed), *Landolt-Börnstein, Group VIII: Advanced Materials and Technologies, Vol. 3: Energy Technologies, Subvol. C: Renewable Energies*, Springer Verlag, Heidelberg-Berlin, 493-604.

Compound	Mineral	c (kJ kg ⁻¹ K ⁻¹) at T in °C						A_1	$2A_2 \times 10^4$	A_3	Δc (%); T-range (°C)
		-200	0	200	400	800	1200				
	<i>sillimanite</i>	0.133	0.743	1	1.08	1.16	1.22	1.054	1.23	25700	3; 0-1200
Al ₆ Si ₂ O ₁₃	<i>mullite</i>		0.77	0.97	1.03	1.09	1.13	1.030	0.75	21000	3; 0-1100
Al ₈ Si ₃ O ₁₈	<i>kaolinite</i>		0.93	1.02				0.806	4.63	0	4; 0-300
Al ₂ Si ₂ O ₇ ·2H ₂ O	<i>kaolin</i>		0.99	1.17	1.35			0.641	9.04	0	3; 0-500
Al ₂ Si ₂ O ₇	<i>metakaolin</i>		0.71	1	1.1	1.2	1.27	1.062	1.51	28900	2; 0-1300
2(AlF)O·SiO ₂	<i>topaz</i>	0.83 at 50 °C									
Au	<i>native gold</i>		0.127	0.13	0.14	0.15		0.119	0.306	0	2; 0-1063
	<i>liquid</i>						0.15				5; 1063-1300
BaCO ₃	<i>α-witherite</i>	0.197	0.44	0.5	0.55	0.66		0.366	2.78	0	5; 0-810
	<i>β-witherite</i>					0.64		0.640	0	0	30; 810-950
BaSO ₄	<i>barite</i>	0.197	0.45	0.5	0.55	0.65		0.383	2.53	0	5; 0-1050
BeAl ₂ O ₄	<i>chrysoberyl</i>	0.84 at 50 °C									
Be ₃ Al ₂ Si ₆ O ₁₈	<i>beryl</i>	0.84 at 50 °C									
C	<i>diamond</i>		0.435	1.06	1.37	1.86		0.754	10.67	45440	4; 0-1040
	<i>β-graphite</i>		0.635	1.18	1.45	1.88		0.932	9.13	40700	3; 0-1040
Ca ₂ Al ₂ H ₂ (SiO ₄) ₃	<i>prehnite</i>	0.84 at 50 °C									
Ca ₂ Al ₂ SiO ₇	<i>gehlenite</i>		0.75	0.97	1.03	1.09	1.12	1.042	0.6	22840	2; 0-1300
CaAl ₂ Si ₂ O ₈	<i>anorthite</i>		0.7	0.95	1.05	1.17	1.27	0.950	2.26	23130	1; 0-1400
	<i>glass</i>		0.68	0.96	1.06			1.014	1.58	28200	1; 0-700
CaCO ₃	<i>aragonite</i>	0.26	0.78	1	1.13			0.823	4.97	12860	3; 0-750
	<i>calcite</i>	0.28	0.79	1	1.13			0.823	4.97	12860	5; 0-1200
CaF ₂	<i>fluorite</i>	0.22	0.85	0.89	0.93	1.01	1.1	0.798	2.04	0	
CaMg(CO) ₃	<i>dolomite</i>	0.93 at 60 °C									
CaMgSi ₂ O ₆	<i>diopside</i>		0.69	0.98	1.06	1.15	1.2	1.053	1.11	29000	1; 0-1300
	<i>glass</i>		0.71	0.98	1.07			0.999	1.88	25300	1; 0-700
CaSiO ₃	<i>pseudo-wollastonite</i>	0.174	0.73	0.92	0.99	1.07	1.14	0.926	1.50	17700	2; 0-1400
	<i>(β) wollastonite</i>	0.172	0.67	0.92	1	1.06	1.1	1.007	0.74	26900	2; 0-1300
	<i>glass</i>		0.69	0.92	1.03			0.834	3.48	17500	2; 0-700
CaSO ₄	<i>anhydrite</i>		0.52	0.58	0.6	0.64		0.569	6.75	4800	5; 0-1100
CaSO ₄ ·2H ₂ O	<i>gypsum</i>	0.322	1.03								
CaWO ₄	<i>scheelite</i>	0.40 at 50 °C									
CdS	<i>greenockite</i>		0.445	0.5	0.55	0.65		0.374	2.605	0	?.; 0-1000
Cu	<i>native copper</i>	0.161	0.384	0.4	0.42	0.46		0.358	0.96	0	2; 0-1084
	<i>liquid</i>							0.493	0	0	3; 1084-1300
Cu ₂ O	<i>cuprite</i>		0.47	0.51	0.54	0.61		0.419	1.81	0	5; 0-950
CuO	<i>tenorite</i>		0.52	0.63	0.68			0.572	1.88	7900	2; 0-537
2CuO·CO ₂ ·H ₂ O	<i>malachite</i>	0.74 at 57 °C									
CuFeS ₂	<i>chalcopyrite</i>	0.54 at 50 °C									
CuPbSbS ₃	<i>bourmonite</i>	0.31 at 50 °C									
Cu ₂ Se	<i>α-berzelianite</i>		0.42					0.420	0	0	5; 0-100
	<i>β-berzelianite</i>			0.41				0.410	0	0	5; 100-200
Cu ₂ S	<i>α-chalcocite</i>	0.255	0.47					0.247	8.2	0	3; 0-103

Compound	Mineral	c (kJ kg ⁻¹ K ⁻¹) at T in °C						A ₁	2A ₂ × 10 ⁴	A ₃	Δc (%); T-range (°C)
		-200	0	200	400	800	1200				
	<i>β-chalcocite</i>			0.55	0.55	0.55		0.550	0	0	10; 103-900
CuS	<i>covellite</i>	0.228	0.49	0.52	0.54	0.59		0.464	1.15	0	?; 0-1000
CuSiO ₃ ·H ₂ O	<i>diopside</i>	0.77 at 34 °C									
Fe	<i>α-iron</i>		0.44	0.52	0.6			0.330	4	0	3; 0-755
	<i>β-iron</i>					0.73		0.460	2.5	0	3; 755-903
	<i>γ-iron</i>						0.63	0.630	0	0	5; 903-1401
	<i>δ-iron</i>							0.750	0	0	5; 1401-1530
	<i>liquid</i>							0.610	0	0	5; 1530-1600
FeAsS	<i>arsenopyrite</i>	0.43 at 55 °C									
FeCO ₃	<i>siderite</i>	0.234	0.68								
Fe ₂ O ₃	<i>hematite</i>		0.61	0.79	0.9	1.08		0.640	4.2	11100	3; 0-800
Fe ₃ O ₄	<i>α-magnetite</i>		0.6	0.83	0.93			0.744	3.4	17700	3; 0-576
	<i>β-magnetite</i>					1.03		0.640	3.62	0	5; 576-800
2Fe ₂ O ₃ ·3H ₂ O	<i>limonite</i>	0.94 at 60 °C									
Fe ₂ SiO ₄	<i>fayalite</i>		0.55	0.79	0.91	1.1		0.690	3.92	18100	3; 0-900
Fe ₂ Si ₂ O ₆	<i>hypersthene</i>	0.80 at 60 °C									
FeS	<i>α-troilite</i>	0.238	0.606					1.000	18.5	0	7; 0-138
	<i>β-troilite</i>			0.64	0.66	0.71	0.574	0.574	1.3	0	3; 138-1195
FeS ₂	<i>pyrite</i>	0.075	0.5	0.59	0.69			0.373	4.66	0	7; 0-500
Fe ₇ S ₈	<i>pyrrhotite</i>		0.594	0.77				0.406	28.1	43100	3; 0-350
H ₂ O	<i>ice</i>	0.653	2.06								
Hg	<i>native mercury</i>		0.138	0.14				0.138	0	0	1; 0-347
HgS	<i>α-cinnabar</i>		0.214	0.23	0.24			0.196	0.66	0	2; 0-580
KAlSi ₂ O ₆	<i>leucite</i>	0.74 at 80 °C									
	<i>glass</i>	0.73 at 60 °C									
KAlSi ₂ O ₈	<i>adularia</i>		0.732	0.84	1						
	<i>microcline</i>		0.68	0.95	1.04	1.14		0.988	1.66	26300	1; 0-1100
	<i>orthoclase</i>		0.61	0.94	1.05	1.15		1.043	1.24	35100	1; 0-1100
	<i>glass</i>		0.7	0.97	1.07	1.19		0.976	0.216	24700	2; 0-1100
KCl	<i>sylvite</i>	0.418	0.682	0.72	0.75			0.682	1.68	0	2; 0-770
KNO ₃	<i>α-niter</i>	0.326						0.266	2.19	0	10; 0-128
	<i>β-niter</i>		1.19					1.190	0	0	5; 128-338
	<i>liquid</i>			1.22				1.220	0	0	10; 338-410
LiAlSi ₂ O ₅	<i>petalite</i>	0.85 at 58 °C									
LiAlSi ₂ O ₆	<i>spodumene</i>	0.90 at 60 °C									
	<i>glass</i>	0.91 at 60 °C									
Mg ₃ Al ₂ Si ₃ O ₁₂	<i>garnet</i>	0.74 at 58 °C									
Mg ₇ B ₁₆ Cl ₂ O ₂₅	<i>α-boracite</i>		0.796	1.18				0.275	19.09	0	5; 0-265
	<i>β-boracite</i>				1.41			0.502	13.46	0	5; 265-100
MgCl ₂	<i>chloromagnesite</i>		0.805	0.84	0.87			0.760	1.66	0	?; 0-718
MgCO ₃	<i>magnesite</i>	0.161	0.864								
MgF ₂	<i>sellaite</i>		0.906	1.08	1.21	1.43		0.857	5.42	7360	3; 0-1000

Pre-Print from:

Clauser, C., 2006. Geothermal Energy, In: K. Heinloth (ed), *Landolt-Börnstein, Group VIII: Advanced Materials and Technologies, Vol. 3: Energy Technologies, Subvol. C: Renewable Energies*, Springer Verlag, Heidelberg-Berlin, 493-604.

Compound	Mineral	c (kJ kg ⁻¹ K ⁻¹) at T in °C						A_1	$2A_2 \times 10^4$	A_3	Δc (%); T-range (°C)
		-200	0	200	400	800	1200				
Mg(OH) ₂	<i>brucite</i>	1.30 at 35 °C									
MgO	<i>periclase</i>	0.066	0.87	1.09	1.16	1.24	1.3	1.127	1.24	21700	2; 0-1800
MgSiO ₃	<i>pyroxene</i>	0.752	1.03	1.15				0.973	3.36	23300	1; 0-500
	<i>amphibole</i>	0.74	1.03	1.13	1.24			1.067	1.83	28100	1; 0-1100
	<i>glass</i>	0.756	1.02	1.14				0.971	3.22	22600	1; 0-700
MgSO ₄ ·H ₂ O	<i>kieserite</i>	1.00 at 9 °C									
MgSO ₄ ·7H ₂ O	<i>epsomite</i>	1.51 at 32 °C									
Mg ₂ Fe ₂ SiO ₄	<i>olivine</i>	0.79 at 36 °C									
Mg ₃ H ₂ Si ₄ O ₁₂	<i>talc</i>	0.87 at 59 °C									
MnCO ₃	<i>rhodochrosite</i>	0.203	0.7	1.08	1.46			0.283	15.32	$0.33 \times 10^{-4} T^4$	4; 0-500
MnO ₂	<i>pyrolusite</i>	0.975	1	1.01				0.924	2.27	$0.14 \times 10^{-11} T^4$?; 0-500
Mn ₂ O ₃ · H ₂ O	<i>manganite</i>	0.74 at 36 °C									
MnS	<i>alabandite</i>	0.322	0.569								
MoS ₂	<i>molybdenite</i>	0.537	0.55	0.57				0.515	0.82	0	5; 0-456
NaAlSi ₃ O ₈	<i>albite</i>	0.709	0.99	1.09	1.2			1.018	1.87	26800	1; 0-1100
	<i>glass</i>	0.724	1	1.11	1.26			0.978	2.82	24700	1; 0-900
NaCl	<i>halite</i>	0.466	0.855	0.92	0.98	1.1		0.773	3	0	2; 0-800
	<i>liquid</i>					1.14		1.140	0	0	3; 800-950
NaF	<i>villiaumite</i>	1.034	1.1	1.29				0.473	11.51	-18400	2; 0-700
Na ₂ B ₄ O ₇ ·10H ₂ O	<i>borax</i>	0.161 at 35 °C									
Na ₃ AlF ₆	<i>cryolite</i>	0.909	1.18	1.39	1.78			0.770	9.49	8950	2; 0-1000
NiS	<i>millerite</i>	0.506	0.57					0.426	2.95	0	3; 0-324
PbCO ₄	<i>cerussite</i>	0.177	0.318								
PbS	<i>galena</i>	0.142	0.207	0.22	0.24			0.188	0.7	0	5; 0-600
PbSO ₄	<i>anglesite</i>	0.364 at 60 °C									
Pd	<i>palladium</i>	0.232	0.25	0.26	0.29	0.318		0.212	0.72	0	2; 0-1549
Pt	<i>platinum</i>	0.134	0.14	0.14	0.15	0.164		0.127	0.249	0	1; 0-1600
S ₈	<i>sulfur rhombic</i>							0.482	8.35	0	3; 0-95.6
	"										
	<i>monoclinic</i>							0.572	5.76	0	3; 95.6-119
	" <i>liquid</i>							0.656	6.58	0	?; 119-160
Sb ₂ S ₃	<i>stibnite</i>	0.342	0.38	0.41				0.298	1.63	0	?; 0-548
	<i>α-quartz</i>	0.173	0.698	0.97	1.13			0.757	6.07	16800	1; 0-575
	<i>β-quartz</i>					1.17	1.327	0.763	3.83	0	4; 575-1600
	<i>α-cristobalite</i>	0.186	0.69	1.01				0.254	16	0	4; 0-250
SiO ₂	<i>β-cristobalite</i>				1.07	1.17	1.21	1.191	0.32	6250	2; 250-1700
	<i>glass</i>	0.184	0.7	0.95	1.06	1.21	1.34	0.892	3.11	2100	5; 0-1700
SnO ₃	<i>cassiterite</i>	0.34	0.43	0.48	0.55			0.387	1.57	7000	4; 0-1100
SrCO ₃	<i>strontianite</i>	0.211	0.536								
TiO ₂	<i>rutile, brookite</i>	0.7	0.8	0.88				0.619	3.95	2200	3; 0-450
WO ₃	<i>tungstite</i>	0.33	0.36	0.38	0.44	0.49		0.289	1.4	0	5; 0-1300

Compound	Mineral	$c \text{ (kJ kg}^{-1} \text{ K}^{-1}) \text{ at } T \text{ in } ^\circ\text{C}$						A_1	$2A_2 \times 10^4$	A_3	$\Delta c \text{ (%);}$ $T\text{-range } (^\circ\text{C})$
		-200	0	200	400	800	1200				
ZnCO ₃	smithsonite	0.238	0.632								
ZnO	zincite		0.48	0.58	0.62	0.66	0.69	0.586	0.75	9400	2; 0-1300
ZnS	α -wurtzite, β -sphalerite	0.43	0.45	0.53	0.56	0.59		0.550	0.41	8400	6; 0-900
ZrSiO ₄	zircon	0.61	at 60 °C								

Table 8.6. (a) Variation of specific heat capacity c of oil with oil gravity (in units of specific gravity G_o and $^\circ\text{API}$) and temperature T according to eq. (8.20); (b) Variation of thermal conductivity λ of atmospheric air and light oil with temperature T ; data: [1992Som].

Oil gravity		$c \text{ (kJ kg}^{-1} \text{ K}^{-1}) \text{ at } T \text{ in } ^\circ\text{C}$				(a) (b)	$\lambda \text{ (W m}^{-1} \text{ K}^{-1})$	
$G_o \text{ (-)}$	$^\circ\text{API}$	20	50	100	150		T (°C)	air oil
0.966	15	1.73	1.83	1.98	2.18		20	0.026 0.139
0.934	20	1.75	1.86	2.04	2.21		50	0.027 0.131
0.904	25	1.78	1.89	2.07	2.25		100	0.030 0.128
0.876	30	1.81	1.92	2.10	2.28		150	0.033 0.126
							200	0.037 0.124

Calculating the thermal capacity (ρc) of the solid and fluid phases requires expressions for density. Based on previous work by different researchers Somerton [1992Som] suggests the following relation between density $\rho_x(T)$ in kg m^{-3} , density $\rho_{x,20}$ at 20 °C, temperature T in °C, and volume expansion coefficient α_x in K^{-1} , where the subscript x stands for fluid water, oil or solid rock, respectively:

$$\rho_x(T) = \frac{\rho_{x,20}}{1 + (T - 20)\alpha_x}, \quad x = f, o, s. \quad (8.17)$$

The volumetric thermal expansion coefficient of rocks and minerals ranges roughly from $10 \mu\text{K}^{-1}$ – $70 \mu\text{K}^{-1}$ [1966Ski; 1992Som; 1995Fei], and the following expressions may be used to obtain values for the thermal expansion coefficients of fluid water and oil, respectively:

$$\left. \begin{array}{l} \alpha_f \\ \alpha_o \\ \alpha_s \end{array} \right\} = \left\{ \begin{array}{l} 2.115 \times 10^{-4} + 1.32 \times 10^{-6} T + 1.09 \times 10^{-8} T^2 \\ 4.42 \times 10^{-4} + 1.03 \times 10^{-5} \times ^\circ\text{API} \\ (2...5) \times 10^{-5} \end{array} \right. . \quad (8.18)$$

Here, $^\circ\text{API}$ characterizes oils of different density, which is expressed relative to water density by means of specific gravity G_o at 20 °C [1992Som]:

$$^\circ\text{API} = (141.5/G_o) - 131.5. \quad (8.19)$$

Heat capacity of oil varies with temperature and oil specific gravity G_o [1992Som] (cf. Table 8.6):

$$c_o = (0.389 + 0.00081 T) / \sqrt{G_o}. \quad (8.20)$$

Table 8.6 lists values for specific heat capacity c and thermal conductivity λ of oil and atmospheric air. The thermal capacity of fluid water can be calculated most easily and accurately using either public domain FORTRAN software or an Excel™ spreadsheet add-in based on the most recent industry standard for the thermodynamic and transport properties of water and steam [1998Wag]. Table 8.8 displays a list

™ registered trademark of Microsoft

of selected values at atmospheric pressure and Fig. 8.9 shows the variation of fluid water thermal capacity with pressure and temperature.

Table 8.7 Specific heat capacity c , thermal conductivity λ , and thermal diffusivity κ of different potential pore space fluids at various temperatures T .

Substance	T ($^{\circ}\text{C}$)	c ($\text{kJ kg}^{-1} \text{K}^{-1}$)	λ ($\text{W m}^{-1} \text{K}^{-1}$)	κ ($10^{-6} \text{m}^2 \text{s}^{-1}$)	ρc ($\text{kJ m}^{-3} \text{K}^{-1}$)
air (dry) [1992Som;1996Sch]	0	1.005	0.024	18.7	1.283
	20	1.005	0.026	21.2	1.226
	40	1.009	0.027	24.9	1.084
	100	1.013	0.030	33.8	0.979
methane gas (CH_4) at 0.1 MPa [2000Lid]	1.85	2.182	0.031	20.1	1.540
	26.85	2.238	0.034	23.7	1.436
	76.85	2.369	0.041	31.7	1.292
	126.85	2.537	0.049	40.1	1.221
	176.85	2.712	0.057	48.5	1.175
	226.85	2.892	0.067	60.2	1.113
	326.85	3.198	0.084	81.9	1.026
fluid water (at 0.1 MPa) [1998Wag]	0	4,219	0,561	0,133	4218,8
	10	4,195	0,580	0,138	4194,2
	30	4,180	0,616	0,148	4161,8
	50	4,180	0,644	0,156	4129,6
	70	4,188	0,663	0,162	4095,0
	90	4,205	0,675	0,166	4059,2
water steam (at 0.1 MPa) [1998Wag]	100	2,074	0,025	20,5	1,223
	120	2,019	0,026	23,5	1,126
	140	1,993	0,028	26,6	1,055
	160	1,980	0,030	29,8	0,998
	180	1,976	0,031	33,1	0,950
	200	1,976	0,033	36,6	0,909
	250	1,989	0,038	46,2	0,827
	300	2,012	0,043	57,0	0,762
	350	2,040	0,049	68,9	0,710
water ice (hexagonal I_h) [1982Mil; 2000Lid]	0	2.11	2.14	1.18	1934.2
	-10	2.03	2.32	1.24	1865.0
	-20	1.96	2.4	1.33	1803.8
	-30	1.88	2.5	1.43	1732.6
	-40	1.80	2.6	1.54	1661.0
crude oil [1996Sch]	20	1.88–2.76	0.13–0.14	0.05–0.11	1300–2350

Table 8.8 Variation of fluid water thermal capacity ρc_p with pressure P and temperature T; data: [1998Wag].

T (K)	P (MPa)	ρc_p (kJ m ⁻³ K ⁻¹)	T (K)	P (MPa)	ρc_p (kJ m ⁻³ K ⁻¹)	T (K)	P (MPa)	ρc_p (kJ m ⁻³ K ⁻¹)
273	0.1	4218.777	273	30	4149.336	273	70	4097.503
283	0.1	4194.196	283	30	4151.243	283	70	4120.714
303	0.1	4161.846	303	30	4142.055	303	70	4129.628
323	0.1	4129.598	323	30	4118.927	323	70	4113.534
343	0.1	4095.033	343	30	4088.580	343	70	4086.521
363	0.1	4059.186	363	30	4054.410	363	70	4053.775
373	0.1	1.222	373	30	4036.378	373	70	4035.909
393	0.1	1.125	393	30	3999.021	393	70	3997.876
413	0.1	1.055	413	30	3960.717	413	70	3957.526
433	0.1	0.998	433	30	3922.571	433	70	3915.792
453	0.1	0.950	453	30	3885.909	453	70	3873.683
473	0.1	0.909	473	30	3852.277	473	70	3832.217
523	0.1	0.826	523	30	3794.174	523	70	3737.215
573	0.1	0.762	573	30	3814.319	573	70	3660.831
623	0.1	0.710	623	30	4117.114	623	70	3590.696
273	1	4216.230	273	40	4132.426	273	80	4090.498
283	1	4192.600	283	40	4141.040	283	80	4116.918
303	1	4161.093	303	40	4137.604	303	80	4128.528
323	1	4129.178	323	40	4116.722	323	80	4113.480
343	1	4094.765	343	40	4087.432	343	80	4086.966
363	1	4058.975	363	40	4053.708	363	80	4054.432
373	1	4040.831	373	40	4035.725	373	80	4036.587
393	1	4004.547	393	40	3998.144	393	80	3998.441
413	1	3969.170	413	40	3959.176	413	80	3957.767
433	1	3936.203	433	40	3919.856	433	80	3915.485
453	1	13.948	453	40	3881.387	453	80	3872.571
473	1	11.790	473	40	3845.103	473	80	3829.994
523	1	9.502	523	40	3773.778	523	80	3730.281
573	1	8.298	573	40	3754.486	573	80	3644.226
623	1	7.515	623	40	3858.081	623	80	3554.707
273	10	4192.400	273	50	4118.286	273	90	4085.546
283	10	4177.733	283	50	4132.647	283	90	4114.422
303	10	4154.127	303	50	4134.099	303	90	4128.108
323	10	4125.334	323	50	4115.117	323	90	4113.873
343	10	4092.353	343	50	4086.727	343	90	4087.748
363	10	4057.114	363	50	4053.388	363	90	4055.371
373	10	4038.994	373	50	4035.451	373	90	4037.537
393	10	4002.287	393	50	3997.692	393	90	3999.285
413	10	3965.802	413	50	3958.176	413	90	3958.334
433	10	3930.870	433	50	3917.894	433	90	3915.592
453	10	3899.260	453	50	3877.959	453	90	3872.015
473	10	3873.290	473	50	3839.561	473	90	3828.535
523	10	3857.910	523	50	3758.236	523	90	3725.089
573	10	4064.012	573	50	3712.957	573	90	3631.687

Pre-Print from:

Clauser, C., 2006. Geothermal Energy, In: K. Heinloth (ed), *Landolt-Börnstein, Group VIII: Advanced Materials and Technologies, Vol. 3: Energy Technologies, Subvol. C: Renewable Energies*, Springer Verlag, Heidelberg-Berlin, 493-604.

T (K)	P (MPa)	ρc_p (kJ m ⁻³ K ⁻¹)	T (K)	P (MPa)	ρc_p (kJ m ⁻³ K ⁻¹)	T (K)	P (MPa)	ρc_p (kJ m ⁻³ K ⁻¹)
623	10	178.759	623	50	3722.856	623	90	3529.047
273	20	4169.245	273	60	4106.709	273	100	4082,519
283	20	4163.417	283	60	4125.916	283	100	4113,132
303	20	4147.533	303	60	4131.463	303	100	4128,318
323	20	4121.780	323	60	4114.067	323	100	4114,686
343	20	4090.207	343	60	4086.433	343	100	4088,848
363	20	4055.531	363	60	4053.420	363	100	4056,580
373	20	4037.452	373	60	4035.522	373	100	4038,745
393	20	4000.378	393	60	3997.616	393	100	4000,389
413	20	3962.889	413	60	3957.646	413	100	3959,196
433	20	3926.182	433	60	3916.570	433	100	3916,069
453	20	3891.763	453	60	3875.440	453	100	3871,945
473	20	3861.490	473	60	3835.345	473	100	3827,731
523	20	3821.248	523	60	3746.332	523	100	3721,322
573	20	3906.276	573	60	3682.980	573	100	3622,249
623	20	4868.968	623	60	3642.885	623	100	3510,407

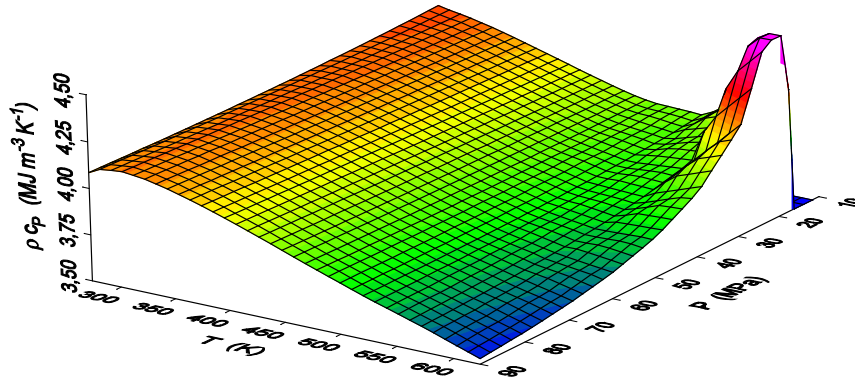


Fig. 8.9 Variation of fluid water thermal capacity ρc_p with pressure P and temperature T data: [1998Wag], see also Table 8.8.

Freezing and thawing of water in soils or rocks liberates or consumes heat, respectively. The latent heat L which corresponds to these additional heat sources and sinks can be elegantly combined with the specific heat capacities of water and ice, c_f and c_{ice} respectively, into an effective specific heat capacity c_{eff} of the pore space. This effective specific water heat capacity then accounts for the entire enthalpy change, including latent heat. In this approach, the latent heat effects are assumed to occur between the solidus and liquidus temperatures T_1 and T_2 , respectively. Weighting by the volume fractions of unfrozen fluid water ϕ_f and ice ϕ_{ice} , the enthalpy change of the water volume becomes $dH = (\phi_f c_f + \phi_{ice} c_{ice}) dT + L d\phi_f$, and the effective water heat capacity c_{eff} is:

$$c_{eff} = \frac{dH}{dT} = \phi_f c_f + \phi_{ice} c_{ice} + L \frac{d\phi_f}{dT}. \quad (8.21)$$

8.1.5 Heat Transport

Heat transport in the Earth is governed mainly by three mechanisms: radiation, advection, and transient diffusion or steady-state conduction. Generally, heat conduction or diffusion dominate within the lithosphere of the Earth. However, there are two exceptions:

- If rock hydraulic permeability is sufficiently large, convection driven heat advection can be equally or even more efficient, provided the associated driving forces are available for the corresponding forced or free convection systems. This is often the case in sedimentary basins [see e.g. 2002Cla for a summary of the literature]. However, fluid driven heat advection can be important also in crystalline rocks and on a crustal scale [e.g. 1983Eth; 1990Tor; 1992Cla; 1999Man; 2000Rat; 2001Cla];
- At ambient temperatures above 600 °C radiation of heat begins to contribute sizably to the overall heat transfer in most polycrystalline materials, but is really efficient only above 1200 °C. However, with single crystals and glasses (e.g. obsidian) radiation becomes important from temperatures as low as 200 °C – 400 °C. For the usual range of crustal temperatures and temperature gradients a linearization of the radiation law yields a "radiative thermal conductivity" which can be formally added to the coefficient of lattice or phonon thermal conductivity in Fourier's law of heat conduction (see below). Thermal conductivities determined at very high temperatures in the laboratory always include this radiative component. Radiative thermal conductivity will therefore not be treated separately here. Interested readers are referred to a review of heat radiation in the Earth [1988Cla].

8.1.5.1 Heat Conduction

Fourier's law of heat conduction defines specific heat flow q_i , i.e. heat flow normalized by area, as the product of the thermal conductivity tensor λ_{ij} and the temperature gradient vector $\partial T/\partial x_j$:

$$q_i = -\lambda_{ij} \frac{\partial T}{\partial x_j}. \quad (8.22)$$

Temperature measurements are usually performed along vertical profiles in boreholes. Therefore only the vertical component of the temperature gradient is generally known from measurements.

Thermal conductivity in some rocks is, to a good approximation, isotropic, particularly for volcanic and plutonic rocks. In these cases heat flow will be predominantly vertical, and it is sufficient to consider only the vertical component of (8.22). Thermal conductivity of many sedimentary and metamorphic rocks, in contrast, is strongly anisotropic, and lateral heat flow will be significant. Hence information on anisotropy is often required, demanding laboratory measurements in different directions. Anisotropy exists on several scales:

- On the microscopic scale many minerals are anisotropic (Table 8.9);
- On the laboratory scale the thermal conductivity of many rocks is also anisotropic. However, even if rocks are composed of anisotropic minerals, random orientation of the crystals within the rock may make the rock's thermal conductivity appear as isotropic on a macroscopic scale;
- On a still larger scale, if rocks are exposed to folding, orogenic or other tectonic processes, the thermal conductivity of the resulting rock formation may be either isotropic or anisotropic.

8.1.5.1.1 Measuring Techniques

Thermal conductivity can be measured in the laboratory on rock samples, i.e. cores or cuttings or in situ either in boreholes or with shallow penetration (3 m – 20 m) marine heat flow probes. There are numerous steady-state and transient techniques available for measuring thermal conductivity, the most prominent being the "divided bar", "needle probe", and "optical scanning". These methods are discussed

in detail in several textbook and review articles [1965Bec; 1969Tye; 1974Des; 1974Kap; 1981Roy; 1988Bec; 1988Dav; 1992Som; 1999Pop^a; 2001Bea]. Here they are therefore neither addressed again nor are the many details involved in performing the actual measurements discussed.

As is the case with most other petrophysical properties, in situ thermal conductivity may deviate significantly from laboratory values, even if the effects of temperature, pressure, and pore fluid are accounted for. The reason for this is a scale dependence in which different aspects are involved: in situ measurements, as a rule, represent an average over a much larger rock volume than laboratory measurements performed on small samples, and small-scale variations may be lost. Thus, the correct scale on which thermal conductivity should be determined depends on the specific question. This is analogous to the similar problem in hydrology of identifying a "representative elementary volume" for which reasonable averages for transport parameters (such as permeability and dispersion lengths) can be defined.

8.1.5.1.2 Indirect Methods

When no data are available or no direct measurements can be performed, thermal conductivity can be inferred indirectly, either from data on mineralogical composition and saturating fluids or from correlations with other physical properties. While some of these methods are based on well defined physical models, others are purely empirical.

Estimation From Mineralogical Composition and Saturating Fluids: Thermal conductivity of rocks may be estimated from their mineral content, as minerals, due to their well defined composition, exhibit a much smaller variance in thermal conductivity than rocks. Similarly, as the bulk thermal conductivity of porous rocks varies with different saturants, it may be of interest to know rock thermal conductivity for other saturants than those used in the laboratory measurement. Numerous models have been proposed for this, but all have their disadvantages: some overestimate while others underestimate systematically the true bulk thermal conductivity. Most of them are valid only for a specific range of volume ratios (or porosities), and yield unreasonable results outside this range.

The parallel and series model for thermal resistance of layered media are easy to understand, but have the disadvantage of being rather special cases, applicable mostly to bedded sediments. They correspond to the well known arithmetic and means harmonic λ_{ari} , and λ_{har} respectively, and define upper and lower limits for all other models. Thus they constrain the maximum variance of possible predictions. Quite successful in describing the data in many cases, but unfortunately without a clearly defined physical model, the geometric mean λ_{geo} falls in between these two extremes. So does the Hashin-Shtrikman mean λ_{HS} [1962Has], whose upper and lower bounds, $\lambda_{\text{HS}}^{\text{U}}$ and $\lambda_{\text{HS}}^{\text{L}}$, respectively, provide tighter constraints for the predictions of different models other than the arithmetic and harmonic means. Finally, effective medium theory [1935Bru; see also 1986Pal] provides a useful effective medium mean λ_{eff} for macroscopically homogeneous and isotropic rocks consisting of randomly distributed grains and pores. If λ_i is the thermal conductivity and n_i the volume fraction of the i -th phase relative to the total volume, where $1 = \sum n_i$, these five means are defined by:

$$\begin{aligned} \text{(a)} \quad \lambda_{\text{max}} = \lambda_{\text{ari}} = \lambda_{\parallel} &= \sum_{i=1}^N n_i \lambda_i ; & \text{(b)} \quad \lambda_{\text{min}} = \lambda_{\text{har}} = \lambda_{\perp} &= \left(\sum_{i=1}^N \frac{n_i}{\lambda_i} \right)^{-1} ; & \text{(c)} \quad \lambda_{\text{mean}} &= \frac{1}{2} (\lambda_{\parallel} + \lambda_{\perp}) ; \\ \text{(d)} \quad \lambda_{\text{geo}} &= \prod_{i=1}^N \lambda_i^{n_i} ; & \text{(e)} \quad \frac{1}{\lambda_{\text{eff}}} &= \sum_{i=1}^N \frac{3 n_i}{2 \lambda_i + \lambda_i} ; & \text{(f)} \quad \lambda_{\text{HS}} &= \frac{1}{2} (\lambda_{\text{HS}}^{\text{U}} + \lambda_{\text{HS}}^{\text{L}}) ; \end{aligned} \quad (8.23)$$

where:

$$\begin{aligned} \lambda_{\text{HS}}^{\text{U}} &= \lambda_{\text{max}} + \frac{A_{\text{max}}}{1 - \alpha_{\text{max}} A_{\text{max}}} ; \quad A_{\text{max}} = \sum_{i=1; \lambda_i \neq \lambda_{\text{max}}}^N \frac{n_i}{\alpha_{\text{max}} + 1/(\lambda_i - \lambda_{\text{max}})} ; \quad \lambda_{\text{max}} = \max(\lambda_1, \dots, \lambda_N) ; \quad \alpha_{\text{max}} = \frac{1}{3\lambda_{\text{max}}} \\ \lambda_{\text{HS}}^{\text{L}} &= \lambda_{\text{min}} + \frac{A_{\text{min}}}{1 - \alpha_{\text{min}} A_{\text{min}}} ; \quad A_{\text{min}} = \sum_{i=1; \lambda_i \neq \lambda_{\text{min}}}^N \frac{n_i}{\alpha_{\text{min}} + 1/(\lambda_i - \lambda_{\text{min}})} ; \quad \lambda_{\text{min}} = \min(\lambda_1, \dots, \lambda_N) ; \quad \alpha_{\text{min}} = \frac{1}{3\lambda_{\text{min}}} . \end{aligned} \quad (8.24)$$

For a two-component system consisting of pore fluid and solid rock with thermal conductivities λ_f and λ_s , respectively, eq. 8.24 simplifies to [1962Has, 1971Hor]:

$$\lambda_{HS}^U = \lambda_s + \frac{\phi}{\frac{1}{\lambda_f - \lambda_s} + \frac{1-\phi}{3\lambda_s}}; \quad \lambda_{HS}^L = \lambda_f + \frac{1-\phi}{\frac{1}{\lambda_s - \lambda_f} + \frac{\phi}{3\lambda_f}}. \quad (8.25)$$

Generally, For a two-component system consisting of pore fluid and solid rock with thermal conductivities λ_f and λ_s , respectively, the implicit definition of λ_{eff} in (8.23e) can be resolved:

$$\lambda_{eff} = \frac{1}{4} \left\{ 3\phi(\lambda_f - \lambda_s) + 2\lambda_s - \lambda_f + \sqrt{9\phi^2\lambda_s^2 + 18\phi\lambda_s\lambda_f - 18\phi^2\lambda_s\lambda_f - 12\phi\lambda_s^2 + \lambda_f^2 - 6\phi\lambda_f^2 + 4\lambda_s\lambda_f + 9\phi^2\lambda_f^2 + 4\lambda_s^2} \right\}. \quad (8.26)$$

The different results obtained by the various methods in eq.(8.23) are illustrated in Fig. 8.10 for a two-phase rock with porosity ϕ consisting of solid rock and pore space. We see that in general:

$$\lambda_{\perp} = \lambda_{har} < \lambda_{HS}^L < \lambda_{mean} < \lambda_{geo} < \lambda_{HS} < \lambda_{eff} < \lambda_{HS}^U < \lambda_{ari} = \lambda_{\parallel}. \quad (8.27)$$

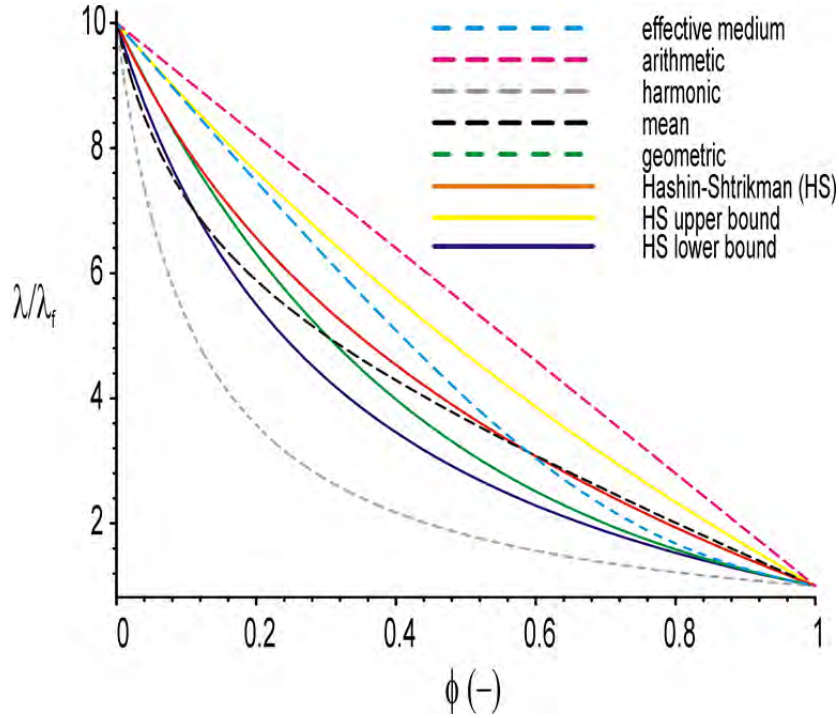


Fig. 8.10. Variation of thermal conductivity λ of a two-phase rock with porosity ϕ according to the five laws in (8.24) for solid and fluid thermal conductivities of $\lambda_s=6 \text{ W m}^{-1} \text{ K}^{-1}$ and $\lambda_f=0.6 \text{ W m}^{-1} \text{ K}^{-1}$, respectively (effective medium= λ_{eff} ; parallel= λ_{ari} ; series= λ_{har} ; mean= λ_{mean} ; geometric= λ_{geo} ; Hashin-Shtrikman= λ_{HS}).

While only these six models are presented and discussed here, various other mixing models are available which take into account additional factors, such as the shape of grains and voids [e.g. 1984Zim; 1989Zim]. Their specific advantages are discussed in considerable detail in the literature [e.g. 1988Bec; 1995Ber; 1996Sch]. Somerton [1992Som] discusses unconsolidated sands, effects of multi-fluid saturation, and provides many examples from hydrocarbon reservoir studies. Horai [1991Hor] tests the results of predictions from several different mixing-models on a remarkable data set in which porosity

virtually varies from 0 % – 100 %. As can be expected, most of the models tested were valid only for certain porosity ranges. Only two more recent two-phase models, assuming that pores can be treated as spheroidal inclusions in a homogeneous and isotropic material, are capable of explaining the complete data set. However, additional information on the spheroids' aspect ratio or orientation is required by these two models.

Given the typical ratios of conductivities we observe in nature, i.e. less than 10, most of the conductivity models work to within 10 % – 15 % accuracy. For larger ratios some break down more than others, and the geometric mean is one of them. The reason why it is still quite popular with many, even in extreme cases, is that it has often been found that errors introduced in the inverse problem (i.e. in predicting the matrix conductivity from measurements on samples saturated with one fluid) are automatically compensated for when using this incorrect matrix value in the subsequent forward calculation (i.e. in predicting the bulk conductivity of the matrix saturated with another fluid).

Correlations With Other Physical Properties: There are three different ways in which other physical properties, in particular those measured in well-logs, can be used to infer estimates for in situ thermal conductivity:

(1) One approach is to establish empirical relationships between thermal conductivity and other properties, such as porosity, bulk density, sonic (compressional elastic wave) velocity or travel times. This approach can be applied to data from both well logs and the laboratory. A useful summary of these different approaches is presented by Blackwell [1989Bla], who also illustrates their application to a specific case;

(2) In a second approach, Williams and Anderson [1990Wil] derive a phonon conduction model for thermal conductivity, which utilizes temperature, acoustic velocity, and bulk density measurements from well-logs. The method is claimed to be accurate to within 15 %, both in isotropic and anisotropic formations. Its application, however, is limited to unfractured rocks, since the effects of fracturing on compressional and shear velocities lead to inaccurate results. There are indications, however, that shear wave birefringence may pose a limit to the application of this method in foliated rocks as well [1993Prib].

(3) The third approach is basically an extension of the mixing-model approach to the borehole scale: The volume fractions V_i of the N different mineral (or fluid) phases are either taken directly from induced gamma ray spectroscopy logs [1990Wil] or determined from a joint analysis of a suitable number J of geophysical logs such as gamma ray (GR), sonic slowness (DT, the inverse of velocity), gamma density (DEN), and neutron porosity (NPHI) [1990Bri; 1991Dem; 2005Har]. If \mathbf{x} and \mathbf{b} are vectors consisting of the N volume fractions n_i and the J theoretical log responses R^j with respect to the N different rock constituents, then:

$$\mathbf{R}^j = \sum_i^N n_i R_i^j, \text{ where: } \sum_i^N n_i = 1, \text{ and } \mathbf{x} = [n_1, \dots, n_N]^T, \mathbf{b} = [R^1, \dots, R^J]^T. \quad (8.28)$$

Arranging the specific responses of each log to the N rock constituents as rows of the matrix \mathbf{A} :

$$\mathbf{A} = \begin{bmatrix} R_1^1 & \dots & R_N^1 \\ \vdots & \ddots & \vdots \\ R_1^J & \dots & R_N^J \end{bmatrix}, \quad (8.29)$$

we can write the direct and inverse problems as:

$$\mathbf{A} \mathbf{x} = \mathbf{b} \text{ and } \mathbf{x} = \mathbf{A}^{-1} \mathbf{b}, \quad (8.30)$$

respectively. Thus in the direct problem, the log response vector \mathbf{b} is computed from the volume fraction vector \mathbf{x} and the specific log response matrix \mathbf{A} . Conversely in the inverse problem, the volume fractions \mathbf{x} are computed from the log responses \mathbf{b} and the inverse of the specific log response matrix, \mathbf{A}^{-1} . Thus,

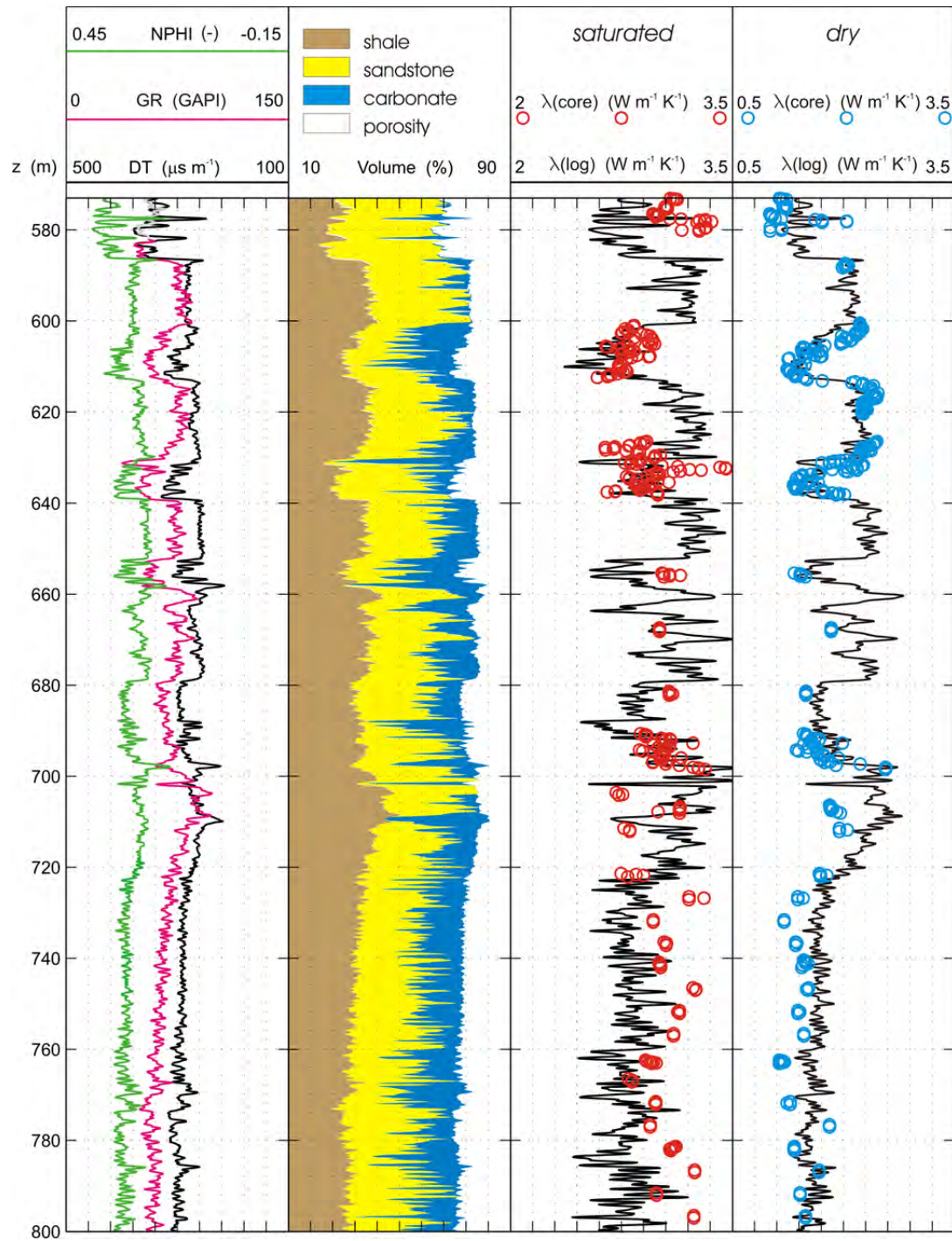


Fig. 8.11 Sand-Shale-Carbonate model for a borehole. Panels (from left to right): (1) Input data: NPHI - neutron porosity; GR - natural gamma radiation (GAPI: gamma ray API units); DT - acoustic slowness. (2) Composition computed from input logs. (3) Log of saturated thermal conductivity $\lambda(\log)$ computed from composition according to the geometric mean, eq. (8.23d). (4) Log of dry thermal conductivity $\lambda(\log)$ computed from composition according to the geometric mean, eq. (8.23d). In panels 3 and 4, thermal conductivity measured on saturated and dry core is shown as red and cyan circles, respectively (after [2005Har]).

solving the inverse requires at least as many logs as solid rock constituents. Porosity is not counted here, because it follows as the difference of one and the sum of the solid rock volume fractions. However, the inverse problem can also be solved in a least-squares sense, if more logs are available making the problem over-determined. Once the volume fractions are known and assigned appropriate thermal conductivities, an appropriate mixing model can be applied to compute rock thermal conductivity. Generally the geometric mean (eq. 8.23d) has turned out quite useful, but other mixing models may be appropriate in specific cases (cf. discussion above).

Assigning representative thermal conductivities to the solid rock constituents is not trivial. For reasons discussed in this text previously, tabulated values of rock thermal conductivity should be used only if they characterize specimens from the logged formations. In all other cases, these formations or their outcrops need to be sampled and these specimens tested in the laboratory. If measurements are performed at ambient conditions the values need to be corrected for the effect of temperature, and in some cases for pressure as well. In general the effect of temperature is more pronounced than that of pressure. However, for greater depth and little or less consolidated rocks it needs to be accounted for, too (for a more detailed discussion, see section 8.1.5.2.1 below).

If commercial log interpretation software is used to perform the inversion, the theoretical log responses R^j with respect to the different rock constituents are usually supplied. Alternatively, values for the log responses R^j can be obtained from the literature [e.g. 1986Cra].

8.1.5.1.3 Thermal Conductivity of Minerals

Data on thermal conductivity of minerals is not as abundant as for rocks. However, thermal conductivity of minerals is much better constrained than that of rocks, as there is a well defined specific crystal structure and chemical formula for each mineral. However there are two specific principal difficulties associated with the measurement of thermal conductivity on mineral samples: purity and sample size. Lattice imperfections in crystals significantly reduce the thermal conductivity of many minerals. Correction of alien mineral phases in samples is possible [1971Hor], but requires further microscopic and X-ray examination of the samples.

Measurements on single crystals or mono-mineral, polycrystalline aggregates require a minimum sample size. But large single crystals which can be machined to the desired size are relatively rare. When single-mineral aggregates are used instead, uncertainty is introduced by porosity. The same is true for needle-probe measurements on finely ground samples of minerals saturated with water [1969Hor; 1971Hor]. This way sample size poses no problem, but all information on anisotropy is lost. Moreover, the interpretation of measurements of thermal conductivity on fragments is not without ambiguity. In their comparison obtained for splits from Horai's and Simmons' [1969Hor] original mineral samples using the transient needle-probe method [1969Hor] and a steady-state divided-bar "cell" method Sass et al. [1971Sas] find that the results of measurements on fragments depend on both the technique and the model used for inferring the thermal conductivity of the solid constituents of the mixture (see e.g. eqs. 8.24a-e).

This review collates a summary of data from original contributions and previous compilations (Table 8.9) comprising data measured on both single crystals as well as natural single-mineral, polycrystalline aggregates, and artificial mono-mineral aggregates produced from a mixture of powdered mineral specimens and distilled water. Data are compiled from four main sources: (1) Diment and Pratt [1988Dim] who report their own measurements as well as those performed or reported previously [1940Bir^a; 1940Bir^b; 1942Bir; 1947Cos; 1954Bir; 1959Rat; 1965Sas; 1966Cla; 1988Rob]; (2) Dreyer [1974Dre], a compilation of data measured by a variety of researchers; (3) Horai [1971Hor, including 1969Hor; 1972Hor]; and finally (4) Popov [1999Pop^a, including 1987Pop].

Table 8.9 Thermal conductivity λ ($\text{W m}^{-1} \text{K}^{-1}$) of different rock-forming minerals. Minerals marked "iso" are isotropic; T: temperature ($^{\circ}\text{C}$: unspecified room temperature); (n): the number of data for mean and standard deviation (always calculated, even if n is statistically insignificant); "state" describes the directional dependence of λ : "x": measurements of unknown orientation on single crystals, "a": on single-mineral aggregates; anisotropy is specified either by (1) the mineral's optical a-, b- or c-axes (100, 010, 001); (2) the diagonal elements of the thermal conductivity tensor (λ_{11} , λ_{22} , λ_{33}), where λ_{33} is parallel to the crystal's optical c-axis, and the optical a-axis lies within the plane defined by λ_{11} and λ_{22} ; (3) the thermal conductivity components normal (\perp) or parallel (\parallel) to the direction of maximum thermal conductivity; Mean values λ_m are calculated as $\lambda_m = (\lambda_{100} + \lambda_{010} + \lambda_{001})/3$ [1987Pop]. Chemical formulas are given as by Ralph [2003Ral].

Mineral	T, state, λ , (n)	Source
MISCELLANEOUS		
diamond, C, (iso)	? $^{\circ}\text{C}$, λ_{11} : 545.3 (?)	[1974Dre]
diamond, C (Type I/IIa/IIb)	(T in K), $T/\lambda_{\text{type I}}/\lambda_{\text{type IIa}}/\lambda_{\text{type IIb}}$: 10/140/317/203, 50/3530/9210/5910, 100/3000/10000/5420, 150/1950/6020/3250, 200/1410/4030/2260, 250/1100/2970/1700, 300/895/2300/1350, 350/755/1850/1110, 400/650/1540/932	[2000Lid]
natural graphite, C	? $^{\circ}\text{C}$, a: 189.7 , λ_{11} : 355.0 , λ_{33} : 89.4 (?)	[1974Dre]
pyrolytic graphite, C (highly purified)	? $^{\circ}\text{C}$, a: 155.0 (?)	[1990Gri]
	(T in K), T/λ_{\parallel} : 10/81.1, 50/2310, 100/4970, 150/4510, 200/3230, 250/2440, 300/1950, 350/1620, 400/1390, 500/1080, 600/892, 800/676, 1000/534, 1200/448, 1400/384, 1600/333, 1800/293, 2000/262	[2000Lid]
	(T in K), T/λ_{\perp} : 10/1.16, 50/15.2, 100/16.8, 150/12.5, 200/9.23, 250/7.11, 300/5.70, 350/4.77, 400/4.09, 500/3.22, 600/2.68, 800/2.01, 1000/1.60, 1200/1.34, 1400/1.16, 1600/1.00, 1800/0.895, 2000/0.807	
water ice, H_2O	0 $^{\circ}\text{C}$, λ_{11} : 1.9 (?), λ_{33} : 2.3 (?), a: 2.0 (?); -125 $^{\circ}\text{C}$, a: 4.0 (?)	[1974Dre]
	(T in $^{\circ}\text{C}$), T/λ_m : 0/2.14, -10/2.32, -20/2.4, -30/2.5, -40/2.6, -60/3.0, -80/3.3, -100/3.7, -120/4.2, -140/4.9, -160/5.7, -180/7.0, -200/8.7, -220/11.8, -240/20, -250/32	[1982Mil, 2000Lid]
ORTHOSILICATES		
olivine group		
olivine (Fa_{xy} : xy % fayalite)	? $^{\circ}\text{C}$, a: Fa_0 – Fa_{10} /5.10, Fa_{10} – Fa_{30} /4.27, Fa_{30} – Fa_{60} /3.60, Fa_{60} – Fa_{90} /3.18, Fa_{90} – Fa_{100} /3.05, Fa_{90} – Fa_{100} /3.14	[1972Hor]
fayalite, Fe_2SiO_4	30 $^{\circ}\text{C}$, a: 3.85 \pm 0.08 (4) (dunite, mostly Fa)	[1988Dim]
	? $^{\circ}\text{C}$, a: 3.16 ($\text{Fo}_4\text{Fa}_{96}$) (1)	[1971Hor]
	? $^{\circ}\text{C}$, λ_m : 3.30 (1)	[1987Pop, 1999Pop ^a]
forsterite, Mg_2SiO_4	30 $^{\circ}\text{C}$, a: 4.68 \pm 0.38 (3) (dunite, 97 % $\text{Fo}_{92}\text{Fa}_8$)	[1940Bir ^a]
	? $^{\circ}\text{C}$, a: 5.03 \pm 0.2 (5) ($\text{Fo}_{98}\text{Fa}_2$ – $\text{Fo}_{91}\text{Fa}_9$)	[1971Hor]
monticellite, CaMgSiO_4	35 $^{\circ}\text{C}$, a: 3.25 \pm 0.04 (3)	[1988Dim]
garnet group		
almandine, $\text{Fe}_3\text{Al}_2[\text{SiO}_4]_3$ iso (cubic)	(Mg, Fe, Mn, Ca) ₃ (Al, Fe) ₂ [SiO_4] ₃	
	? $^{\circ}\text{C}$, a: 3.56 (1)	[1988Dim]
	? $^{\circ}\text{C}$, a: 3.31 (1)	[1971Hor]
	? $^{\circ}\text{C}$, λ_{11} : 3.6 (?)	[1974Dre]
	27 $^{\circ}\text{C}$ (100): 3.53 \pm 0.14 (3), (010): 3.53 \pm 0.14 (3), (001): 3.53 \pm 0.14 (3)	[1987Pop, 1999Pop ^a]
grossular, $\text{Ca}_3\text{Al}_2[\text{SiO}_4]_3$, iso (cubic)	? $^{\circ}\text{C}$, a: 5.32 (1)	[1988Dim]
	? $^{\circ}\text{C}$, a: 5.48 \pm 0.24 (3)	[1971Hor]
	27 $^{\circ}\text{C}$ (100): 5.90 (1), (010): 5.90 (1), (001): 5.90 (1)	[1987Pop, 1999Pop ^a]
hibschite (hydrogrossular), $\text{Ca}_3\text{Al}_2[\text{SiO}_4]_{3-x}[\text{OH}]_{4x}$? $^{\circ}\text{C}$, a: 6.53 (1)	
spessartine, $\text{Mn}_3\text{Al}_2[\text{SiO}_4]_3$ (cubic)	35 $^{\circ}\text{C}$, a: 3.06 \pm 0.10 (3)	[1988Dim]
	27 $^{\circ}\text{C}$ (100): 3.66 (1), (010): 3.66 (1), (001): 3.66 (1)	[1987Pop, 1999Pop ^a]
zircon group		
zircon, ZrSiO_4	? $^{\circ}\text{C}$, λ_{11} : 3.9 (?), λ_{33} : 4.8 (?)	[1974Dre]
	? $^{\circ}\text{C}$, a: 5.54	[1971Hor]
titanite group (sphene)		

Mineral	<i>T</i> , state, λ , (n)	Source
titanite, CaTiSiO_5	? °C, a: 2.34 (1)	[1971Hor]
<i>Al₂SiO₅ group (disthene series)</i>		
andalusite, Al_2SiO_5	35 °C, a: 6.56 ± 0.45 (8) (<5 % quartz impurity) ? °C, a: 7.58 (1)	[1988Dim] [1971Hor]
kyanite, Al_2SiO_5	35 °C, a: 7.15 ± 0.17 (4), a: 12.45 ± 0.71 (3) (< 5 % quartz impurity) ? °C, a: 14.16 (1)	[1988Dim] [1971Hor]
sillimanite, Al_2SiO_5	35 °C, a: 10.73 ± 0.64 (3) ? °C, a: 9.10 (1)	[1988Dim] [1971Hor]
topaz, $\text{Al}_2\text{SiO}_4(\text{F},\text{OH})_2$? °C, λ_m : 20.9 (1)	[1987Pop, 1999Pop ^a]
<i>SOROSILICATES</i>		
allanite, (Y,Ce,Ca) ₂ (Al,Fe ³⁺) ₃ [SiO ₄] ₃ [OH]	? °C, λ_m : 1.44 (1)	[1987Pop, 1999Pop ^a]
epidote, $\text{Ca}_2(\text{Al},\text{Fe})_3[\text{SiO}_4]_3[\text{OH}]$	32 °C, λ : 3.10 (1); 32 °C, λ : 2.93 (1); 31 °C, a: 2.51 ± 0.03 (2) ? °C, a: 2.83 ± 0.3 (2)	[1988Dim] [1971Hor]
ilvaite, $\text{CaFe}_2^{2+}\text{Fe}^{3+}[\text{SiO}_4]_2[\text{OH}]$? °C, λ_m : 1.84 (1)	[1987Pop, 1999Pop ^a]
vesuvianite, (tetragonal) $\text{Ca}_{10}\text{Mg}_2\text{Al}_4[\text{SiO}_4]_5[\text{Si}_2\text{O}_7]_2[\text{OH}]_4$? °C, x: 2.31 ± 0.23 (2), a: 2.86 (1); 27 °C (100): 2.17 ± 0.22 (3), (010): 2.17 ± 0.22 (3), (001): 2.34 ± 0.18 (3)	[1987Pop, 1999Pop ^a]
<i>CYCLOSILICATES</i>		
beryl, $\text{Be}_3\text{Al}_2\text{Si}_6\text{O}_{18}$ (hexagonal)	? °C, x: 3.93 ± 0.08 (2); λ_m : 4.16 (1), a: 3.87 (1); 27 °C (100): 3.81 ± 0.09 (2), (010): 3.81 ± 0.09 (2), (001): 4.31 ± 0.19 (2)	[1987Pop, 1999Pop ^a]
cordierite, $(\text{Mg},\text{Fe})_2\text{Al}_4\text{Si}_5\text{O}_{18}$	35 °C, λ : 3.33 ± 0.04 (3); ? °C, λ : 3.06 ± 0.03 (2) ? °C, λ_m : 2.41 (1)	[1988Dim] [1987Pop, 1999Pop ^a]
eudialyte, $\text{Na}_4(\text{Ca},\text{Ce})_2(\text{Fe}^{2+},\text{Mn},\text{Y})\text{ZrSi}_8\text{O}_{22}(\text{OH},\text{Cl})_2$? °C, a: 1.14 (1)	[1987Pop, 1999Pop ^a]
schorl (tourmaline) (trigonal), $\text{NaFe}_3^{2+}\text{Al}_6[\text{BO}_3]_3\text{Si}_6\text{O}_{18}[\text{OH}]_4$? °C, x: 3.97 ± 0.47 (2); λ_m : 3.64 (1); 27 °C (100): 4.36 ± 0.40 (2), (010): 4.36 ± 0.40 (2), (001): 3.19 ± 0.59 (2)	[1987Pop, 1999Pop ^a]
<i>CHAIN SILICATES</i>		
<i>pyroxene group</i>		
augite, $(\text{Ca},\text{Na})(\text{Mg},\text{Fe},\text{Al},\text{Ti})(\text{Al},\text{Si})_2\text{O}_6$	(Na,Ca)(Mg,Fe,Al)(Al,Si) ₂ O ₆ 35 °C, a: 4.20 ± 0.05 (3)	[1988Dim]
diallage (augite)	? °C, λ_m : 3.17 (1)	[1987Pop, 1999Pop ^a]
diopside, $\text{CaMgSi}_2\text{O}_6$	35 °C, a: 4.40 ± 0.42 (2) ? °C, a: 4.66 ± 0.31 (4) ? °C, λ_m : 4.05 ± 0.03 (3)	[1988Dim] [1971Hor] [1987Pop, 1999Pop ^a]
enstatite, $\text{Mg}_2\text{Si}_2\text{O}_6$? °C, a: 4.47 ± 0.35 (4)	[1971Hor]
jadeite, $\text{Na}(\text{Al},\text{Fe})\text{Si}_2\text{O}_6$	34 °C, a: 5.59 ± 1.22 (2) ? °C, a: 5.64 ± 1.44 (2)	[1988Dim] [1971Hor]
pyroxene (Fs _{xy} : xy % ferrosilite, Fs = Fe ₂ Si ₂ O ₆)	? °C, a: Fs ₀ –Fs ₁₀ /4.73, Fs ₁₀ –Fs ₃₀ /4.93, Fs ₃₀ –Fs ₅₀ /(3.43), Fs ₅₀ –Fs ₇₀ /(3.18), Fs ₇₀ –Fs ₉₀ /(3.14), Fs ₉₀ –Fs ₁₀₀ /(3.22)	[1972Hor]
spodumene, $\text{LiAlSi}_2\text{O}_6$? °C, λ_m : 5.28 ± 0.77 (2)	[1987Pop, 1999Pop ^a]
<i>amphibole group</i>		
actinolite, $\text{Ca}_2(\text{Mg},\text{Fe}^{2+})_5[\text{Si}_8\text{O}_{22}][\text{OH}]_2$	$\text{NaCa}_2(\text{Mg},\text{Fe},\text{Al})(\text{Al},\text{Si})_8\text{O}_{22}(\text{OH})_2$ 31 °C, λ : 5.34 ± 0.12 (2); ? °C, λ : 2.96 (1)	[1988Dim]
nephrite (actinolite)	? °C, a: 3.64 ± 0.50 (2)	[1987Pop, 1999Pop ^a]
hornblende, $\text{Ca}_2(\text{Mg},\text{Fe}^{2+})_4(\text{Al},\text{Fe}^{3+})[\text{Si}_7\text{Al}]\text{O}_{22}[\text{OH}]_2$? °C, λ : 2.75 ± 0.18 (2); 35 °C, λ : 1.88 (1) 20 °C, a: 2.91 ± 0.09 (2) ? °C, a: 2.81 ± 0.27 (2) ? °C, λ_{11} : 3.0 , λ_{33} : 2.4 (?) ? °C, λ_m : 1.82 ± 0.01 (2)	[1988Dim] [1966Cla] [1971Hor] [1974Dre] [1987Pop, 1999Pop ^a]
pargasite, $\text{NaCa}_2(\text{Mg},\text{Fe}^{2+})_4\text{Al}[\text{Si}_6\text{Al}_2]\text{O}_{22}[\text{OH}]_2$? °C, λ_m : 2.65 (1)	[1987Pop, 1999Pop ^a]
rhodonite, $(\text{Mn}^{2+},\text{Fe}^{2+},\text{Mg},\text{Ca})\text{SiO}_3$? °C, λ_m : 2.35 (1)	[1987Pop, 1999Pop ^a]
tremolite, $[\text{Ca}_2\text{Mg}_5][\text{Si}_8\text{O}_{22}][\text{OH}]_2$	31 °C, λ : 5.79 ± 0.28 (2); 32 °C, λ : 4.54 ± 0.14 (2)	[1988Dim]

Mineral	<i>T</i> , state, λ , (n)	Source
wollastonite, CaSiO_3	? °C, a: 6.36 (1)	[1987Pop, 1999Pop ^a]
PHYLLOSILICATES		
<i>mica group</i>		
biotite (monoclinic), $\text{K}(\text{Mg,Fe})_3(\text{Al,Fe}^{3+})\text{Si}_3\text{O}_{10}(\text{OH,F})_2$	33 °C, H^+ : 3.14 ; 32 °C, \perp : 0.52 ± 0.01 (2) ? °C, a: 2.02 ± 0.32 (2) ? °C, λ_m : 2.29 ± 0.26 (2), x: 2.10 (1); 27 °C (100): 2.61 (1), (010): 2.61 (1), (001): 1.30 (1)	[1988Dim] [1971Hor] [1987Pop, 1999Pop ^a]
clinochlore, $(\text{Mg,Fe}^{2+})_5\text{Al}[\text{Si}_3\text{Al}]\text{O}_{10}[\text{OH}]_8$	29 °C, H^+ : 10.34 ± 0.57 (2), \perp : 1.97 ± 0.06 (2)	[1988Dim]
chlorite (monoclinic), $(\text{Mg,Fe})_3[(\text{Si,Al})_4\text{O}_{10}[\text{OH}]_2] \cdot (\text{Mg,Fe,Al})_3[\text{OH}]_6$	30 °C, a: 3.06 ± 1.32 (5) ? °C, a: 5.2 (?), λ_{11} : 5.5 (?), λ_{33} : 5.1 (?) ? °C, a: 5.15 ± 0.94 (3) ? °C, λ_m : 3.77 (1), x: 7.87 (1); 27 °C (100): 11.1 (1), (010): 11.1 (1), (001): 1.38 (1)	[1988Dim] [1974Dre] [1971Hor] [1987Pop, 1999Pop ^a]
chrysotile, $\text{Mg}_3\text{Si}_2\text{O}_5[\text{OH}]_4$? °C, a: 1.95 (1)	[1987Pop, 1999Pop ^a]
muscovite (monoclinic), $\text{KA}l_2[\text{Si}_3\text{Al}]\text{O}_{10}[\text{OH}]_2$	30 °C, H^+ : 3.89 ± 0.0 (2); 32-45 °C, \perp : 0.62 ± 0.13 (4) ? °C, a: 2.28 ± 0.07 (3) ? °C, λ_m : 2.34 (1), x: 2.88 (1); ; 27 °C (100): 3.80 (1), (010): 3.80 (1), (001): 1.03 (1)	[1988Dim] [1971Hor] [1987Pop, 1999Pop ^a]
phlogopite, $\text{KMg}_3\text{Si}_3\text{AlO}_{10}(\text{F,OH})_2$	30 °C, H^+ : 4.01 (3), \perp : 0.48 ± 0.02 (4) ? °C, λ_m : 1.57 (1)	[1988Dim] [1987Pop, 1999Pop ^a]
prochlorite, $(\text{Mg,Fe}^{2+},\text{Al})_6\text{Al}[\text{Si}_{2.5}\text{Al}_{1.5}]\text{O}_{10}[\text{OH}]_8$	29-34 °C, a: 2.61 ± 0.40 (10)	[1988Dim]
pyrophyllite, $\text{Al}_2\text{Si}_4\text{O}_{10}[\text{OH}]_2$	30 °C, H^+ : 6.17 ± 0.73 (5), \perp : 1.12 ± 0.42 (2) 30-35 °C, a: 4.47 ± 0.47 (7) (<i>T</i> in °C), <i>T</i> / λ_m : 0/4.98, 100/4.17, 200/3.59, 300/3.14, 400/2.81	[1988Dim] [1966Cla]
serpentine (antigorite), $(\text{Mg,Fe})_3[\text{Si}_2\text{O}_5][\text{OH}]_4$? °C, H^+ : 2.76 ± 0.03 (4); 32 °C, \perp : 2.41 ± 0.15 (2) 30-34 °C, a: 2.61 ± 0.40 (10) ? °C, a: 2.1 (?), λ_{11} : 2.6 (?), λ_{33} : 2.3 (?) ? °C, a: 3.53 ± 1.57 (3) ? °C, a: 2.80 ± 0.20 (4) ? °C, λ_m : 2.78 (1)	[1988Dim] [1988Dim] [1974Dre] [1971Hor] [1987Pop, 1999Pop ^a]
talc, $\text{Mg}_3\text{Si}_4\text{O}_{10}[\text{OH}]_2$	29-34 °C, H^+ : 10.69 ± 1.50 (5); 30 °C, \perp : 1.76 ± 0.0 (2) 30 °C, a: 2.97 (1) ? °C, a: 6.1 ± 1.27 (2) ? °C, λ_{11} : 3.1 (?), λ_{33} : 2.9 (?)	[1988Dim] [1954Bir] [1971Hor] [1974Dre]
TECTOSILICATES		
<i>feldspar group</i>		
albite, $\text{NaAlSi}_3\text{O}_8$	25 °C, a: 2.34 (1) ? °C, a: 2.14 ± 0.22 (4) ? °C, λ_{11} : 2.1 (?), λ_{33} : 2.9 (?) ? °C, λ_m : 2.04 ± 0.25 (6)	[1965Sas] [1971Hor] [1974Dre] [1987Pop, 1999Pop ^a]
anorthite, $\text{CaAl}_2\text{Si}_2\text{O}_8$	25 °C, a: 2.72 (1) ? °C, a: 1.68 (1)	[1965Sas] [1971Hor]
cancrinite, $\text{Na}_6\text{Ca}_2\text{Al}_6\text{Si}_6\text{O}_{24}[\text{CO}_3]_2$? °C, λ_m : 1.36 (1)	[1987Pop, 1999Pop ^a]
labradorite, $(\text{Ca,Na})(\text{Si,Al})_4\text{O}_8$? °C, a: 1.71 (1)	[1987Pop, 1999Pop ^a]
microcline, KAlSi_3O_8	? °C, (001): 2.04 (1) ? °C, a: 2.49 ± 0.10 (3) ? °C, a: 2.41 ± 0.11 (3)	[1965Sas] [1971Hor] [1987Pop, 1999Pop ^a]
natrolite, $\text{Na}_2\text{Al}_2\text{Si}_3\text{O}_{10} \cdot 2\text{H}_2\text{O}$? °C, λ_m : 1.73 (1)	[1987Pop, 1999Pop ^a]
nepheline, $(\text{Na,K})\text{AlSiO}_4$	35 °C, a: 1.39 ± 0.15 (3) ? °C, a: 1.36 (1)	[1988Dim] [1987Pop, 1999Pop ^a]
oligoclase, $(\text{Na,Ca})(\text{Si,Al})_4\text{O}_8$? °C, λ_m : 2.11 (1)	[1987Pop, 1999Pop ^a]
orthoclase, KAlSi_3O_8	30 °C, (100): 2.34 ± 0.11 (2), (010): 2.68 (1), (001): 2.30 ± 0.3 (2) ? °C, a: 2.31 (1)	[1965Sas] [1971Hor]

Pre-Print from:

Clauser, C., 2006. Geothermal Energy, In: K. Heinloth (ed), *Landolt-Börnstein, Group VIII: Advanced Materials and Technologies, Vol. 3: Energy Technologies, Subvol. C: Renewable Energies*, Springer Verlag, Heidelberg-Berlin, 493-604.

Mineral	T , state, λ , (n)	Source
	? °C, \perp : 2.9 , \parallel_1 : 4.2 , \parallel_2 : 4.6 , λ_{11} : 2.94 , λ_{22} : 4.2 , λ_{33} : 4.63 (1)	[1974Dre]
	? °C, a: 2.15 ± 0.05 (2)	[1987Pop, 1999Pop ^a]
plagioclase (An _{xy} : xy % anorthite)	? °C, a: An ₀ –An ₅ / 2.34 , An ₅ –An ₁₅ / 1.92 , An ₁₅ –An ₃₀ / 1.63 , An ₃₀ –An ₅₀ / 1.46 , An ₅₀ –An ₇₀ / 1.46 , An ₇₀ –An ₈₅ / 1.59 , An ₈₅ –An ₁₀₀ / 1.72	[1972Hor]
sanidine, (K,Na)(Si,Al) ₄ O ₈	? °C, λ_m : 1.73 (1)	[1987Pop, 1999Pop ^a]
scapolite (tetragonal)	35 °C, x _X : 1.76 ± 0.00 (3), x _Z : 1.95 ± 0.04 (2)	[1988Dim]
(Na,Ca) ₄ (Si,Al) ₁₂ O ₂₄ (Cl,CO ₃ ,SO ₄)	? °C, x: 1.42 (1); ; 27 °C (100): 1.34 (1), (010): 1.34 (1), (001): 1.59 (1)	[1987Pop, 1999Pop ^a]
sodalite, Na ₄ Al ₃ Si ₃ O ₁₂ Cl	35 °C, a: 3.16 ± 0.12 (3)	[1988Dim]
silica group	<i>SiO₂</i>	
α quartz, SiO ₂ (trigonal)	30 °C, \parallel : 10.17 (1)	[1940Bir ^a]
	30 °C, \perp : 6.15 (1)	[1959Rat]
	? °C, a: 8.1 , λ_{11} : 6.5 (?), λ_{33} : 11.3 (?)	[1974Dre]
	? °C, a: 7.69 (1)	[1971Hor]
	? °C, x: 7.60 ± 0.0 (4); 27 °C (100): 6.05 ± 0.0 (4), (010): 6.05 ± 0.0 (4), (001): 10.7 ± 0.0 (4)	[1987Pop, 1999Pop ^a]
α quartz \perp	(T in °C), T/λ , x: 0/ 6.82 , 50/ 5.65 , 100/ 4.94 , 150/ 4.44 , 200/ 4.06 , 250/ 3.73 , 300/ 3.52 , 350/ 3.31	[1940Bir ^a]
α quartz \parallel	(T in °C), T/λ , x: 0/ 11.43 , 50/ 9.38 , 100/ 7.95 , 150/ 7.03 , 200/ 6.32 , 250/ 5.69 , 300/ 5.15 , 350/ 4.73	[1940Bir ^a]
chalcedony, SiO ₂	? °C, a: 3.17 (1)	[1987Pop, 1999Pop ^a]
pyrex 774 glass	(T in °C), amorphous: T/λ : 0/ 1.21 , 50/ 1.26 , 100/ 1.32 , 150/ 1.38 , 200/ 1.44 , 250/ 1.49 , 300/ 1.55 , 350/ 1.61 , 400/ 1.66 , 450/ 1.72 , 500/ 1.83 (T in °C)	[1940Bir ^a]
silica glass	30 °C, amorphous: 1.38 (?)	[1959Rat]
	? °C, amorphous: 1.2 (?)	[1974Dre]
silica glass	(T in °C), amorphous: T/λ : 0/ 1.36 , 50/ 1.44 , 100/ 1.48 , 150/ 1.53 , 200/ 1.58 , 250/ 1.64 , 300/ 1.70 , 350/ 1.78 , 400/ 1.85 , 450/ 1.94 , 500/ 2.07	[1940Bir ^a]
Non-Silicates		
oxides		
cassiterite, SnO ₂	? °C, λ_m : 12.3 (1)	[1987Pop, 1999Pop ^a]
chromite, iso, FeCr ₂ O ₄	35 °C, a: 2.20 ± 0.27 (3)	[1974Dre]
	? °C, a: 2.52 (1)	[1971Hor]
	? °C, a: 2.62 (1)	[1987Pop, 1999Pop ^a]
corundum, Al ₂ O ₃	26–70 °C, \parallel : 18.37 ± 3.86 (5); 23–77 °C, \perp : 17.70 ± 3.60 (4)	[1988Dim]
	? °C, λ_{11} : 31.2 (?), λ_{33} : 38.9 (?)	[1974Dre]
hematite, Fe ₂ O ₃	30 °C, a: 12.42 ± 1.74 (3)	[1954Bir, 1966Cla]
	? °C, λ_{11} : 14.7 (?), λ_{33} : 12.1 (?)	[1974Dre]
	? °C, a: 11.28 (1)	[1971Hor]
	? °C, λ_m : 18.25 ± 1.25 (2)	[1987Pop, 1999Pop ^a]
ilmenite, FeTiO ₃	35 °C, a: 2.50 ± 0.02 (3)	[1988Dim]
	? °C, a: 2.38 ± 0.25 (2)	[1971Hor]
	? °C, a: 2.92 (1)	[1987Pop, 1999Pop ^a]
magnetite, iso, Fe ²⁺ Fe ³⁺ ₂ O ₄	22–33 °C, a: 4.61 ± 0.39 (8)	[1988Dim]
	? °C, λ_{11} : 9.7 (?)	[1974Dre]
	? °C, a: 5.10 (1)	[1971Hor]
	? °C, λ_m : 4.34 ± 0.90 (2)	[1987Pop, 1999Pop ^a]
periclase, MgO, iso	? °C, λ_{11} : 33.5 (?)	[1974Dre]
artificial periclase	400 K, λ_{11} : 41.05 (1)	[1968Kan]
pyrochlore, (Na,Ca) ₂ Nb ₂ O ₆ (OH,F)	? °C, a: 1.52 (1)	[1987Pop, 1999Pop ^a]
rutile, TiO ₂ (tetragonal)	44–67 °C, \perp : 7.95 ± 1.198 (2)	[1988Dim]
	36–67 °C, \perp : 13.19 ± 0.89 (2); ? °C, a: 4.90 ± 0.21 (3)	[1966Cla]
	? °C, λ_{11} : 9.3 (?), λ_{33} : 12.9 (?)	[1974Dre]

Mineral	T , state, λ , (n)	Source
scheelite, CaWO_4	? °C, a: 5.12 (1)	[1971Hor]
	? °C, x: 4.89 (1),	[1987Pop,
	27 °C (100): 4.38 (1), (010): 4.38 (1), (001): 5.92 (1)	1999Pop ^a]
	? °C, λ_m : 2.53 ± 0.20 (4)	[[1987Pop,
		1999Pop ^a]
spinel, iso, MgAl_2O_4	35-70 °C, a: 12.14 ± 1.51 (3)	[1966Cla]
	? °C, λ_{11} : 13.8 (?)	[1974Dre]
	? °C, a: 9.48 (1)	[1971Hor]
wolframite, $(\text{Fe,Mn})\text{WO}_4$? °C, λ_m : 2.81 ± 0.38 (5)	[1987Pop,
wulfenite, PbMoO_4		1999Pop ^a]
	? °C, λ_m : 1.82 (1)	[1987Pop,
sulfides		
arsenopyrite, FeAsS	? °C, a: 7.24 (1)	[1987Pop,
chalcopyrite, CuFeS_2		1999Pop ^a]
	35 °C, a: 7.55 ± 0.33 (3)	[1988Dim]
	? °C, a: 10.7 (1)	[1987Pop,
galena, PbS iso (cubic)		1999Pop ^a]
	35 °C, a: 2.76 ± 0.22 (3)	[1988Dim]
	? °C, a: 2.28 (1)	[1971Hor]
	? °C, a: 1.99 (1), x: 2.02 (1),	[1987Pop,
pyrite, FeS_2 , iso (cubic)	27 °C (100): 2.02 (1), (010): 2.02 (1), (001): 2.02 (1)	1999Pop ^a]
	35 °C, a: 23.15 ± 2.45 (3)	[1988Dim]
	? °C, a: 19.21 (1)	[1971Hor]
	? °C, a: 23.7 (1)	[1987Pop,
pyrrhotite, FeS (hexagonal)	27 °C (100): 41.4 (1), (010): 41.4 (1), (001): 41.4 (1)	1999Pop ^a]
	? °C, x: 41.4 (1), λ_{11} : 37.9 (?)	[1974Dre]
	35 °C, a: 3.53 ± 0.06 (3)	[1988Dim]
	? °C, a: 4.60 (1)	[1971Hor]
	? °C, a: 3.52 (1),	[1987Pop,
sphalerite, $(\text{Zn,Fe}^{2+})\text{S}$	27 °C (100): 3.43 (1), (010): 3.43 (1), (001): 3.71 (1)	1999Pop ^a]
	35 °C, a: 11.20 ± 0.02 (3)	[1988Dim]
sphalerite (marmitite), $(\text{Zn,Fe}^{2+})\text{S}$? °C, a: 18.9 (1)	[1987Pop,
sphalerite (cleiophane), ZnS	? °C, a: 4.67 (1)	1999Pop ^a]
wurtzite, $(\text{Zn,Fe})\text{S}$? °C, a: 4.19 (1)	[1987Pop,
sulfates		
anhydrite, CaSO_4	25-35 °C, a: 5.36 ± 0.30 (6)	[1988Dim]
	? °C, a: 4.76 (1)	[1971Hor]
barite, BaSO_4	25-100 °C, λ : 2.92 ± 0.09 (4), \perp : 2.07 ± 0.03 (2)	[1988Dim]
	25-35 °C, a: 1.72 ± 0.05 (4)	
	? °C, a: 1.51 ± 0.12 (2)	[1987Pop,
celestine, SrSO_4		1999Pop ^a]
	35 °C, λ : 1.38 (1); 35 °C, \perp : 1.29 ± 0.11 (3)	[1988Dim]
	? °C, λ_m : 1.32 (1)	[1987Pop,
gypsum, $\text{CaSO}_4 \cdot 2\text{H}_2\text{O}$		1999Pop ^a]
	? °C, a: 1.30 (1)	[1988Dim]
	? °C, a: 1.22 (1)	[1987Pop,
		1999Pop ^a]
	? °C, \perp : 1.6 , λ_{11} : 2.5 , λ_{12} : 3.8 , λ_{11} : 2.6 , λ_{22} : 1.6 , λ_{33} : 3.7 (1)	[1974Dre]
carbonates		
aragonite, CaCO_3	25-100 °C, a: 2.37 ± 0.23 (11)	[1988Dim]
calcite, CaCO_3 (trigonal)	? °C, a: 2.24 (1)	[1971Hor]
	? °C, λ_{11} : 4.2 (?), λ_{33} : 5.0 (?)	[1974Dre]
	? °C, x: 3.13 (1);	[1987Pop,
	27 °C (100): 3.21 (1), (010): 3.21 (1), (001): 3.50 (1)	1999Pop ^a]
	? °C, λ_m : 3.28 ± 0.04 (2), a: 3.59 (1)	[1971Hor]
calcite \parallel	(T in °C), T/λ , x: 0/4.00, 30/3.63, 50/3.40, 100/2.99, 150/2.73, 200/2.55, 250/2.41, 300/2.29, 350/2.20, 400/2.13	[1940Bir ^a]
calcite \perp	(T in °C), T/λ , x: 0/3.48, 30/3.16, 50/3.00, 100/2.72, 150/2.52, 200/2.37, 250/2.25, 300/2.16, 350/2.09, 400/2.06	
cerussite, PbCO_3	35 °C, a: 1.35 ± 0.02 (3)	[1988Dim]
dolomite, $\text{CaMg}[\text{CO}_3]_2$	25-35 °C, a: 4.85 ± 0.26 (73)	[1988Dim]
	? °C, λ_{11} : 4.7 (?), λ_{33} : 4.3 (?)	[1974Dre]
	? °C, a: 5.51 (1)	[1971Hor]

Pre-Print from:

Clauser, C., 2006. Geothermal Energy, In: K. Heinloth (ed), *Landolt-Börnstein, Group VIII: Advanced Materials and Technologies, Vol. 3: Energy Technologies, Subvol. C: Renewable Energies*, Springer Verlag, Heidelberg-Berlin, 493-604.

Mineral	T , state, λ , (n)	Source
	? °C, a: 5.97 ± 0.44 (2)	[1987Pop, 1999Pop ^a]
magnesite, MgCO ₃	25-100 °C, λ : 7.86 ± 0.20 (4); \perp : 7.32 ± 0.36 (4) 34-35 °C, a: 8.18 ± 1.34 (5)	[1988Dim] [1988Dim]
	? °C, a: 5.84 (1)	[1971Hor]
siderite, FeCO ₃	35 °C, a: 2.99 ± 0.15 (3)	[1988Dim]
	? °C, a: 3.01 (1)	[1971Hor]
strontianite, SrCO ₃	35 °C, a: 1.38 ± 0.07 (4)	[1988Dim]
witherrite, BaCO ₃	35 °C, a: 2.26 ± 0.02 (3)	[1988Dim]
phosphates		
apatite, Ca ₅ [PO ₄] ₃ (F,Cl,OH)	35 °C, a: 1.27 ± 0.02 (3)	[1988Dim]
(hexagonal)	? °C, a: 1.38 ± 0.01 (2)	[1971Hor]
	? °C, x: 1.58 ± 0.06 (3); 27 °C (100): 1.53 ± 0.07 (3), (010): 1.53 ± 0.07 (3), (001): 1.70 ± 0.07 (3)	[1987Pop, 1999Pop ^a]
halides		
fluorite, CaF ₂ , iso	0-36 °C, x: 8.62 ± 1.11 (6)	[1988Dim]
	? °C, λ_{11} : 10.1 (?)	[1974Dre]
	? °C, a: 9.51 (1)	[1971Hor]
	? °C, a: 8.64 (1)	[1987Pop, 1999Pop ^a]
halite, NaCl, iso (cubic)	0-35 °C, x: 5.55 ± 1.09 (8)	[1966Cla]
	? °C, a: 6.1 (?)	[1974Dre]
	? °C, a: 5.88 (1), λ_m : 5.90 (1); 27 °C (100): 5.89 ± 0.01 (2), (010): 5.89 ± 0.01 (2), (001): 5.89 ± 0.01 (2)	[1987Pop, 1999Pop ^a]
halite, NaCl, iso	(T in °C), $T\lambda$, x: 0/6.11, 50/5.02, 70/5.44, 100/4.21, 150/3.59, 200/3.12, 250/2.76, 300/2.49, 350/2.30, 400/2.09	[1940Bir ^a]
rock salt, NaCl, iso	27 °C, x: 6.05 ± 0.87 (5)	[1988Dim]
rock salt, NaCl, iso	(T in K), $T\lambda$: 0.4/0.95, 0.5/1.78, 0.6/3.13, 0.7/4.97, 0.8/7.40, 0.9/10.0, 1/14.0, 2/99.3, 3/270, 4/443, 5/595, 6/735, 7/829, 8/880, 9/870, 10/836, 15/502, 20/306, 25/191, 30/130, 40/75.0, 50/54.0, 75/34.9, 100/24.3, 150/15.0, 200/10.9, 250/8.24, 293/6.65, 300/6.57, 400/4.80, 500/3.67, 600/2.98, 700/2.47, 800/2.08, 900/1.85, 1000/1.67	[1981Yan]
sylvite, KCl, iso	0-12 °C, x: 6.74 ± 0.3 (2)	[1966Cla]
	? °C, λ_{11} : 6.4 (?)	[1974Dre]

Table 8.10. Thermal diffusivity κ ($10^{-6} \text{ m}^2 \text{ s}^{-1}$, upper number) and thermal conductivity λ ($\text{W m}^{-1} \text{ K}^{-1}$, lower number, *in italics*) at different temperatures for quartz, fused silica, olivine, and synthetic periclase; "x" denotes measurements of unknown orientation on single crystals, "a" on single-mineral aggregates; directions of anisotropy are specified either by the mineral's optical a-, b- or c-axes (100, 010, 001); Temperature conversion: $T(^{\circ}\text{C}) = T(\text{K}) - 273.15$; data: [1968Kan;].

mineral	300 K	400 K	500 K	600 K	700 K	800 K	900 K	1000 K	1100 K
quartz, (001)	7.14	3.57	2.38	1.69	1.37	1.14	1.41	1.54	1.64
	13.93	8.20	6.24	4.81	3.91	3.56	3.87	4.56	5.15
quartz, (010)	3.33	2.00	1.45	1.15	0.96	0.89	1.00	1.14	1.28
	6.49	4.60	3.83	3.29	2.90	2.79	2.75	3.39	4.03
fused silica	0.725	0.715	0.705	0.700	0.715	0.741	0.800	0.885	-
	1.147	1.348	1.499	1.612	1.725	1.854	2.060	2.323	-
olivine (Fo ₈₂ Fa ₁₈) (001)	1.85	1.49	1.22	1.08	1.03	1.04	1.09	1.2	1.35
	5.07	4.73	4.23	3.89	3.86	3.98	4.23	4.77	5.44
periclase (MgO) (001)	-	12.5	8.70	6.67	5.56	4.65	4.00	3.57	3.23
	-	46.05	34.12	27.21	23.19	19.63	17.12	15.61	14.32
jadeite	1.54	1.28	1.11	0.97	0.88	0.84	0.83	0.89	0.96
(Na(Al,Fe)Si ₂ O ₆), a	-	-	-	-	-	-	-	-	-
garnet (mean of two), x	1.10	1.00	0.91	0.85	0.81	0.79	0.80	0.81	0.83
	-	-	-	-	-	-	-	-	-
spinel (MgAl ₂ O ₄), x	-	-	3.45	3.13	2.86	2.56	2.44	2.25	2.13
	-	-	-	-	-	-	-	-	-
corundum (Al ₂ O ₃), x	-	6.06	4.55	3.45	2.86	2.50	2.13	1.85	1.64
	-	-	-	-	-	-	-	-	-
alkali feldspar (moonstone), x	7.09	6.67	6.49	6.71	6.99	7.30	7.81	8.33	8.93
	-	-	-	-	-	-	-	-	-

As for rocks, data on the temperature dependence of mineral thermal conductivity is not very abundant. Yang's temperature dependent data for rock salt [1981Yan] represent "recommended values" based on a great number of individual determinations and cover the temperature range 0.4 K – 1000 K. Table 8.10 lists thermal conductivity and thermal diffusivity as functions of temperature for some rock-forming minerals [1968Kan].

For single-mineral aggregates a linear relationship between temperature and thermal resistivity λ^{-1} discriminates between temperature-dependent contributions and other factors which are independent of temperature, such as micro-cracks, grain boundaries, shape and orientation of crystals and their fragments:

$$\frac{1}{\lambda(T)} = m + n T, \quad (8.31)$$

where λ is in $\text{W m}^{-1} \text{K}^{-1}$ and T is in K. By measuring thermal conductivity λ and plotting its inverse, thermal resistivity λ^{-1} , versus temperature m and n may be determined as intercept and slope of a linear regression. Table 8.11 provides values for the constants m and n in eq. (8.31) which may be used to infer the temperature dependence of thermal resistivity for some single-mineral aggregates [1969Cla].

Table 8.11 Values of m and n in eq. (8.31) for single-mineral aggregates; data: [1969Cla].

mineral	T (°C)	m ($10^{-3} \text{ W}^{-1} \text{ m K}$)	n ($10^{-3} \text{ W}^{-1} \text{ m}$)
halite, NaCl	0 – 400	-52.55	0.788
periclase, MgO	100 – 800	-21.50	0.127
corundum, Al_2O_3	100 – 800	-28.66	0.155
quartz, SiO_2 (*)	100 – 400	62.10	0.387
spinel, MgAl_2O_4	100 – 1000	19.11	0.122
Zircon, ZrSiO_4	100 – 800	131.37	0.093
forsterite, Mg_2SiO_4 ,	100 – 600	85.98	0.282
enstatite, ferrosilite, $(\text{Mg}_2, \text{Fe}_2)\text{SiO}_3$	100 – 300	200.63	0.222

(*): single SiO_2 crystal, heat flowing \perp to optical axis

According to eq. (8.15) thermal diffusivity can be expressed by thermal conductivity, density and isobaric specific heat capacity:

$$\kappa = \lambda / (\rho c). \quad (8.32)$$

Based on eq. (8.32), Robertson [1988Rob] converts the feldspar diffusivity data of Kanamori et al. [1968Kan] into conductivity, using a constant density of $\rho = 2600 \text{ kg m}^{-3}$ and a temperature dependent specific heat capacity. However, a comparison of this data set with results from temperature dependent measurements of feldspar conductivity performed by other authors yields a somewhat ambiguous result: Some measurements contradict the increase in conductivity with temperature displayed by Kanamori et al.'s [1968Kan] converted data while those performed by Birch and Clark [1940Bir^a; 1940Bir^b], seem to confirm it, at least in the temperature range 25 °C – 300 °C.

8.1.5.2 Thermal Conductivity of Rocks

For a large number of rocks thermal conductivity data are available and classified according to rock name and origin in several extensive compilations [1942Bir; 1966Cla; 1974Des; 1974Kap; 1981Roy; 1982Čer; 1988Rob; 1988Sun; 1996Sch]. However, it is important to realize that these compilations comprise rocks which are heterogeneous in important aspects, such as mineral composition, porosity, saturation, and experimental conditions. This is the reason for the great variability of thermal conductivity within each particular rock type. Indeed, rock type as such is a rather poor descriptor for thermal and most other physical rock properties. This limits the usefulness of such tabulations, except for the rare instance when

they comprise data for the exact location of particular interest. In all other cases, predictions based only on data collated according to general rock type may be seriously in error. For all practical applications it is therefore strongly recommended to obtain genuine, representative data of thermal conductivity, either by direct measurement (cf. section 8.1.5.1.1) or by inference from geophysical logs (cf. section 8.1.5.1.2).

Therefore, the complementary approach taken previously by Clauser and Huenges [1995Cla] is extended here with new data: Rather than arranging individual measurements of rock thermal conductivity in tables, data from earlier compilations [1940Bir^a; 1940Bir^b; 1966Cla; 1974Des; 1974Kap; 1981Roy; 1982Čer; 1988Rob] supplemented by a large amount of new data which have become available since [1988Sun; 1990Kob; 1995Pop; 1996Pop, 1998Pop^a; 1998Pop^b; 1999Pop^b; 1999Pop^c; 2002Pop; 2003Pop^a; 2005Rat; 2005Mot] is presented in a statistical way and arranged as in [1995Cla] according to the four basic rock types: sedimentary, volcanic, plutonic, and metamorphic.

Inspection of any of the available compilations shows that thermal conductivity varies by as much as a factor of two to three. This is due to the natural variation of rock mineral content as well as to several physical and diagenetic factors. All rocks are therefore arranged according to the conditions at the time of their formation as sedimentary, volcanic, plutonic or metamorphic rocks. Each group is described in a statistical way by histograms, median, mean, and standard deviation (Table 8.12). This illustrates the variation of thermal conductivity with those factors which have the most pronounced effect on each rock type. These are petrological aspects or petrophysical influences such as porosity (in sedimentary and volcanic rocks), the dominant mineral phase (in metamorphic and plutonic rocks), and anisotropy (in sedimentary and metamorphic rocks).

8.1.5.2.1 Thermal Conductivity of Sedimentary, Volcanic, Plutonic, and Metamorphic Rocks

Fig. 8.12 shows thermal conductivity histograms for the four basic rock types: sedimentary, volcanic, plutonic, and metamorphic. For *sediments*, a distinction is made between (1) chemical sediments comprising limestone, coal, dolomite, hematite, chert, anhydrite, gypsum, rock salt, and sylvinit; (2) low porosity ($< 30\%$) physical sediments comprising shale (dolomitic, pyritic, carbonaceous), marl, clayey marl, marlstone, conglomerate, tuff conglomerate, impact conglomerate, tuffite, breccia, quartz breccia, and sandstone (including limy and quartz sandstone); and (3) high porosity ($> 80\%$) physical sediments comprising ocean and lake-bottom sediments. For *volcanic rocks* a distinction is made between (1) high porosity rocks (lava, tuff, tuff breccia, and mod-ocean ridge basalt (MORB)); and (2) low porosity rocks (rhyolite, liparite, trachodolerite, andesite, and basalt, other than MORB). For *plutonic rocks* a distinction is made between (1) rocks with high feldspar content ($> 60\%$; syenite (including alkali and nepheline syenite), grano-syenite, syenite porphyry, and anorthosite); and (2) low feldspar content ($< 60\%$; granite (including alkali granite, plagiogranite, granodiorite, tonalite, quartz monzonite), quartz- and quartz-feldspar porphyry, diorite (including monzonite), gabbro (including quartz and olivine gabbro), porphyrite dykes (lamprophyre, diabase, quartz dolerite) and ultra mafic rocks (pyroxenite, peridotite, lherzolite, hypersthene, bronzite, dunite, olivinite, hornblendite, cumberlandite). For *metamorphic rocks* a distinction is made between (1) rocks with high quartz content (quartzites); and (2) low quartz content (quartz-mica schist, gneiss)

Influence of Porosity and the Dominant Mineral Phase: For *sedimentary rocks* the factors controlling thermal conductivity are porosity and sediment type (Fig. 8.12a): Both chemical sediments (formed mainly by precipitation of dissolved minerals or by compaction of organic material) and low porosity physical sediments ($\phi < 30\%$, formed by compaction and cementation of clastic material) have similar frequency distributions, means, medians, and first and third quartiles (Table 8.12). In contrast, the distribution of marine, high porosity ($\phi > 80\%$) physical sediments is skewed towards low conductivities, and mean and median are about half the size of those of the previous two distributions. Clearly, this is due to the low conductivity of the void filling fluid, either air or water.

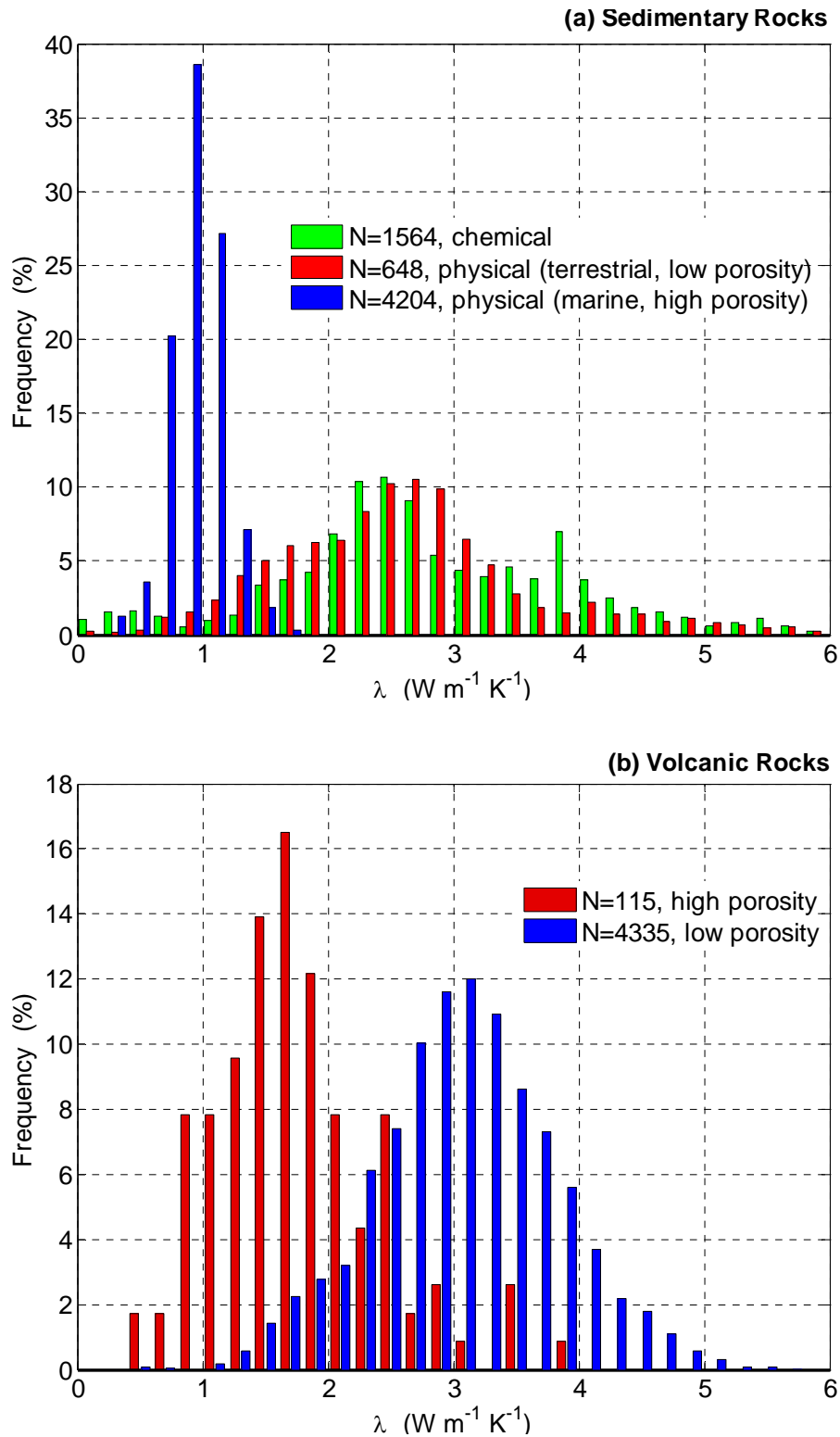


Fig. 8.12 Histograms of thermal conductivity for (a) sedimentary and (b) volcanic rocks (see text for details; plots by courtesy of Andreas Hartmann, RWTH Aachen University).

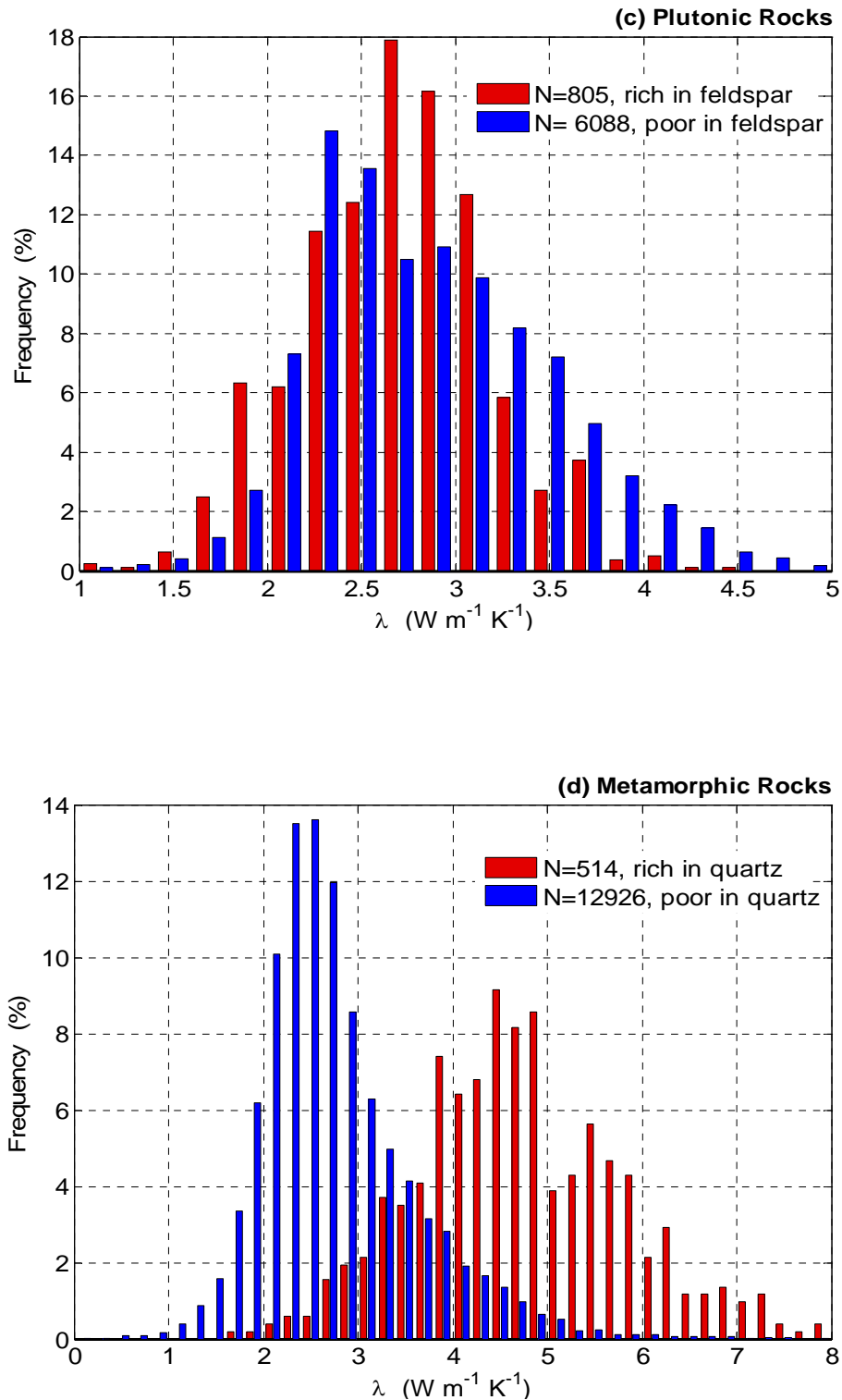


Fig. 8.12 (continued). Histograms of thermal conductivity of (c) plutonic and (d) metamorphic rocks (see text for details; plots by courtesy of Andreas Hartmann, RWTH Aachen University).

For *volcanic rocks* (Fig. 8.12b), spanning nearly the total possible range of porosity from 0 % – 100 %, porosity is clearly the controlling factor on thermal conductivity: mean and median of the high and low porosity histograms differ by nearly a factor of two, and the high porosity distribution is clearly skewed towards low conductivities (Table 8.12).

Plutonic and metamorphic rocks are generally much less porous. Here, the controlling factor is the dominant mineral phase. For *plutonic rocks* (Fig. 8.12c) the feldspar content determines the nature of the histogram: Rocks with a high feldspar content (i.e. > 60 %) show a nearly symmetrical conductivity distribution about a lower mean conductivity than rocks with low feldspar content. In spite of these differences, the means and medians for both distributions are nearly identical within the given standard deviation (Table 8.12).

For *metamorphic rocks* quartz content controls thermal conductivity (Fig. 8.12d). Mean and median of the distributions for high and low quartz content differ by nearly a factor of two. While the histogram for high quartz content rocks (mostly quartzites) is nearly symmetrical, that for low quartz content rocks is strongly skewed towards low conductivities (Table 8.12).

Table 8.12 Statistical moments of the histograms in Fig. 8.12: Number of measurements N; mean value μ ; standard deviation σ ; median M; and first and third quartile Q1 and Q3, respectively. Total number of data is 27230.

Rock Type		N	N _{total}	μ	σ	Q1	M	Q3
Sedimentary rocks	physical, marine ($\phi > 80$ %)	648	6416	0,94	0,21	0,80	0,94	1,06
	physical, terrestrial ($\phi < 30$ %)	4204		2,65	1,08	1,93	2,57	3,09
	chemical	1564		2,80	1,19	2,15	2,64	3,61
Volcanic rocks	high porosity	115	4450	1,75	0,64	1,31	1,66	2,10
	low porosity	4335		3,08	0,73	2,63	3,07	3,55
Plutonic rocks	rich in feldspar	805	6893	2,70	0,50	2,37	2,73	3,02
	poor in feldspar	6088		2,86	0,63	2,38	2,79	3,28
Metamorphic rocks	rich in quartz	514	13476	4,71	1,10	3,98	4,63	5,48
	poor in quartz	12962		2,70	0,82	2,20	2,54	3,00

Influence of Ambient Temperature: Thermal conductivity varies with temperature. This is primarily due to the decrease of lattice (or phonon) thermal conductivity with temperature and to a lesser extent to thermal cracking. Since the thermal expansion coefficient increases with temperature (but differently for all minerals) differential expansion may create contact resistances between mineral grains. This effect is less pronounced in water-saturated rocks than in dry rocks, the condition in which most rocks are tested at elevated temperatures. In contrast, the radiative contribution to thermal conductivity (cf. section 8.1.5.4) increases with the cube of temperature [see e.g. 1988Cla; 1999Hof]. Thus measurements of thermal conductivity as function of temperature generally first show a decrease with temperature, until – from about 1000 °C – 1200 °C onwards – the radiative component balances and sometimes even reverses this decreasing trend. Radiation is more important for rocks with a larger free mean path of radiation corresponding to smaller values of absorption coefficient and opacity (cf. section 8.1.5.4).

Fig. 8.13a illustrates the temperature variation of thermal conductivity for *sedimentary rocks*. Up to 300 °C there is a reduction by nearly a factor of two, both for physical and chemical sediments. Above 300 °C the decrease in thermal conductivity is less pronounced, for chemical still a little stronger than for physical sediments. However, there are very few data for this temperature range, which makes this last observation statistically weak. Above 300 °C, the mean thermal conductivity of sediments varies between $1.0 \text{ W m}^{-1} \text{ K}^{-1}$ – $1.5 \text{ W m}^{-1} \text{ K}^{-1}$.

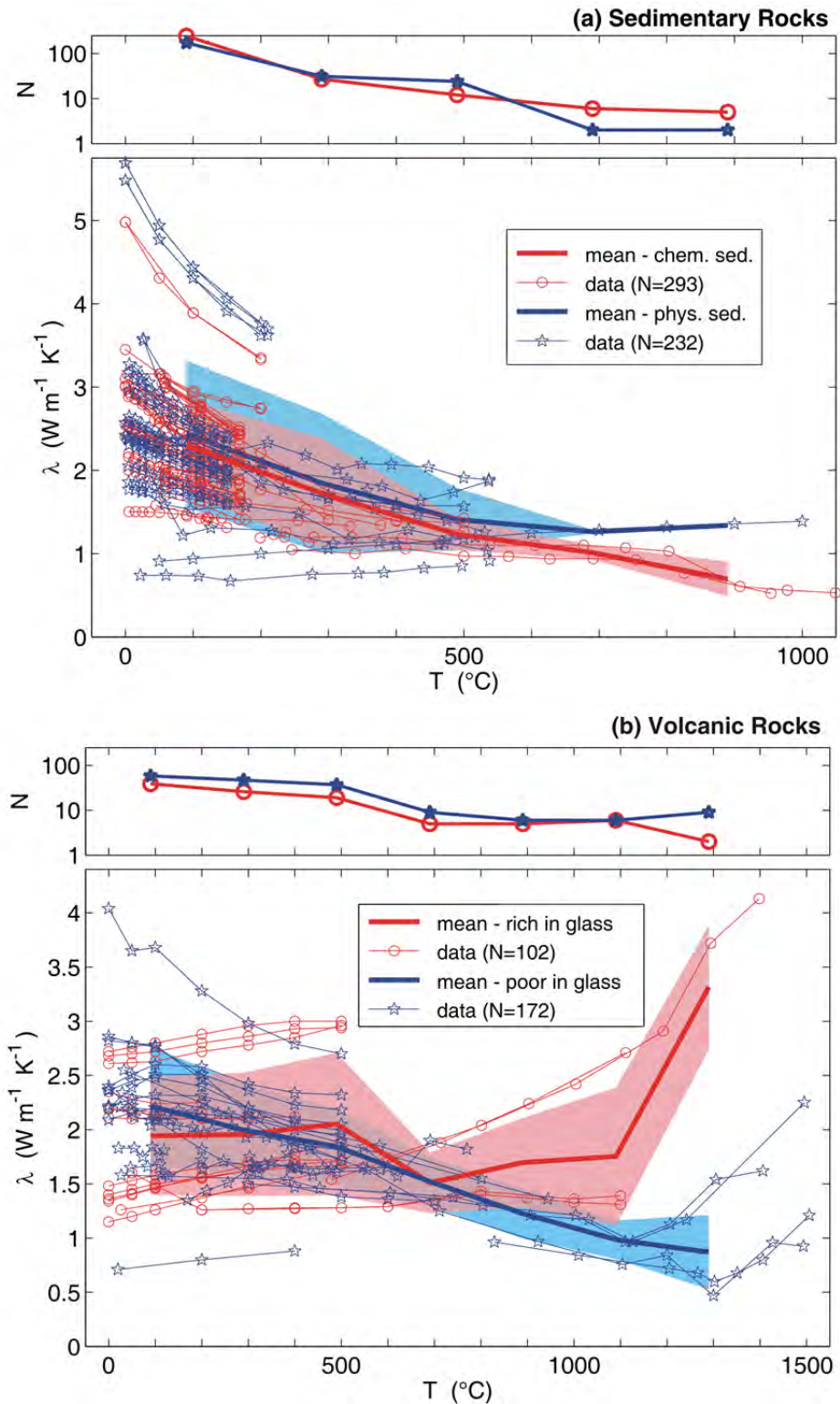


Fig. 8.13 Variation of thermal conductivity of (a) sedimentary and (b) volcanic rocks with temperature. Color shading indicates a range defined by plus and minus one standard deviation (see text for details; plots by courtesy of Andreas Hartmann, RWTH Aachen University).

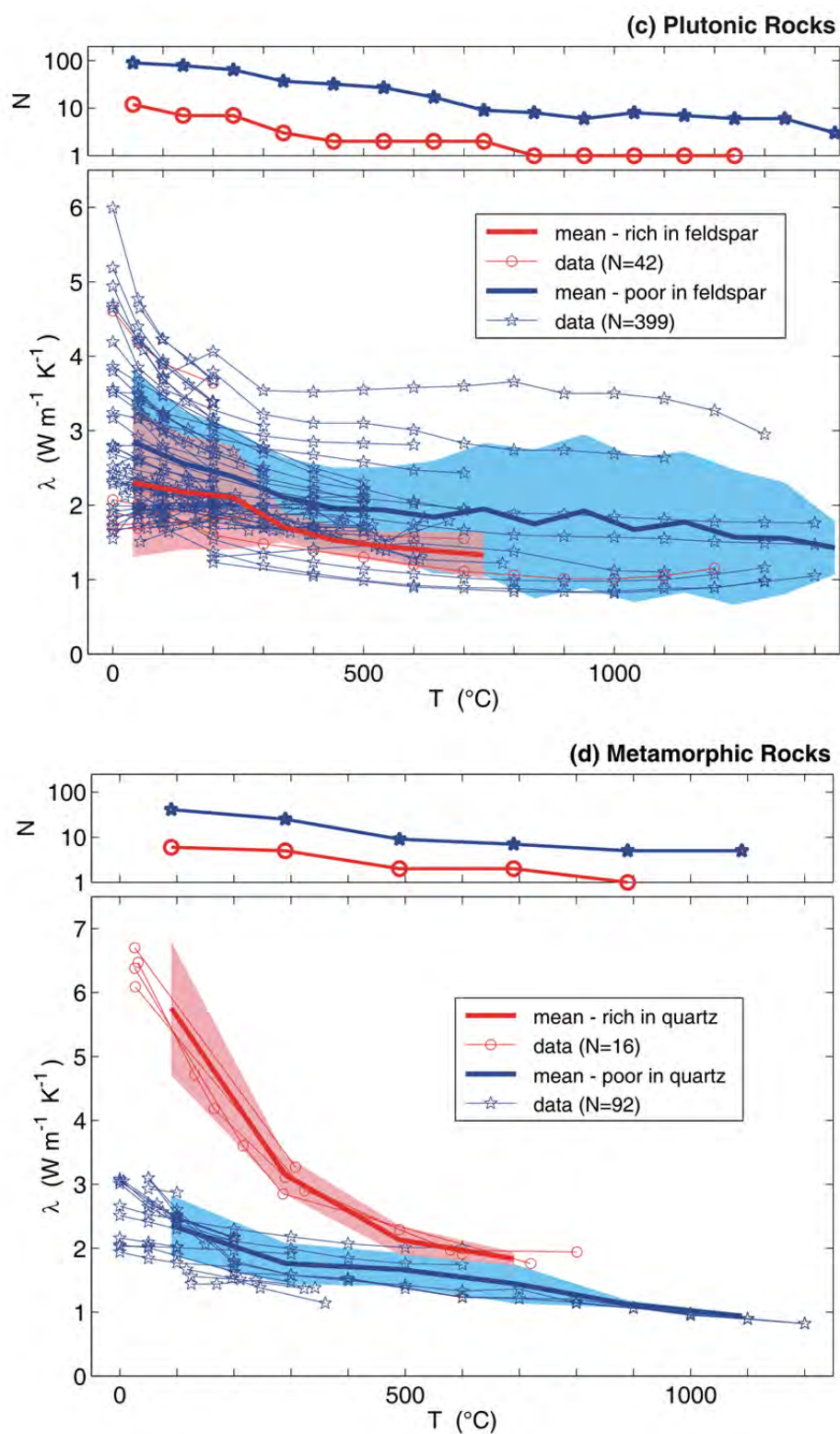


Fig. 8.13 (continued). Variation of thermal conductivity of (c) plutonic and (d) metamorphic rocks with temperature, Color shading indicates a range defined by plus and minus one standard deviation (see text for details; plots by courtesy of Andreas Hartmann, RWTH Aachen University).

Volcanic rocks (Fig. 8.13b) show a quite different behavior, depending on their opacity, i.e. on how well they transmit thermal energy by radiation. Due to this additional "radiative thermal conductivity", volcanic glasses and rocks with a small iron content experience an increase in thermal conductivity for temperatures above 800 °C – 1000 °C (cf. section 8.1.5.4 and e.g. [1988Cla] and [1999Hof]). In contrast, the thermal conductivity of conduction dominated rocks, such as volcanic glasses and rocks with high iron content, again decreases with temperature. An inversion of this trend is indicated by few available high-temperature measurements (above 1300 °C) but with too few measurements to calculate statistically meaningful means and standard deviations. At about 1000 °C thermal conductivity for these rocks is at about 50 % of the room-temperature value. Again, there are few data points above 700 °C.

In *plutonic rocks* there seems to be no strong radiative contribution (Fig. 8.13c). At temperatures above 600 °C thermal conductivity decreases only very little. However, the variation of thermal conductivity with temperature depends on the feldspar content of the rocks. For rocks enriched in feldspar, thermal conductivity decreases little up to 300 °C, while for those poor in feldspar the decrease is stronger, becoming more gentle above 300 °C, and spreading an additional 20 % over the next 1000 K. Interestingly, there is a large amount of data available for this high temperature range. The different behavior of rocks with high feldspar content is due to the increase in thermal conductivity with temperature of some plagioclase feldspars [1940Bir^a] which compensates the decrease in thermal conductivity with temperature observed for most other minerals and rocks. Other notable exceptions are fused silica as well as volcanic and silica glasses (see also discussion of empirical relationships below).

For *metamorphic rocks*, the decrease of thermal conductivity with temperature depends on the content in a dominant mineral phase, similar to plutonic rocks. For quartzites the decrease is rapid, by nearly a factor of three up to a temperature of about 500 °C. Above, there is only a very mild further decrease. For rocks that are poor in quartz the decrease in conductivity is not quite as dramatic, amounting to about one third of the room-temperature value up to 300 °C. Then it remains roughly constant up to 500 °C. Up to 750 °C, it decreases again to about one third of the room-temperature value.

Often data on thermal conductivity is available for room-temperature conditions only, even though it is required at elevated temperatures. For this purpose empirical relationships have been proposed based on measurements at elevated temperatures. With care, they can be used for extrapolation. It is strongly emphasized, however, that there is no real substitute for genuine measurements.

It has been long recognized that for moderate temperatures thermal conductivity, in general, varies with the inverse of temperature [1940Bir^b]. For this temperature range several approaches are available for inferring thermal conductivity at elevated temperatures. Based on the analysis of available tabulated data of thermal conductivity as function of temperature Zoth and Hänel [1988Zot] suggested the following relationship:

$$\lambda(T) = A + \frac{B}{350 + T}, \quad (8.33)$$

where λ is in $\text{W m}^{-1} \text{K}^{-1}$, T in °C, and the empirical constants A and B are determined from a least-squares fit versus temperature of data for different rock types (Table 8.12).

Linear relationships between temperature and thermal resistivity, such as eqs. (8.31) and (8.33), discriminate between temperature-dependent contributions and other factors, which are independent of temperature, such as micro-cracks, grain boundaries, pore volume, mineralogical composition, shape and orientation of crystals and their fragments. As discussed for minerals, the coefficients m and n in eq. (8.31) may be determined as intercept and slope of a linear regression of thermal resistivity versus temperature. Buntebarth [1991Bun] determined m and n from measurements on 113 samples of metamorphic rocks from the KTB research borehole in Germany (mostly gneisses and metabasites) in the temperature range 50 °C – 200 °C. The arithmetic means of 66 individual values determined for gneiss are

Table 8.13. Values for the constants A and B in eq. (8.33) for different rock types; data: [1988Zot].

rock type	T (°C)	A (W m ⁻¹ K ⁻¹)	B (W m ⁻¹)
(1) rock salt	-20 – 0	-2.11	2960
(2) limestones	0 – 500	0.13	1073
(3) metamorphic rocks	0 – 1200	0.75	705
(4) acid rocks	0 – 1400	0.64	807
(5) basic rocks	50 – 1100	1.18	474
(6) ultra-basic rocks	20 – 1400	0.73	1293
(7) rock types (2)-(5)	0 – 800	0.70	770

$\bar{m} = 0.16 \pm 0.03 \text{ m K W}^{-1}$ and $\bar{n} = (0.37 \pm 0.14) \times 10^{-3} \text{ m W}^{-1}$. The corresponding means determined on 36 metabasite samples are $\bar{m} = 0.33 \pm 0.03 \text{ m K W}^{-1}$ and $\bar{n} = (0.22 \pm 0.14) \times 10^{-3} \text{ m W}^{-1}$.

Sass et al. [1992Sas] and Vosteen and Schellschmidt [2003Vos] also distinguish between the effects of composition and temperature. They propose a general empirical relation for $\lambda(T)$, the thermal conductivity in $\text{W m}^{-1} \text{ K}^{-1}$ at temperature T in °C, as a function of λ_0 , the thermal conductivity at 0 °C:

$$\lambda(T) = \frac{\lambda_0}{a + T(b - c/\lambda_0)} \quad \text{or} \quad \lambda_0/\lambda(T) = \underbrace{a}_{\text{intercept}} + \underbrace{(b - c/\lambda_0)}_{\text{slope}} T. \quad (8.34)$$

For different rock types, slopes and intercepts can be determined from linear regressions of eq. (8.34), yielding a mean intercept \bar{a} and its uncertainty Δa . Coefficients b and c and associated uncertainties σ_b and σ_c are determined from a second linear regression of the different slopes $(b - c/\lambda_0)$ as a function of $1/\lambda_0$ (Table 8.14).

Table 8.14. Coefficients \bar{a} , b, and c in eq. (8.34) and associated uncertainties Δa , and σ_b , σ_c ; Δa is the error of the mean intercept \bar{a} for all rock types of the linear regressions of the normalized thermal resistance $\lambda_0/\lambda(T)$ as a function of temperature T; σ_b and σ_c are the errors defined by the linear regression of the slopes $(b - c/\lambda_0)$ as a function of the thermal resistance $1/\lambda_0$ (see eq. (8.34)).

rock type	\bar{a} (–)	Δa (%)	b (K ⁻¹)	σ_b (K ⁻¹)	c (W m ⁻¹ K ⁻²)	σ_c (W m ⁻¹ K ⁻²)	T (°C)	Reference
Basement Rocks I (from felsic gneiss to amphibolite)	1.007	–	0.0036	–	0.0072	–	0-250	[1992Sas]
Basement Rocks II (magmatic and metamorphic)	0.99	1	0.0030	0.0015	0.0042	0.0006	0-500	[2003Vos]
Sediments	0.99	1	0.0034	0.0006	0.0039	0.0014	0-300	[2003Vos]

Since thermal conductivity is usually measured at room temperature, λ_0 is expressed as a function of λ_{25} , the room temperature thermal conductivity, by Sass et al. [1992Sas] for crystalline rocks (felsic gneiss to amphibolite) as:

$$\lambda_0 = \lambda_{25} \left[1.007 + 25 (0.0037 - 0.0074/\lambda_{25}) \right]. \quad (8.35)$$

Vosteen and Schellschmidt [2003Vos] find for magmatic and metamorphic rocks:

$$\lambda_0 = 0.53 \lambda_{25} + 0.5 \sqrt{1.13 \lambda_{25}^2 - 0.42 \lambda_{25}}, \quad (8.36)$$

and for sedimentary rocks:

$$\lambda_0 = 0.54 \lambda_{25} + 0.5 \sqrt{1.16 \lambda_{25}^2 - 0.39 \lambda_{25}}. \quad (8.37)$$

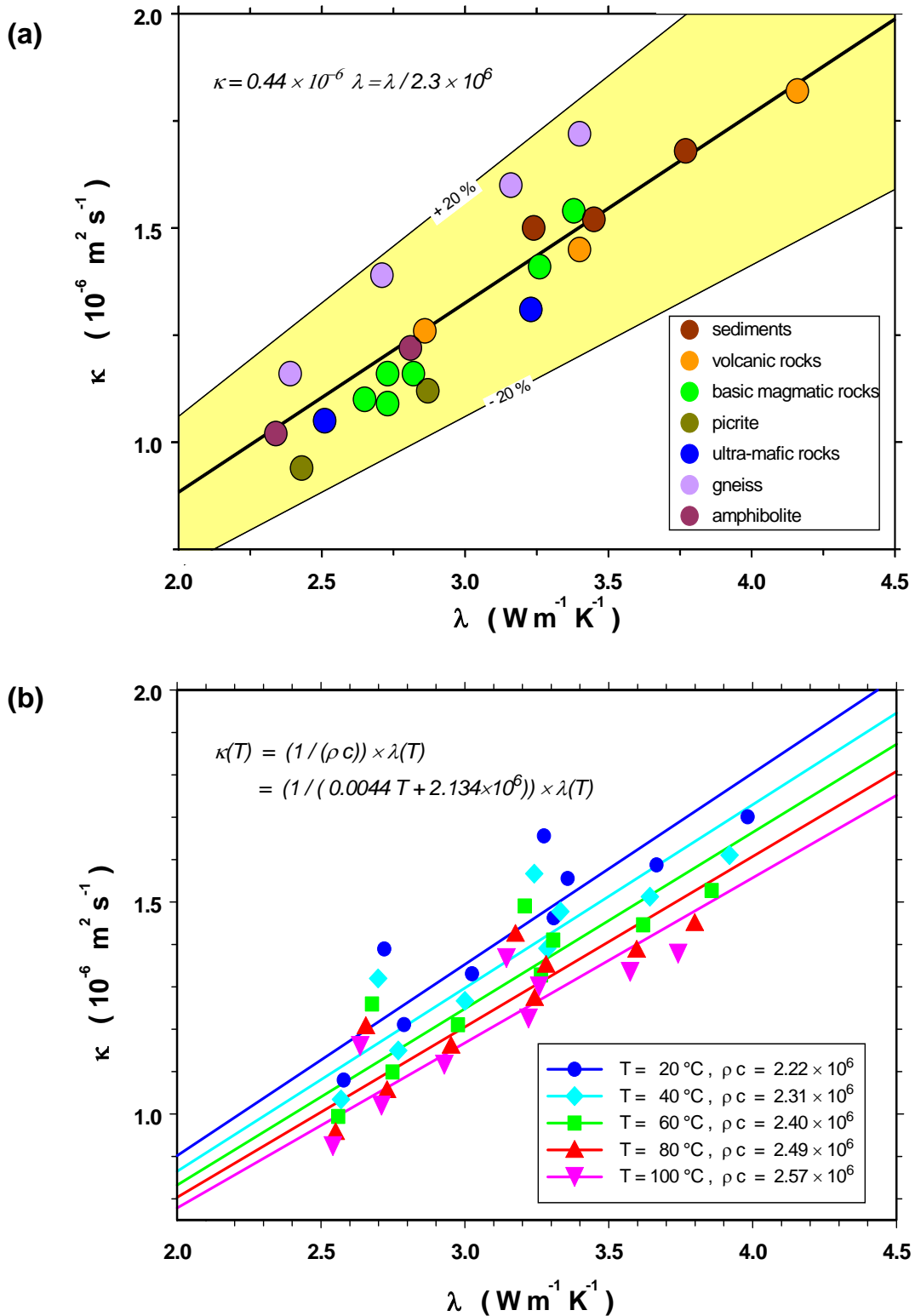


Fig. 8.14 Variation of thermal diffusivity κ with thermal conductivity λ for a suite of meta-sedimentary, volcanic, magmatic, and metamorphic rocks; (a) at room temperature; (b) as a function of temperature [2005Mot].

Sass et al. [1992Sas] derived eqs. (8.34) and (8.35) from thermal conductivity measured as function of temperature in the range 0 °C – 200 °C and higher on 38 samples from a large suite of materials including volcanic, metamorphic, plutonic, and sedimentary rocks [1940Bir^a; 1940Bir^b]. Their results for granites demonstrate the coupled effect of composition and temperature: The normalized thermal resistivity $\lambda_0/\lambda(T)$ is a linear function of temperature, while the slope increases with λ_0 . Sass et al. [1992Sas] tested eqs. (8.34) and (8.35) on an independent data set over a temperature range of 0 °C – 250 °C for rocks ranging in composition from felsic gneiss to amphibolite. In spite of some slight systematic differences, the deviations between measured and predicted values were well within the experimental error range. This suggests that eq. (8.35) yields useful estimates of the temperature dependence of thermal conductivity for crystalline rocks, independent of mineralogy, in the temperature interval 0 °C – 250 °C. Vosteen and Schellschmidt [2003Vos] used a similar approach to obtain thermal conductivity for different crystalline and sedimentary rocks from the Eastern Alps in the temperature range 0 °C – 500 °C and 0 °C – 300 °C, respectively.

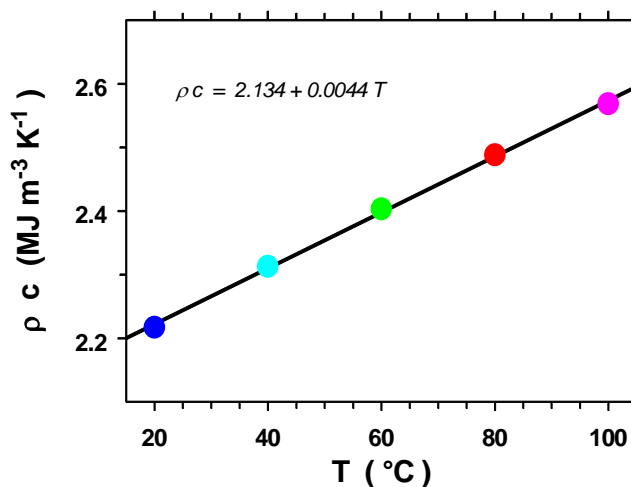


Fig. 8.15 Variation of thermal capacity ρc with temperature (after [2005Mot]); color code: as in Fig. 8.14.

For crystalline rocks up to a temperature of 100 °C, predictions based on the coefficients of Sass et al. [1992Sas] and Vosteen and Schellschmidt [2003Vos] yield comparable results with errors of ± 15 %. From 100 °C – 500 °C predictions based on the coefficients of Vosteen and Schellschmidt [2003Vos] remain within this error range, while those based on the coefficients of Sass et al. [1992Sas] show a systematic increase and shift of the error range with temperature from +5 % – -30 % at 200 °C to -10 % – -55 % at 500 °C [2003Vos].

For sedimentary rocks up to a temperature of 80 °C, predictions based on the coefficients of Sass et al. [1992Sas] and Vosteen and Schellschmidt [2003Vos] yield comparable results with errors ranging from +5 % – -18 %. From 80 °C – 300 °C the errors of the predictions based on the coefficients of Vosteen and Schellschmidt [2003Vos] range from +8 % – -34 %, while those based on the coefficients of Sass et al. [1992Sas] systematically increase and vary in the range of -5 % – -60 % [2003Vos]. Thus predictions based on the coefficients of Vosteen and Schellschmidt [2003Vos] appear to be more accurate at higher temperature and, in particular, for sedimentary rocks.

Thermal diffusivity of rocks varies even more strongly with temperature than thermal conductivity. This is caused by the opposite behavior of thermal conductivity and thermal capacity (ρc) with respect to temperature: While thermal conductivity decreases by 4 % – 7 % in the range 1 °C – 100 °C, thermal diffusivity decreases by 18 % – 22 %. Fig. 8.14a shows the variation of thermal diffusivity with thermal conductivity at ambient temperature for a suite of meta-sedimentary, volcanic, magmatic, and metamorphic rocks [2005Mot]. A linear regression through the origin yields:

$$\kappa = \frac{\lambda}{\rho c} = 0.44 \times 10^{-6} \lambda = \frac{\lambda}{2.3 \times 10^6} . \quad (8.38)$$

Because of several self-compensating factors, thermal capacity (ρc) with few exceptions generally varies within ± 20 % of $2.3 \text{ MJ m}^{-3} \text{ K}^{-1}$ for the great majority of minerals and rocks [1988Bec]. Fig. 8.14b shows the variation of thermal diffusivity for the previous rock suite [2005Mot] with thermal conductivity at

temperatures up to 100 °C. Thermal capacity (ρc) is the inverse slope of each of these linear regressions and varies linearly with temperature, too (Fig. 8.15). A linear regression of thermal capacity as a function of temperature again yields a linear relationship from which the variation of thermal diffusivity $\kappa(T)$ with temperature can be derived from the variation of thermal conductivity $\lambda(T)$ with temperature:

$$\kappa(T) = \frac{\lambda(T)}{2.134 \times 10^6 + 0.0044 T} \quad (8.39)$$

Similar relationships have been reported by Kukkonen and Suppala [1999Kuk] and Vosteen and Schell-schmidt [2003Vos].

8.1.5.2.2 Influence of Various Factors on Thermal Conductivity

Apart from temperature, thermal conductivity also varies with pressure, saturation, pore fluid, dominant mineral phase, and anisotropy of different rock types.

Pressure: The effect of overburden pressure is twofold, different for two distinct pressure ranges. First, fractures and micro-cracks (developed during stress release, when samples are brought to the surface) begin to close with increasing pressure. This reduces thermal contact resistance as well as porosity, which is usually filled with a low conductivity fluid. When an overburden pressure of about 15 MPa is reached, this process comes to an end. A compilation of measurements on various sedimentary, volcanic, plutonic and metamorphic rocks [1995Cla] indicates that this effect accounts for an increase of about 20 % relative to thermal conductivity at ambient conditions. A further pressure increase to 40 MPa does not affect thermal conductivity significantly. If pressure is increased further, however, a second process becomes effective, the reduction of intrinsic porosity, i.e. voids which are not created by stress release. For granite and for metamorphic rocks data indicate a corresponding increase of thermal conductivity on the order of 10 % over the pressure range 50 MPa – 500 MPa.

Porosity and Saturating Fluid: For large porosities (i.e. $\phi \gg 1\%$) the thermal conductivity of the saturating fluid affects significantly the bulk rock thermal conductivity. The influence varies with the thermal conductivity of the saturating fluids: water, oil, natural gas or air (cf. Table 8.7). The resulting bulk thermal conductivity can be estimated from a suitable mixing model (e.g. eqs. 8.23 – 8.26; see also Fig. 8.10). This effect is illustrated in Fig. 8.16 for data obtained by Robertson and Peck [1974Rob] from Hawaiian marine basalt saturated by air and water. This data set is remarkable as it comprises nearly the total possible range of porosity from 0 % – 100 %.

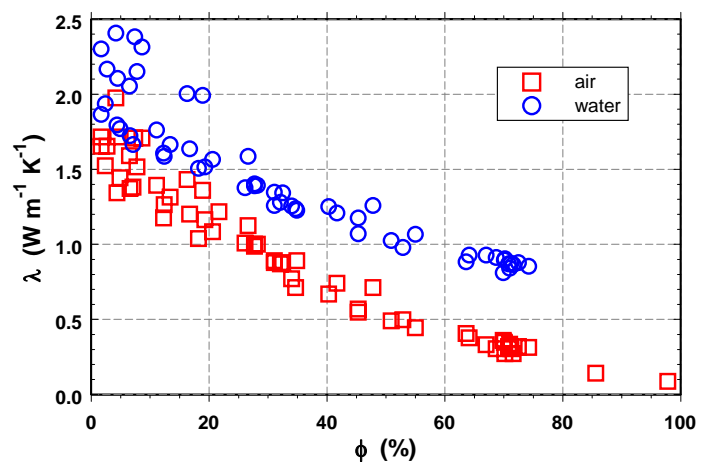


Fig. 8.16 Variation of thermal conductivity λ with porosity ϕ for Hawaiian basalt [1974Rob], measured dry (air) and saturated with water.

Partial Saturation: The effect of partial saturation is different for porous or fractured rocks. Porosity in porous rocks consists of the bulk pore space and bottlenecks in between formed by the contact between individual grains. Dry bottlenecks act as thermal contact resistances between grains, while the bulk pore volume contributes proportionally to the effective rock thermal conductivity. In fractured rocks, in con-

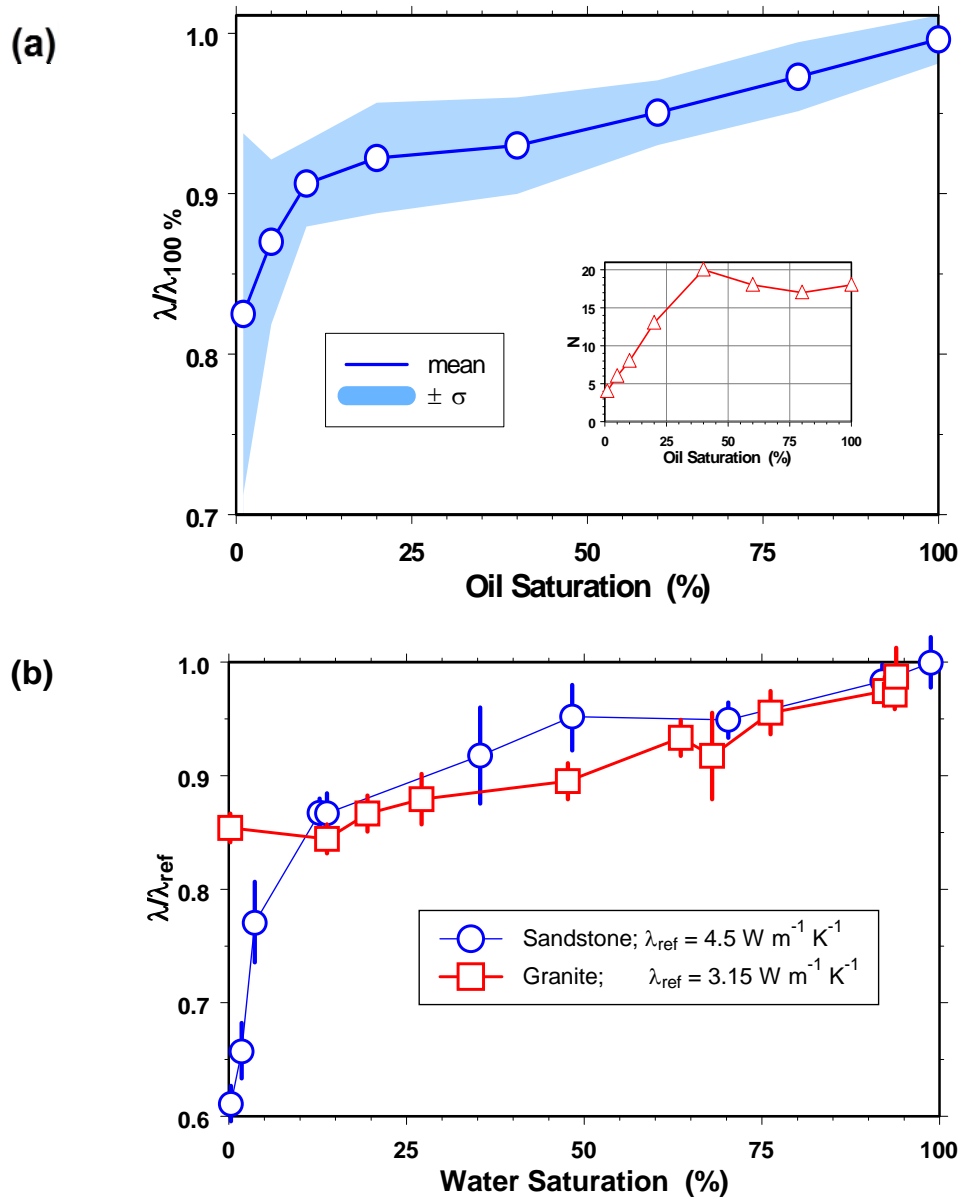


Fig. 8.17 Variation of thermal conductivity with partial saturation. (a) Sandstones ($3\% \leq \phi \leq 30\%$) saturated with oil; values normalized by thermal conductivity at full saturation (circles); data: [1965Mes; 1974Des]; (b) Sandstone ($\phi = 18\%$) (circles) and granite ($\phi = 1\%$) (squares) saturated with water and standard deviations (bars); values normalized by reference thermal conductivities shown in legend; data: [1991Rei].

trast, there are no bottlenecks between grains as in porous rocks, and the small void volume in the fractures corresponds to the bulk pores space of porous rocks.

Saturating these two basic types of voids results in a completely different variation of thermal conductivity with saturation. Fig. 8.17a illustrates the variation of thermal conductivity with the degree of oil saturation in sandstones of low- to medium-porosity. Initially, there is a rapid increase in conductivity with saturation: Starting from completely unsaturated conditions (where conductivity is only about 80 %

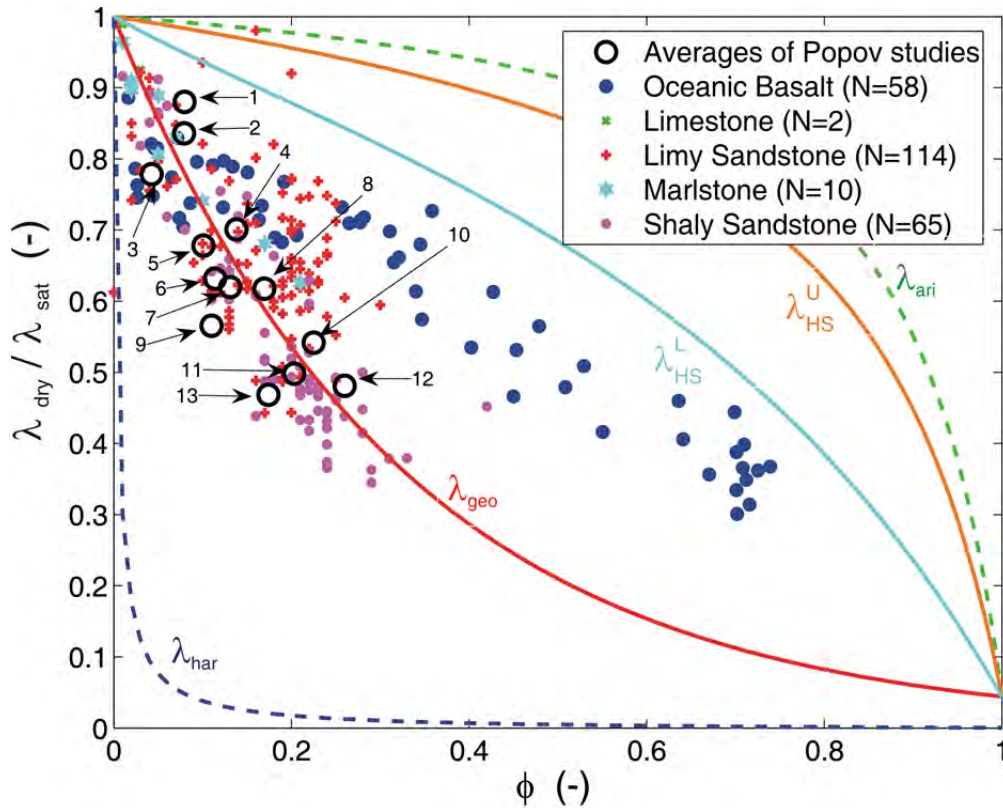


Fig. 8.18. Variation of thermal conductivity ratio $\lambda_{\text{dry}}/\lambda_{\text{sat}}$ (dry and saturated measurements) with porosity ϕ for different rock types. Open circles represent mean values of Popov's measurements on sedimentary rocks [1990Kob; 1995Pop; 1996Pop; 1998Pop^b; 1999Pop^b; 2002Pop]; (1) 21 limestones (North Khasedayu); (2) 54 limestones (Kaliningrad); (3) 13 quartz sandstones (Talinskoe); (4) 44 quartz siltstones (Povkhovskoe, Vat-Eganskoe); (5) 35 conglomerates (Talinskoe); (6) 141 quartz sandstones (Samotlorskoe); (7) 33 claystones (Samotlorskoe); (8) 99 polymictic sandstones (Orenburgskoe); (9) 30 quartz sandstones (East European platform); (10) 22 claystones (Povkhovskoe, Vat-Eganskoe); (11) 65 quartz siltstones (EM-Egovskoe); (12) 99 quartz siltstones (EM-Egovskoe); (13) 241 quartz siltstones (Samotlorskoe); curves labeled λ_{ari} , $\lambda_{\text{HS}}^{\text{U}}$, $\lambda_{\text{HS}}^{\text{L}}$, λ_{geo} , and λ_{har} correspond to the arithmetic, upper and lower Hashin-Shtrikman bound, geometric and harmonic mixing laws, λ_{ari} , $\lambda_{\text{HS}}^{\text{U}}$, $\lambda_{\text{HS}}^{\text{L}}$, λ_{geo} , and λ_{har} , respectively (eq. 8.23); plots by courtesy of Andreas Hartmann, RWTH Aachen University.

of the saturated value), a level of 90 % is reached at about 10 % saturation. The 10 % conductivity residual is spread almost linearly over the remaining 90 % of saturation. Fig. 8.17b illustrates these two effects for the case of water-saturation and a medium-porosity sandstone. The behavior is quite similar to the preceding case: Starting from a completely unsaturated conductivity of only about 60 % of the saturated value, a level of 85 % is reached again at about 10 % saturation. The 15 % conductivity residual is again spread almost linearly over the remaining 90 % of saturation. Physically this observation indicates that the filling of inter-granular bottlenecks, which accounts for only about 10 % – 15 % of the total porosity, significantly reduces the contact resistances between the individual grains. The replacement of low conductivity air by a more conductive fluid in the major part of the pore volume accounts for the second effect. If only fractures contribute to the total porosity, such as in crystalline rock, there are no bottlenecks and we observe only the second effect. This is shown in Fig. 8.17b for granite with a porosity of 1 %. Starting from completely unsaturated conditions at a level of only about 85 % of the saturated conductivity, there is a quasi linear increase until the 100 % level is reached for complete saturation. Obviously, porous rocks whose pore volume comprises many bottlenecks experience this